PV and HP Disaggregation for Transmission System Applications

by

Hediyeh Safari

A thesis
presented to the University of Waterloo
in fulfillment of the
thesis requirement for the degree of
Doctor of Philosophy
in
Electrical and Computer Engineering

Waterloo, Ontario, Canada, 2026

© Hediyeh Safari 2026

Examining Committee Membership

The following served on the Examining Committee for this thesis. The decision of the Examining Committee is by majority vote.

Supervisor	Claudio Cañizares University Professor Department of Electrical and Computer Engineering University of Waterloo
Co-Supervisor	Maurice B. Dusseault University Professor Department of Earth Science University of Waterloo
Internal Member	Mehrdad Kazerani Professor Department of Electrical and Computer Engineering University of Waterloo
Internal Member	Ramadan El Shatshat Professor Department of Electrical and Computer Engineering University of Waterloo
Internal–External Member	Mehrdad Pirnia Professor Department of Management Science and Engineering University of Waterloo
External Examiner	Pierluigi Mancarella Professor Department of Electrical and Electronic Engineering University of Melbourne

Author's Declaration

I hereby declare that I am the sole author of this thesis. This is a true copy of the thesis, including any required final revisions, as accepted by my examiners.

I understand that my thesis may be made electronically available to the public.

Abstract

Utility customers in Canada and across the globe are installing Photovoltaic (PV) and Heat Pump (HP) systems at the Low Voltage (LV) level of distribution grids. Current projections indicate a continued global increase in the integration of these systems. The responsibility for managing the electric grid at this level primarily falls to Distribution System Operators (DSOs). However, the growing integration of these systems into distribution networks has limited visibility for transmission system operators, as the power output of those low-power systems is not typically monitored. Since the increased presence of PV and HP systems significantly impacts the grid, more detailed information is needed than what is currently provided by existing measurements. Hence, leveraging data to identify the capacity and aggregate signature of PV and HP systems from net-load measurements at the High Voltage (HV)/ Medium Voltage (MV) level in the transmission system is required to address this information gap, which is the focus of the proposed research.

The research presented in this thesis first introduces a novel approach for disaggregating PV generation from net-load measurements recorded at the HV level. The proposed technique is applied to actual data from an existing transmission line feeder to identify PV generation from net demand measurements. The methodology incorporates Geographical Information Systems (GIS) for detecting PV panels based on an algorithm that provides an accurate estimate of solar PV capacity. These estimations are validated against actual data from a local utility, showing a close match with the observed results. This information is then used in software tools to simulate PV power generation in the studied region, which is then used to estimate and disaggregate the generated power from net-load data by applying multiple Machine Learning (ML) and Deep Learning (DL) models. The results obtained for the Waterloo region in connection with the Independent Electricity System Operator (IESO) demonstrate that it is feasible to adequately disaggregate in practice PV power generation from transmission feeder net-load measurements with minimal or no additional sensor infrastructure.

The second part of this thesis focuses on identifying HP loads at the transmission system level, since the widespread adoption of HPs, particularly as replacements for fossil-based furnaces, raises concerns about potential grid issues at the HV level, where

existing infrastructure may be insufficient to manage the increased load. Additionally, the implementation of sub-metering infrastructure to monitor energy consumption specifically for HPs' LV loads is often expensive and not really available. In this context, understanding the power consumption of HPs is important, considering the frequency of their on-off transitions that significantly influence their demand patterns. However, the power demand of HPs in real-world operations has not been thoroughly characterized, and effective methods for detecting aggregated patterns are still underdeveloped. Thus, the presented research investigates how single smart meter data can be utilized to extract key indicators of HP demand profiles under varying outdoor temperature conditions. The proposed framework generates synthetic HP load consumption profiles and aggregates them at the transmission level. These aggregated profiles are then used to disaggregate HP loads from total power measurements using simulation models, data-driven approaches, and supervised ML and DL techniques for net load disaggregation. The results obtained using actual data provided by IESO from an HV/MV substation in Milton, Ontario, Canada, indicate that the proposed framework successfully captures temperature-dependent HP behavior and provides a reasonable approximation of aggregated real-world HP loads at the transmission system level, highlighting the practical relevance of the proposed technique for the IESO.

Acknowledgments

This thesis would not have been possible without the help of so many people in so many ways. I would like to express my sincere appreciation to all those who supported me throughout my journey to complete the Ph.D. program at the University of Waterloo.

I have had the honor and privilege to work under the supervision of Professors Claudio Cañizares and Maurice B. Dusseault, who guided me through the first steps of becoming a researcher. Their guidance and support have been invaluable in shaping my academic research and writing from the very first day of the Ph.D. program. Apart from their immense wisdom and insight, their enthusiasm to explore new research directions and novel ideas has been a constant source of inspiration to me. Their patience, kindness, understanding, and empathy towards their students are truly admirable, and they have been extremely caring during my days of struggle. Although I have immensely benefited from their technical expertise, I continue to learn from their superior discipline and kind disposition.

I also received significant advice and guidance from Daniel Sohm and Elyas Ahmad at the IESO. Discussions with them were always an exceptional source of new ideas. Without their continuous support, encouragement, and inspiration, preparing this thesis would have been much more challenging. I am deeply grateful for the guidance of Professors Mehrdad Kazerani, Ramadan ElShatshat, and Mehrdad Pirnia, my thesis readers, for their efforts in polishing and revising this thesis. I am also thankful to Professor Pierluigi Mancarella, Chair Professor of Electrical Power Systems at the University of Melbourne, Australia, for agreeing to be on my final public oral committee.

I would also like to extend my appreciation to all the instructors who taught me during my coursework at the University of Waterloo. Their dedication and expertise provided a strong academic foundation that supported my research journey. The faculty in the Electrical Engineering and Computer Science Departments have been a phenomenal source of knowledge and guidance, and I sincerely thank all of them.

I am also thankful to have group-mates like Pablo Verdugo, Carlos Ceja-Espinosa, Muhammad Abuelhamd, and many others, whose support and camaraderie I will al-

ways cherish. I am especially grateful to my fellow researchers at the University of Waterloo for their collaboration and friendship. I would like to express my sincere gratitude towards Professor and Associate Dean Christopher Nielsen, Jessica Rossi, Susan Widdifield, and others, who have been extremely helpful throughout my time in the Department of Electrical Engineering. I also appreciate the help I received from my friends who have made this journey unforgettable. I have shared so many great moments with them. To my close friends back home, your encouragement and belief in me have been deeply appreciated, even across the distance. Special thanks to those who stood by me through the most difficult times; I have been fortunate to have them in my life.

Finally, above all, I dedicate this thesis to my family for their unwavering love and sacrifice. My heartfelt thanks go to my beloved parents, to the memory of my late grandparents, and to my wonderful brother. I would not have been able to accomplish anything without their unconditional love, support, and understanding.

I gratefully acknowledge the financial support provided by the IESO and the University of Waterloo, which made this research possible.

AI Disclosure Statement

The language editing tool ChatGPT was employed for editing purposes.

Dedication

To my beloved parents and family,
for their unwavering support, endless encouragement,
and constant belief in me throughout my academic journey.

To myself,

for choosing growth over comfort,
for facing adversity with courage and dignity,
for remaining resilient through uncertainty,
for practicing discipline when it mattered most,
and for becoming stronger, steadier, more grounded,
and a more dependable and responsible human being...

Table of Contents

List of Figures **xiv**

List of Tables **xvii**

List of Abbreviations **xviii**

1 Introduction **1**

1.1 Motivation 1

1.1.1 PV Power Disaggregation 3

1.1.2 Heat Pump Load Disaggregation 4

1.1.3 Practical and Operational Applications 5

1.2 Literature Review 6

1.2.1 Distributed PV Power Disaggregation in Transmission Systems . 7

1.2.2 Heat Pump Modeling in Smart Residential Application 13

1.2.3 Heat Pump Load Disaggregation Techniques for Transmission Systems 16

1.2.4 Relevant Knowledge Gaps 19

1.3 Objectives 20

1.3.1 PV Power Disaggregation 21

1.3.2 Modeling and Validation of Heat Pump Loads 21

1.3.3 Heat Pump Load Disaggregation 21

1.4 Content Overview 22

2 Background Review **24**

2.1 Introduction . . . 24
2.2 Distributed PV Power . . . 25
2.3 Heat Pump Demand . . . 26
2.4 Geographical Information Systems Overview . . . 31
2.5 Machine Learning/Deep Learning Techniques . . . 32
2.5.1 Model Development . . . 33
2.5.2 Forecasting . . . 34
2.5.3 Image Processing . . . 35
2.6 Stochastic Analysis . . . 36
2.7 Synthetic Data . . . 37
2.7.1 Synthetic PV Generation Profiles . . . 38
2.7.2 Synthetic Heat Pump Load Profiles . . . 40
2.8 Summary . . . 42

3 Disaggregation of PV Generation at the Transmission System Level 43
Nomenclature . . . 43
3.1 Introduction . . . 45
3.2 General Approach . . . 45
3.3 Solar PV Output Estimation . . . 47
3.4 Solar and Load Power Disaggregation . . . 53
3.5 Machine Learning Models . . . 54
3.5.1 Regression Model . . . 54
3.5.2 KNN Model . . . 55
3.5.3 SVM Model . . . 55
3.6 Deep Learning Models . . . 56
3.6.1 LSTM Model . . . 56
3.6.2 CNN-LSTM Model . . . 57
3.6.3 BiLSTM Model . . . 59
3.7 Results and Discussion . . . 61
3.7.1 Data Sets . . . 61
3.7.2 Feature Extraction and Correlation Analysis . . . 62
3.7.3 Mask R-CNN PV Detection . . . 64

3.7.4 PV Capacity Estimation . . . 69
3.7.5 Hyperparameters Settings . . . 70
3.7.6 Forecasting Error Metrics . . . 73
3.7.7 Application and Comparison . . . 74
3.8 Summary . . . 83

4 Modeling of Heat Pumps for Smart Residential Applications 84
Nomenclature . . . 84
4.1 Introduction . . . 85
4.2 Machine Learning Models . . . 86
4.2.1 ANN Model . . . 87
4.2.2 LSTM Model . . . 87
4.2.3 Evaluation Metrics . . . 88
4.3 Results and Discussion . . . 89
4.3.1 Household and Heat Pump Description . . . 89
4.3.2 Data Collection and Preprocessing . . . 90
4.3.3 Hyperparameters . . . 91
4.3.4 Application and Comparison . . . 92
4.4 Summary . . . 96

5 Heat Pump Load Disaggregation for Transmission System Applications 97
Nomenclature . . . 97
5.1 Introduction . . . 98
5.2 Methodology . . . 99
5.2.1 Heat Pump Modeling and Synthetic Load Generation . . . 101
5.2.2 Heat Pump Demand Disaggregation . . . 105
5.3 Results, Validation and Verification . . . 107
5.3.1 Data Description and Processing . . . 107
5.3.2 Synthetic Heat Pump Load Generation . . . 110
5.3.3 Heat Pump Capacity Estimation . . . 114
5.3.4 Machine Learning Model . . . 115

5.3.5 Verification 116
5.3.6 Heat Pump and Demand Load Power Disaggregation 118
5.4 Summary 119

6 Conclusions, Contributions and Future Work **121**
6.1 Summary and Conclusions 121
6.2 Contributions 124
6.2.1 PV Power Disaggregation 124
6.2.2 Modeling and Validation of Heat Pump Loads 124
6.2.3 Heat Pump Load Disaggregation 125
6.2.4 Applicability 125
6.3 Future Work 127

References **128**

List of Figures

2.1 DPV generation system. 25
2.2 HP operation [141]. 28
2.3 Simplified HP control model. 30

3.1 PV generation identification at the transmission system level from net-load measurements in power grid feeders. 46
3.2 Waterloo region in Ontario, Canada. 48
3.3 Overview of the proposed PV generation and demand disaggregation approach. 49
3.4 Mask R-CNN architecture for detecting and segmenting PV solar panels. 50
3.5 Example of false positive segmentation of solar PV panels: (a) shadows from surrounding structures, (b) water pool, (c) dark-colored roofing materials, (d) skylights and car roofs. 52
3.6 Proposed approach for disaggregating net-load components. 54
3.7 Structure of LSTM cell with input x_t and output y_t [160]. 56
3.8 1D-CNN computational process. 58
3.9 CNN-LSTM hybrid model. 59
3.10 Structure of BiLSTM cell with time series inputs x_t and outputs y_t [213]. 60
3.11 Solar PV panels segmentation in the Waterloo region. 63
3.12 Simulated PV power output from SAM software with the colors signifying the probability of the PV output values, with red for more likely values and green-blue for least likely. 63

3.13 Time series for four days showing (a) PV power generation versus solar irradiance and (b) net-load versus ambient temperature for May 2020. . 65
3.14 Time series for four days showing (a) PV power generation versus solar irradiance and (b) net-load versus ambient temperature for December 2020. 66
3.15 Correlation metrics between solar power output and various factors in May 2020. 67
3.16 Measured and disaggregated powers for May 2021: (a) PV generation forecast and (b) BiLSTM disaggregation results. 75
3.17 Measured and disaggregated powers for July 2021: (a) PV generation forecast and (b) BiLSTM disaggregation results. 76
3.18 Measured and disaggregated powers for December 2021: (a) PV generation forecast and (b) BiLSTM disaggregation results. 77
3.19 Rolling window performance metric analysis for different algorithms over the specified date range in May 2021: (a) MAE and (b) RMSE. 79
3.20 Rolling window performance metric analysis for different algorithms over the specified date range in July 2021: (a) MAE and (b) RMSE. 80
3.21 Rolling window performance metric analysis for different algorithms over the specified date range of December 2021: (a) MAE and (b) RMSE. . 81
3.22 RMSE boxplots across models and months. 82
3.23 MAE boxplots across models and months. 82

4.1 Framework for ML-based model for HPs. 86
4.2 Structure of an LSTM cell. 88
4.3 Case study of a detached house in Milton, Ontario, Canada, equipped with a Mitsubishi Zuba HP [233]. 89
4.4 Overview of the datasets utilized. 91
4.5 Measured vs. LSTM, ANN, and physics-based load estimates, outdoor temperature T_a and indoor temperature T_i for some cold days at the end of February 2025. 94

5.1 HP load identification at the transmission system level from net-load measurements. 100
5.2 Generation of stochastic synthetic HP load data. 101
5.3 Detailed overview of proposed physics-based HP synthetic data generation. 103
5.4 Proposed approach for disaggregating net-load components. 106
5.5 Milton region in Ontario, Canada. 108
5.6 Simulated HP electrical load for January to March in (a) 2022 and (b) 2025. 111
5.7 Milton area for random house size selection. 112
5.8 Nominal and probabilistic COP values for the 7 HP types used, assuming a ±8% variability and normal pdf. 113
5.9 Probability scenarios employed to generate synthetic HP load profiles based on standard stochastic analysis. 114
5.10 LSTM pre-training and fine-tuning workflow for aggregated HP load forecasting. 116
5.11 Aggregated HP load profiles in Milton for February (a) 2022 and (b) 2025. 117
5.12 Kernel Density Estimation-based pdf of the 2022 dataset spanning January 01 to March 25. 117
5.13 Disaggregation of HP demand using net-load measurements for (a) March 2022 and (b) February 2025. 119

List of Tables

3.1 Performance Metrics for Mask-RCNN Model Evaluation 69
3.2 Actual Installed PV Capacity at Relevant HV/MV Transformer. 70
3.3 Hyperparameter Settings for LSTM, CNN-LSTM, and BiLSTM Models 71
3.4 Hyperparameter Settings for Linear Regression, KNN, and SVM Models 73
3.5 Quantitative Comparison of ML/DL Models for Photovoltaic (PV) Generation Forecasting 78

4.1 Hyperparameters of LSTM and ANN Models 92
4.2 Energy Modeling of Proposed Models 93
4.3 Power Estimation Errors for the Proposed Models 95

5.1 Probability of Thermostat Setpoints [237] 112

List of Abbreviations

AC	Alternating Current
ACKF	Augmented Complex Kalman Filter
AI	Artificial Intelligence
AMI	Advanced Metering Infrastructure
ANN	Artificial Neural Network
AR	Auto-Regressive
ARIMA	Auto Regressive Integrated Moving Average
ARMA	Auto Regressive Moving Average
ASHP	Air Source Heat Pumps
BiLSTM	Bidirectional Long Short-Term Memory
CNN	Convolutional Neural Network
COP	Coefficient of Performance
DC	Direct Current
DER	Distributed Energy Resources
DHI	Diffuse Horizontal Irradiance

DL	Deep Learning
DNI	Direct Normal Irradiance
DNN	Deep Neural Network
DPV	Distributed Photovoltaic
DR	Demand Response
EMS	Energy Management System
ESS	Energy Storage System
EV	Electric Vehicle
GAN	Generative Adversarial Network
GB	Gradient Boosting
GHG	Greenhouse Gas
GHI	Global Horizontal Irradiance
GIS	Geographical Information Systems
GSHP	Ground-Source Heat Pumps
HDI	Highest Density Interval
HP	Heat Pump
HV	High Voltage
HVAC	Heating, Ventilation, and Air Conditioning
IESO	Independent Electricity System Operator
IoU	Intersection over Union
IQR	Interquartile Range

KDE	Kernel Density Estimation
KNN	K-Nearest Neighbors
LSTM	Long Short-Term Memory
LV	Low Voltage
MAE	Mean Absolute Error
MAPE	Mean Absolute Percentage Error
ML	Machine Learning
MLP	Multi-Layer Perceptron
MPC	Model Predictive Control
MSE	Mean Squared Error
MV	Medium Voltage
NN	Neural Network
NRCan	Natural Resources Canada
NREL	National Renewable Energy Laboratory
PCA	Principal Component Analysis
PCC	Point of Common Coupling
pdf	probability density function
PV	Photovoltaic
RBF	Radial Basis Function
ReLU	Rectified Linear Unit
RF	Random Forest

RMSE	Root Mean Squared Error
RNN	Recurrent Neural Network
SAM	System Advisor Model
SGD	Stochastic Gradient Descent
SVM	Support Vector Machines
SVR	Support Vector Regression
TEC	Thermal Equivalent Circuit

Chapter 1

Introduction

This chapter outlines the motivation for the proposed research, beginning with an exploration of the need for improved techniques in disaggregating PV generation and Heat Pump (HP) consumption from net-load measurements at the transmission system level. It then provides a review of existing methodologies and approaches in the existing technical literature relevant to the research topics, identifying the gap that the present work addresses. Building on the insights gained from the motivation and literature review, the specific objectives of the presented research are then defined. Finally, the chapter concludes with an overview of the structure and content of the thesis.

1.1 Motivation

As clean energy and energy-efficient technologies, such as PV systems and HP, gain prominence in the quest to achieve global carbon emissions targets toward a net-zero 2050, the need for accurate real-time information about Distributed Energy Resources (DER) becomes increasingly important. Among these DERs, solar PV, a key element in the renewable energy transition, offers a sustainable pathway to reduce carbon emissions [1]. Global PV capacity has experienced rapid expansion in recent years, increasing from 480 GW in 2018 to 583.5 GW by the end of 2019, partly driven by the addition of 16 GW of rooftop PV capacity [2,3]. This upward trajectory has continued, with global solar installations reaching record levels. In the first half of 2025 alone,

approximately 380 GW of new solar capacity were added worldwide, representing a 64% increase compared to the same period in 2024 [4].

High-efficiency electric HPs play a key role in reducing emissions in the building sector. These systems, which are at least three times more efficient than conventional fossil fuel boilers, are projected to see a substantial increase in global installations, rising from 180 million units in 2020, with approximately 1.5 million HP installed each month, to nearly 600 million by 2030 [5]. To meet existing national energy and climate commitments, HP are expected to supply nearly 20% of global building heating demand by 2030 [5]. In this context, global deployment of HP has accelerated significantly, with an 11% increase in 2022 marking a second consecutive year of double-digit growth [5], reflecting their increasing importance in achieving global emissions reduction targets [6], and reinforcing their central role in the transition toward secure and sustainable heating.

In 2021, Ontario accounted for approximately 80% of Canada's solar capacity, with 2,669 MW installed [7]. In the same year, HP served as the primary heating source for a growing share of homes [8], offering a low-carbon alternative to conventional fossil fuel systems. According to Natural Resources Canada (NRCan), the total number of newly installed HPs across the country rose from 144,736 units in July 2024 to 260,389 units in July 2025 with federal support [9,10]; within Ontario specifically, installations increased from 49,558 to 102,535 over the same period. Analysis based on the Independent Electricity System Operator (IESO) projected 2030 electricity supply mix indicates that deploying high-efficiency HPs could reduce Greenhouse Gas (GHG) emissions from Ontario's gas-fired power plants by up to 18%, corresponding to approximately 2.2 Megatonnes of annual GHG reductions, or about 4.0 Megatonnes when lifecycle emissions are considered. Nevertheless, gas furnaces remain the dominant residential heating technology in the province, contributing substantially to GHG emissions, which were estimated at 157 Megatonnes in 2022 [11,12]. This highlights the continuing need to expand low-carbon technologies, such as HP and distributed solar generation, to reduce emissions and support a sustainable energy transition in Ontario.

The increasing complexity in net load behavior has important implications for power system operation and planning. In particular, the growing penetration of both Distributed Photovoltaic (DPV) and HP technologies introduces additional variability and

shifts in demand patterns, especially during peak heating and cooling periods. Such effects can lead to operational challenges, including the "duck curve" phenomenon, where solar generation profiles lead to generation dispatch issues [13–15]. HPs can exacerbate supply-demand imbalances, particularly during peak heating/cooling periods, resulting in heightened demand and complicating grid management. Beyond operational variability, these changes directly affect the estimation of the capacity of Demand Response (DR), which is essential for aggregators and system operators in market participation and grid management. Since DR capacity is strongly dependent on underlying load profiles, inaccuracies in representing embedded DPV and HP capacities can propagate into errors in demand response baselines, forecasting models, and network planning decisions [16–19]. Under these conditions, accurate representation of net demand becomes challenging, typically requiring either direct measurement approaches, which depend on additional metering infrastructure and increase deployment cost, or indirect approaches that infer underlying consumption and DPV generation from existing measurements through disaggregation techniques [20–22]. As a result, improved visibility and disaggregation of DERs are critical for reliable system operation under high renewable penetration.

1.1.1 PV Power Disaggregation

The integration of DPV systems into power grids presents challenges due to their behind-the-meter nature, which limits visibility for utilities and system operators [23–25]. Unregistered or decommissioned rooftop PV systems can create significant gaps, particularly at the transmission feeder level, where broad geographic coverage makes accurate tracking difficult [26, 27]. Errors in utility datasets can also arise from manual data entry mistakes or inconsistencies between reported and actual system configurations. Transmission system operators often have limited access to distribution-level network data, which in some cases may not be really shared, further complicating accurate assessment. Studies have shown that a significant portion of residential rooftop PV capacity often goes unrecorded in many regions, leading to gaps in utility data [26, 27].

In Canada, the rapid growth of small-scale solar PV systems has increased the need for high-quality data on their location, capacity, and generation [28]. Accurate

estimation of PV generation improves visibility of masked feeder load, enabling system operators to anticipate steep ramp events, such as the evening drop in solar output coinciding with residential demand peaks [28]. This has driven the development of load disaggregation methods to better characterize DPV behavior and support more reliable and resilient grid operation [15, 29, 30].

1.1.2 Heat Pump Load Disaggregation

HP provides efficient heating and cooling solutions, enabling substantial reductions in the carbon footprint of buildings [31]. With increasing HP adoption, integrating these systems into demand response strategies offers an opportunity to enhance grid stability and accommodate the variability of renewable energy. HPs are increasingly adopted in Ontario as low-carbon, cost-effective heating solutions that reduce GHG emissions [8, 11, 12]. Despite HP benefits, large-scale adoption in regions such as the UK and Europe has revealed challenges for Low Voltage (LV) networks, particularly voltage drops caused by the induction motors driving compressors during start-up that must be addressed to fully realize their potential [32, 33].

The electricity consumption of HP can vary considerably due to factors such as improper sizing, non-optimal settings, and frequent on-off cycling [31]. This variability, in turn, affects their efficiency and lifetime. However, a significant challenge lies in the absence of data on HP operation and its impact on power consumption. While manufacturers are developing digital monitoring solutions, these tend to focus more on system breakdown prevention rather than optimizing efficiency, and a lack of standardization among manufacturers limits broader data integration [31, 34]. Moreover, many HP lack network connectivity, leaving them outside the scope of metering digital services [35].

Limited visibility of aggregated HP penetration and demand at the High Voltage (HV)/Medium Voltage (MV) transmission level creates operational challenges [36]. The integration of HPs across various voltage levels, including HV/MV networks, alters consumption profiles [13]. Transmission and distribution operators must anticipate these shifts to prevent instabilities in the grid. To do so effectively, they require accurate information about the installed capacity and load patterns of HPs, as these technologies

are closely linked to weather conditions. However, this data is often incomplete or unavailable, particularly when installations are small-scale.

Understanding the installed capacity and generation/consumption profile of DPVs and HPs, given their increased deployment, is important for assessing their active participation in and influence on energy generation/consumption patterns [37], as previously discussed in more detail. This thesis addresses these challenges by first proposing methods for estimating the capacity and disaggregation of DPV profiles. Then, it incorporates methods for estimating capacity and generating HP load profiles to enable HP load disaggregation at the transmission level. Machine Learning (ML) and Deep Learning (DL) techniques are widely used throughout the presented research, providing a useful framework for understanding the dynamic interactions between PV and HP technologies and their impact on grid operations.

1.1.3 Practical and Operational Applications

Disaggregating unmonitored solar generation and residential heat pump loads is essential for bulk power system reliability. Thus, identifying unmonitored distributed photovoltaic output allows operators to decouple steep net-load ramps and effectively mitigate duck-curve transitions, since the rapid drop in solar generation during late afternoon hours typically coincides with rising residential consumption, creating severe upward ramp rates on bulk supply points. By disaggregating gross photovoltaic generation from feeder net load, system operators can anticipate ramp events, optimize operating reserves, and manage generation and load resources more reliably.

On the heating side, isolating heat pump demand is critical for better winter peak load forecasting, as severe cold snaps degrade the coefficient of performance and trigger auxiliary resistance spikes. Separating these temperature-sensitive loads from substation measurements allows us to better manage peak load events and enables the proactive dispatch of fast-ramping reserves to manage steep heating ramps.

In addition to normal operating conditions, disaggregating behind-the-meter resources is vital for power system security and contingency assessment. In traditional $N-1$ security analysis, transmission operators assess the grid's ability to withstand

sudden line or transformer outages based primarily on net-load readings. However, composite measurements can severely mask true operating risk. For instance, high penetrations of unmonitored distributed solar can conceal substantial electrical demand, leading operators to underestimate post-contingency line flows should an outage coincide with sudden solar curtailment, cloud transients, or widespread inverter voltage trips. Similarly, isolating temperature-sensitive heat pump loads allows operators to identify feeders vulnerable to thermal violations and severe voltage depressions during extreme winter weather. By decoupling customer demand from distributed generation and flexible thermal loads, system operators gain situational awareness to improve system operation, evaluate transfer limits, and coordinate targeted demand response actions to maintain system security without resorting to indiscriminate load shedding.

Beyond real-time operations, load disaggregation plays a pivotal role in demand-side management. Disaggregating underlying thermal flexible loads establishes reliable baselines for residential demand response programs, ensuring that participating resources are properly managed such as improving load curtailment during grid stress. Simultaneously, tracking localized heating and solar penetration directly from existing transformer net-load data improves transformer loading assessments and asset utilization, allowing utilities to properly manage overloads while maintaining reliability under increasing electrification.

1.2 Literature Review

A comprehensive literature review is undertaken in this section to gain insights into the current state of research and identify gaps relevant to this thesis. The review is organized into the following four main sections that are discussed next: DPV power disaggregation in transmission systems, residential HP modeling in smart residential applications, HP load disaggregation techniques for transmission systems, and research gaps.

1.2.1 Distributed PV Power Disaggregation in Transmission Systems

The process of identifying, estimating, and separating the electricity generated by small-scale PV installations, such as rooftop solar systems, from aggregated power measurements recorded at HV transmission substations or feeders generally involves two main components: (i) estimating the installed DPV capacity and (ii) reconstructing time-varying PV generation profiles based on the identified capacity. Recent research has investigated a range of techniques, including satellite-based approaches [38], statistical methods [27], and machine learning algorithms [23] to enhance the accuracy and reliability of DPV estimation at the transmission level. Building on these advances, researchers have developed numerous methodologies to estimate both the installed generation capacity and the real-time production of solar systems.

One common approach to identifying DPV power profiles involves the use of satellite and aerial imagery to detect solar PV systems and assess their physical characteristics, such as size, tilt, and orientation [27]. While this technique offers a broad estimate of PV installations' peak capacity, it falls short of accurately predicting real-time solar generation. Another common strategy for estimating PV output is model-based, utilizing localized irradiance measurements or estimations of beam, diffuse, and global solar irradiance derived from satellite data [39, 40]. These methodologies, although effective in certain contexts, often lack the precision needed for comprehensive real-time monitoring and analysis, particularly when dealing with diverse environmental conditions and large geographical areas.

The following sections examine two key aspects of DPV disaggregation. The first focuses on PV capacity identification, including statistical methods, time series–driven ML models, and image-based ML approaches. The second addresses the time-varying PV generation profiles using model-based techniques, data-driven approaches, and hybrid methods, with the objective of improving the fidelity of PV generation estimates at the transmission level.

1.2.1.1 PV Capacity Identification

The core problem of detecting PV generation capacity and profiles lies in the lack of visibility of small-scale, rooftop PV systems [41]. Unlike utility-scale solar farms that are monitored and recorded individually, rooftop PV systems are often behind the meter, meaning their real-time generation is not directly observable by grid operators. In addition to the operational challenges associated with distributed generation, privacy concerns and regulatory frameworks, such as the Data Access and Privacy Framework, further limit the accessibility of individual meter data for grid operators, thereby exacerbating the difficulty of accurate system-level PV visibility [42]. To address this limitation, a range of non-intrusive and data-driven methodologies has been proposed for PV capacity identification that avoid the need for direct metering infrastructure. Advanced data analytics and indirect measurement techniques enable accurate estimation of regional PV capacity, supporting improved grid visibility and management while preserving privacy and minimizing operational costs [43].

Recent studies have further investigated scaling techniques for small-scale PV estimation, where data from a limited number of monitored sites is used to infer generation behavior across larger regions. However, such approaches often rely on the assumption of known or well-characterized installed capacity and may not fully capture site-specific variability, which can introduce estimation errors [44]. Based on these developments, existing methodologies for rooftop PV capacity estimation can generally be categorized into three main groups, as discussed next.

Statistical Models

State estimation algorithms play an important role in determining the most likely system state. In [38], a statistical method is proposed for detecting and estimating residential PV installations using change-point detection to identify abnormal consumption patterns, including unauthorized PV systems. The approach is further validated using a permutation test based on Spearman's rank coefficient and load profiles before and after the detected change-point, estimated via a Gaussian kernel density method. To improve PV size estimation, local cloud cover data is integrated with smart meter measurements. The method is validated using real smart meter data across multiple scenarios. However, this approach is not applicable to large-scale transmission feeder studies, as it requires detailed customer-level measurements and historical consumption

data that are typically unavailable.

Time Series-Driven Machine Learning Models

A two-stage ML approach based on Support Vector Machines (SVM) is proposed in [23], where customers with installed DPVs are first identified using net load deviations via a support vector classifier, followed by capacity estimation using a bootstrap-Support Vector Regression (SVR) model. The method is validated on real data from Austin, Texas, demonstrating accurate residential PV capacity estimation. In [45], decision tree classifiers are used to distinguish between solar and non-solar daily consumption profiles derived from smart meter data, achieving up to 92% accuracy after preprocessing and model evaluation. Researchers in [46] propose semi-supervised and one-class autoencoder-based methods to detect solar customers under limited labeling conditions, leveraging both synthetic and utility data to learn nonlinear consumption patterns. However, these data-driven approaches typically require detailed smart meter data, labeled datasets, or system-specific training, which limits their applicability in transmission-level settings where only aggregated net-load measurements are available.

Image-based Machine Learning Models

The use of Geographical Information Systems (GIS) for automated identification and capacity estimation of DPV systems across large regions is gaining significant traction [27]. Advances in computer vision, particularly semantic segmentation and DL methods, have improved the accuracy and efficiency of these processes [47]. Prior studies have successfully applied GIS to detect buildings, roads, and rooftops [27,48,49], while PV-specific applications remain more limited but promising [50]. Nevertheless, challenges remain in DPV detection due to the need for very high-resolution imagery and the issue of distinguishing these systems from similar structures such as skylights, solar thermal systems, and other rooftop elements [27].

Supervised ML methods, particularly Random Forest (RF) [51], Neural Network (NN) [52–54], and SVM [55], have been widely used for DPV detection. RF, in particular, has proven effective in remote sensing classification tasks [56,57], distinguishing PV arrays from buildings, vegetation, and other surfaces. More recently, DL approaches such as Convolutional Neural Network (CNN) have significantly advanced automated

DPV detection [58]. When trained on labeled datasets, these models can efficiently identify DPV systems from aerial imagery, reducing manual effort and enabling scalable large-area analysis.

Several studies also estimate DPV capacity using object detection and segmentation models. For example, [59] detects rooftop PV systems from satellite imagery but relies on manual annotations and provides coarse capacity estimates. Similarly, [60], [61], and [62] use CNN-based or U-Net architectures to estimate DPV potential, often relying on empirical coefficients and focusing on city-scale rooftop analysis. Hybrid and data-driven approaches further integrate satellite-derived irradiance and spatial interpolation to improve DPV generation estimates [15]. However, these methods often assume uniform PV characteristics and do not fully capture variability in system size, configuration, and placement.

Many satellite imagery studies focus on regions with dense labels and homogeneous conditions, limiting their generalization to more complex environments. To address this, recent work such as [63] integrates DPV detection and quantification using Generative Adversarial Network (GAN)-based data augmentation, improving performance in low-observability regions by combining satellite data with geographic and meteorological information. Despite these advancements, most existing methods are designed for high-resolution, data-rich environments and do not generalize well to large-scale systems with heterogeneous and partially observable DPV installations.

1.2.1.2 PV Power Generation Identification

Several studies address load disaggregation for DPV power identification using approaches such as online learning, Dynamic Fixed Share, and linear regression models (e.g., [15]). While promising, these methods are constrained by limitations in existing metering infrastructure. For example, although DPV systems above a certain size require metering, the data is typically low-resolution (e.g., 30-minute intervals) and often unavailable for smaller residential systems. This creates limited visibility into the actual impact of PV generation on load profiles. Despite increasing utility interest in real-time inverter monitoring, communication infrastructure requirements remain costly [64], highlighting the need for more accurate and reliable net-load disaggregation

for DPVs identification.

High DPV penetration, particularly behind-the-meter systems, often remains invisible to utilities and operators, making accurate estimation both essential and challenging due to factors such as net metering. A notable approach uses a dual-phase estimation of DPV generation via SVM based on customer load profiles [23], showing potential for improving estimation accuracy. While existing studies on load disaggregation and DPV profiling focus mainly on distribution systems [15,65], transmission-level analysis remains limited, despite its importance for system planning and operation.

Recent studies have introduced various methodologies for estimating the PV generation in a feeder. Among these, model-based techniques are outlined in [66], which focuses on adjusting solar irradiance measurements to account for the orientation of the PV panels. In addition, data-driven techniques are explored in [44, 67, 68], leveraging historical data and machine learning algorithms to enhance estimation accuracy. Furthermore, [69] presents a hybrid approach that integrates both models and data-driven methods, aiming to capitalize on the strengths of each to provide a more comprehensive assessment of DPV generation.

Model-based Techniques

Model-based approaches provide an alternative to data-driven methods for PV power identification, requiring limited calibration data while leveraging system characteristics such as capacity and orientation. These methods are applicable to both estimation and forecasting tasks [70]. For example, [71] combines a clear-sky model with a physical PV model for solar disaggregation using limited net-load data. To reduce dependency on location-specific inputs, [70] proposes an unsupervised framework integrating a physical PV model with a Hidden Markov Regression model, enabling joint estimation of PV generation and load without geographical information.

In distribution systems, [72] introduces an Augmented Complex Kalman Filter (ACKF)-based state estimation framework for feeders with high PV penetration, improving robustness to unobserved PV injections. Traditional model-based approaches also rely on Global Horizontal Irradiance (GHI)-based irradiance conversion to Direct Normal Irradiance (DNI) and Diffuse Horizontal Irradiance (DHI), where conversion and parameter uncertainties (e.g., tilt, azimuth, efficiency) can significantly reduce ac-

curacy [73–75]. Orientation-aware modeling can partially mitigate these errors, achieving notable accuracy improvements [66]. Overall, while physical approaches provide interpretability, they remain dependent on detailed system parameters, weather inputs, and calibration data, limiting scalability in large-scale systems.

Data-driven Techniques

Recent advancements in PV generation identification have increasingly focused on data-driven approaches. In [44], a hybrid method combining k-means clustering and Principal Component Analysis (PCA) is used to identify regions with similar generation patterns and upscale limited measurements to estimate total PV output. The approach relies on historical 15-minute data and updates cluster representations to account for new installations. Similarly, [67] applies clustering with NN models to estimate regional PV generation, showing improved performance when separate models are trained per cluster, although limited by hourly data resolution and lack of adaptation to new installations. In contrast, [68] exploits higher-frequency measurements and spectral similarity between irradiance and net-load signals to perform feeder-level disaggregation, demonstrating effectiveness when detailed temporal data is available.

In [76], net load is decomposed into load and PV components using a virtual equivalent system characterized by estimated parameters such as capacity, tilt, and orientation. This enables both real-time estimation and forecasting of aggregated PV generation. In a similar direction, [77] proposes irradiance-proxy-based regression and optimization-based decomposition methods using active and reactive power measurements, which are further extended in [15] through additional regularization and contextual variables to improve robustness. Game-theoretic and feature-based approaches are explored in [20] and [78], where net-load patterns under different weather conditions are used for PV capacity estimation and disaggregation. Furthermore, [79] introduces a Bayesian structural time-series model to jointly estimate PV generation and load, providing probabilistic outputs but suffering from high computational cost. While these data-driven methods perform well in data-rich settings, they typically depend on high-resolution measurements, detailed customer-level data, or system-specific calibration.

Hybrid Techniques

Based on a hybrid approach, [69] combines satellite-derived GHI estimates with measurements from reference PV systems to estimate generation across geographic regions. The method spatially interpolates discrepancies between measured and satellite-predicted PV output to derive correction factors, which provide more granular PV generation profiles, helping system operators better assess short-term variability and its impact on voltage regulation. Similarly, [80] integrates accurate ground-based measurements with satellite-derived irradiance data from the Heliosat method. Three interpolation techniques are evaluated: nearest neighbor, gravity interpolation, and Kriging, with Kriging achieving the best performance, particularly under low irradiance conditions.

The work in [81] focuses on improving GHI forecasting for solar-rich island grids by combining ground measurements, satellite data, and Numerical Weather Prediction inputs. Several statistical models, including Auto-Regressive (AR), Auto Regressive Moving Average (ARMA), and NN, are evaluated, with neural networks providing the best accuracy when incorporating exogenous data. Likewise, [82] highlights the benefits of integrating satellite and measurement data to improve regional PV power production assessments and forecasting accuracy. However, these methods depend on the availability of reference PV systems, irradiance measurements, and weather data, which limits their applicability in data-scarce environments.

1.2.2 Heat Pump Modeling in Smart Residential Application

Residential Air Source Heat Pumps (ASHP) modeling has become increasingly important due to rapid growth in adoption and its impact on power system operation. Higher HP penetration in residential buildings contributes to rising peak demand, highlighting the need for accurate models that capture thermal dynamics and electrical consumption for grid planning and flexibility assessment [36]. Accurate modeling also enables reliable carbon footprint estimation [31] and supports integration with renewable generation and storage in home energy systems [83]. Modern HP systems can provide heating, cooling, and domestic hot water through a single unit, with improved efficiency and reliability enhancing their residential adoption [84]. The increasing integration of on-site

renewables, particularly PV, further strengthens their role in low-carbon residential energy systems.

Accurate modeling of HP operation is challenging due to its temperature-sensitive and dynamic behavior. Efficiency and power consumption vary throughout heating and cooling seasons as outdoor conditions change [85]. Operation is also influenced by thermal demand, control strategies, and system design, with partial-load conditions playing a key role in seasonal performance. Additional variability arises from building envelope characteristics, thermostat settings, and occupant behavior, contributing to diverse residential load profiles [85–87].

In smart residential applications, accurate HP models are essential for enabling demand response, peak shaving, and load shifting strategies. They also support predictive control frameworks that optimize energy consumption while maintaining occupant comfort [88]. This is particularly relevant in building energy management, where heating, ventilation, and Heating, Ventilation, and Air Conditioning (HVAC) systems account for a large share of residential energy use. Using predictive control methods such as Model Predictive Control (MPC), HP operation can be optimized to leverage thermal storage, reduce peak demand, and lower energy consumption while maintaining comfort under varying weather and occupancy conditions [88, 89].

HP load modeling can be broadly divided into two categories: physics-based and ML-based data-driven models. Physics-based models rely on thermodynamic and heat transfer principles, offering interpretability and suitability for long-term analysis. In contrast, ML-based models capture complex relationships among building, behavioral, and environmental factors to enable accurate load forecasting. These two approaches are reviewed next.

1.2.2.1 Physics-Based HP Modeling

Despite the need for accurate HP models, high-resolution physics-based modeling of individual residential units remains limited. For instance, [90] uses archetype-based and aggregated Coefficient of Performance (COP) modeling without experimental validation or distinction between centralized and room-based systems, while [91] incorporates field data into a semi-theoretical model capturing defrost and cycling losses only for

fixed-speed HPs, which do not consider variable-speed systems. Furthermore, [92] applies a simplified hourly cooling model lacking sufficient resolution for energy management, and [93] proposes a hybrid model using fan coil power as a proxy with 60-minute sampling, but without detailed thermal modeling or system–building interaction.

More detailed TRNSYS-based models provide comprehensive representations of HP behavior [94]. These high-fidelity simulations support evaluation of system performance and control strategies, including Ground-Source Heat Pumps (GSHP) applications that demonstrate improved efficiency through dynamic modeling [95]. Such models also enable the generation of data for control-oriented applications. Physics-based models further capture effects such as temperature-dependent COP variation and compressor cycling constraints, improving physical realism and consistency [96]. As a result, they provide a benchmark for assessing flexibility, peak reduction potential, and system performance under varying conditions.

Despite extensive developments in residential HP modeling, most existing studies do not sufficiently address system-wide, high-resolution representation of HP demand under realistic grid conditions. In particular, the dependence of these methods on detailed system parameters and calibrated inputs restricts their applicability in settings with limited observability.

1.2.2.2 Machine Learning-Based HP Modeling

ML-based models have emerged as effective tools for short-term and high-resolution HP load modeling [97]. They capture complex interactions among weather conditions, building characteristics, occupancy behavior, and system operation that influence HP demand [98]. Compared to physics-based approaches, these models can adapt to temporal variations and improve prediction accuracy without explicit physical calibration, making them suitable for residential load forecasting [99]. However, they require high-resolution data and often lack physical interpretability. Recent advances in ML have further enhanced these methods through architectures such as Artificial Neural Network (ANN), Recurrent Neural Network (RNN), and Long Short-Term Memory (LSTM), which have demonstrated superior performance compared to traditional statistical models in time-series projection tasks [100, 101]. However, despite these devel-

opments, their application to HP systems remains limited and is often restricted to controlled or small-scale datasets. As a result, data-driven HP modeling frameworks that are both scalable and robust under realistic grid conditions remain underdeveloped, particularly in settings with limited or aggregated observability.

1.2.3 Heat Pump Load Disaggregation Techniques for Transmission Systems

The rapid growth of HP installations reflects their increasing penetration in the residential sector, with continued expansion expected. While smart meters provide high-resolution consumption data for improved monitoring, dedicated HP sub-metering remains costly and rarely deployed, limiting accurate tracking of device-level behavior. As a result, reliable estimation of aggregated HP operation under varying conditions remains limited, creating potential operational risks for power systems, especially during winter peak demand.

Researchers in [33] use dynamic simulations in DIgSILENT PowerFactory to study starting currents, voltage variations, and switching transients, highlighting the need for careful planning to manage growing HP penetration. In addition, MPC-based approaches such as [102] propose a plug-and-play framework using only smart thermostat and meter data, enabling nonintrusive HP load modeling through disaggregation and improving scalability while reducing hardware requirements. These methods help enhance grid integration of residential HPs by improving robustness and reducing overfitting. Accordingly, the following subsections examine three key aspects of HP load disaggregation: HP detection and characterization, synthetic data generation, and HP load disaggregation.

1.2.3.1 HP Detection and Characterization

The deployment of HPs is often not directly observable. In this context, smart meters provide a promising opportunity for detection. For example, a hierarchical LSTM-based framework can classify household heating types using smart meter sequences and weather data, distinguishing district heating, exhaust air HPs, and direct

electric heating. Including outdoor weather data further improves performance [103].

Few studies focus on detecting and characterizing HP installations at the distribution level using monitoring data. In Switzerland, data from 397 households combined with weather and geographic information showed that HP usage can be reliably identified, especially when focusing on heating-season data. Restricting analysis to colder months (e.g., November to February) improves accuracy and reduces data requirements [104]. Similarly, a semi-supervised Bayesian approach in [105] uses low-resolution smart meter data to isolate HP activity via sparse signal decomposition, achieving strong performance on EcoGrid EU data. In addition, [31] proposes a monitoring method using 15-minute smart meter data, capturing cycling behavior across 503 ASHP and GSHP and revealing significant differences in operational patterns and efficiency.

To support demand-side management, [106] analyzes hourly load profiles from 139 Danish households with HPs using clustering and regression. Two main consumption patterns are identified, primarily driven by building characteristics such as size, construction year, and heating system type, while socio-economic factors show limited influence except for household composition. These results highlight the combined role of technical and behavioral factors in HP load modeling, which is important for effective demand-side management and grid planning.

Most existing approaches have been developed for household- or community-scale applications and have not been designed for transmission-level analysis of aggregated loads. In addition, there is limited work that links detailed HP behavior modeling with large-scale grid applications such as system-level demand estimation and operational planning. As a result, scalable frameworks capable of translating individual HP dynamics into aggregated demand signals for power system analysis remain largely unexplored.

1.2.3.2 HP Synthetic Data Generation

Accurate HP load modeling captures variability driven by weather, occupancy, and building characteristics, supporting load profiling, demand estimation, and transmission-level disaggregation for grid planning and demand-side management. In this context,

the generation of synthetic HP load profiles is essential for energy system modeling and scenario analysis. For example, [107] applies k-means clustering to water-to-water HP measurements to generate representative synthetic profiles, validated using statistical similarity metrics.

To address limitations in real-world data availability, several studies have proposed synthetic residential load generation methods. These include ANN-based approaches driven by weather data [108], stochastic models incorporating socio-economic and seasonal effects [109, 110], and probabilistic and top-down frameworks for household consumption modeling [111, 112]. More recent work explores data-driven techniques, including ML and GANs, to generate realistic demand and renewable scenarios [113,114].

Overall, most existing methods focus primarily on household-level load modeling and do not explicitly capture aggregated HP demand behavior at larger spatial scales. In particular, scalable synthetic HP generation frameworks that reflect transmission-level diversity and limited observability remain unexplored.

1.2.3.3 HP Load Disaggregation

Assessing HP system-level impact requires high-resolution real-world data that can complement traditional modeling approaches and improve understanding of peak demand and network stress. Recent studies using detailed measurement datasets, such as two-minute interval data from nearly 700 domestic HP installations in the UK, show that aggregated HP demand exhibits distinct daily peak patterns, particularly during winter conditions. However, the impact on ramp rates remains limited, suggesting that HPs mainly affect peak magnitude rather than demand variability [115].

System-level studies further show that large-scale adoption could significantly increase electricity demand, with simulations indicating up to a 60% rise under full HP penetration in Great Britain [116]. Additional analyses suggest that when HP penetration exceeds 20%–30%, distribution networks may face operational challenges [117]. Similar studies in Denmark report 14% increase in peak load compared to other electrification technologies [94]. However, many of these studies rely on proprietary or limited-access datasets, restricting reproducibility and broader validation.

A large-scale demand-response study involving over 300 residential buildings equipped

with HPs uses outdoor temperature measurements to quantify and predict aggregate demand-response potential [118]. However, extending these approaches to multi-household aggregation for transmission-level analysis remains challenging due to increased variability and uncertainty in aggregated HP behavior, as well as the limited availability of transmission-level data despite widespread smart meter deployment [34]. Public datasets such as AMPds [119] provide only single-household measurements, while larger-scale datasets like When2Heat in [120] offer national-level HP profiles and COP values for multiple countries, supporting macro-scale studies but not detailed system-level analysis.

Despite recent progress in HP modeling and load estimation, only a limited number of studies have focused on HP load disaggregation, focusing their applicability on LV distribution-level analysis. Furthermore, many existing approaches rely on high-resolution smart meter data and do not adequately account for seasonal, behavioral, and weather-driven variations under realistic grid operating conditions. These limitations highlight the need for scalable HP modeling frameworks capable of representing aggregated demand under limited data availability, thereby enabling reliable system-level analysis and planning under increasing HP penetration in modern power systems.

1.2.4 Relevant Knowledge Gaps

This literature review reveals the following knowledge gaps in existing studies on PV and HP disaggregation:

- Dependence on PV and HP specific historical data: Many PV and HP disaggregation models rely on large amounts of historical data for each of these individual power sources and loads to train supervised learning algorithms. However, mostly aggregated load data is available to network operators, limiting the scalability and applicability of these models.

- Limited generalizability and integration: Current synthetic PV and HP datasets are often derived from limited brands, technologies, or local conditions, reducing their applicability across diverse regions and system types. Additionally, limited research explores the integration of multiple data sources, such as satellite im-

agery and weather data, which could enhance the accuracy and robustness of PV and HP disaggregation models.

- PV generation disaggregation: There has been limited research focused on the disaggregation of PV power at the transmission level, which is important for utilities to enhance the planning and operation of power grids.

- High-resolution HP modeling: Physical models that accurately capture the thermal–electrical dynamics of residential HPs in the context of the power grid are limited, and the application of advanced ML techniques for HP modeling is still underexplored, resulting in few frameworks that effectively develop physical systems and data-driven HP models for power grid applications. Furthermore, these simulations do not account for stochastic user behavior or dynamic control strategies.

- HP load disaggregation: There has been limited research focused on the disaggregation of HP load demand at the distribution level and no published research at the transmission level, particularly in the absence of smart-meter data, which is important for utilities to accurately estimate HP demand and support grid planning and operation.

- Scalability: Current PV generation and HP load disaggregation methods often struggle to scale effectively across large systems, especially when dealing with diverse voltage levels. Given the increasing penetration of DERs, scalable solutions are needed to support real-time monitoring and decision-making.

1.3 Objectives

The main objectives of this research are presented next, in the context of a collaborative project between the University of Waterloo and the IESO of Ontario, Canada. The primary objective is to develop transmission-level net-load disaggregation methodologies for estimating DPV generation, HP power consumption, and net demand using transmission-level measurements.

1.3.1 PV Power Disaggregation

- Propose an approach to estimate PV capacity based on satellite imagery and image-based DL techniques, using GIS tools for PV panel detection and capacity estimation.
- Develop a generalizable and scalable method for PV disaggregation from net load data designed to function effectively in scenarios where other data sources are unavailable, unreliable, or not properly and timely updated.
- Propose a synthetic data generation technique and multiple ML/DL models to predict PV power generation for net-load disaggregation.
- Apply the developed PV capacity and generation profile estimation techniques to actual transmission feeder-head power measurements to disaggregate PV generation and demand load downstream, considering residential and farm PV installations in the Waterloo region of Ontario.

1.3.2 Modeling and Validation of Heat Pump Loads

- Propose ML-based HP models using indoor temperature, weather, and load data from smart thermostats and smart meter measurements.
- Validate and compare the ML models with respect to a physics-based model, highlighting the benefits and shortcomings of the proposed modeling approach.

1.3.3 Heat Pump Load Disaggregation

- Use a physics-based HP simulation model and real-world measurements to ensure realistic representation of HP load behavior for a comprehensive characterization of HP operational dynamics, including thermodynamic performance, ambient-temperature dependence, cycling behavior, comfort level, and COP variability.
- Propose a flexible and scalable framework for generating aggregated synthetic HP load profiles from a limited dataset to enable the simulation of diverse operating conditions and stochastic temporal variability. This is accomplished through the

use of satellite imagery and ML-based random sampling to identify residential building characteristics within the study region, complemented by accounting for typical occupancy patterns and comfort levels, as well as a probabilistic approach to generate realistic HP load profiles.

- Develop an approach to estimate installed HP capacity based on publicly available data on regional installation rates, housing types, and penetration levels. This is used to scale up the aggregated synthetic HP load profile for the region for which HV/MV data is available.

- Propose an HP load disaggregation framework to extract aggregated HP load profiles from real HV/MV feeder-head measurements based on aggregated synthetic data and DL techniques.

- Demonstrate and verify the proposed overall disaggregation approaches for multiple years based on real data for Milton, Ontario, that do not rely on extensive Advanced Metering Infrastructure (AMI) datasets, showcasing the practical relevance of the proposed framework.

1.4 Content Overview

The rest of this research thesis is structured as follows:

- Chapter 2 provides a comprehensive review of the concepts and background relevant to this study. It begins with key definitions and an overview of PV generation, followed by a discussion of HP systems. The roles of GIS and ML/DL methods for modeling and load disaggregation are also discussed. Finally, the chapter provides an overview of synthetic data generation and stochastic analysis in PV and HP systems.

- Chapter 3 presents the approach developed to identify and disaggregate PV generation from aggregated power measurement at HV/MV substation. It discusses the methodology for detecting DPV panels and estimating their power generation

proposed at the transmission system level. Thus, this chapter proposes an approach for PV power capacity estimation based on GIS techniques for PV panel detection and a method for solar PV generation profile estimation through a simulation approach. The PV power disaggregation techniques that incorporate various ML/DL methodologies are also described in detail. Finally, the results of applying these techniques to actual HV/MV aggregated power data at the Waterloo Region in Ontario, Canada, are presented and discussed.

- Chapter 4 presents an ML-based framework for residential HP modeling based on real measurements and environmental inputs, including a comparative analysis of the proposed data-driven models against a physical model in terms of their ability to capture power and energy usage.

- Chapter 5 presents a methodology for generating and disaggregating residential HP load profiles at the transmission system level. The approach combines publicly available statistics, GIS data, typical house characteristics, physics-based simulations, and ML models to create probabilistic synthetic HP load profiles. An ML framework for load forecasting is also presented, and the practical application of the proposed methodology is demonstrated using actual HV/MV substation data from Milton, Ontario, Canada.

- Chapter 6 concludes the thesis by summarizing the main findings and contributions of the presented research and discusses potential directions for further study of DER load disaggregation in HV/MV transmission and distribution systems.

Chapter 2

Background Review

2.1 Introduction

This chapter outlines the essential foundational concepts, models, and methodologies for the proposed research. Thus, first an overview of DPV generation is presented, focusing on the growing penetration of DPV systems and their impact on grid management, outlining key challenges and strategies for accurate PV generation estimation, particularly in large-scale grids. Then, an overview of the HP system is provided, focusing on describing the operational characteristics of HPs, their energy consumption patterns, and their integration into electrical grids. Next, a brief description of the use of GIS for capacity estimation of PV systems is presented. Similarly, the use of GIS data to analyze the spatial distribution of residential buildings for supporting the estimation of aggregated HP capacity is also described.

A review of ML/DL methods is provided, focusing on their application to forecasting and load disaggregation. The section compares various algorithms used for energy data analysis, forecasting, and disaggregation, emphasizing their potential to improve PV power generation disaggregation and HP load disaggregation. Finally, the application of synthetic data generation and stochastic analysis is discussed to address operational uncertainties and limited real-world measurements, highlighting its potential to improve both PV generation and HP demand profile modeling.

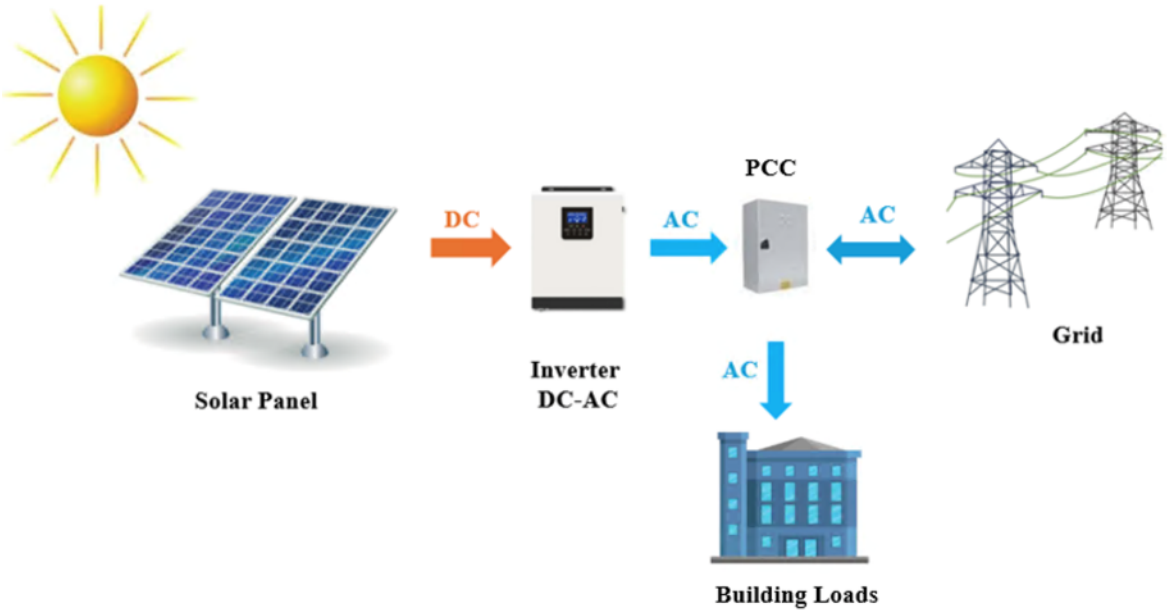

Figure 2.1: DPV generation system.

2.2 Distributed PV Power

DPV generation refers to the process of converting sunlight into electricity using semiconductor materials through the PV effect. This technology can be integrated into the power grid at various levels, including residential, commercial, and utility-scale installations. These systems operate by absorbing sunlight and converting it into Direct Current (DC) electricity, which is then transformed into Alternating Current (AC) using an inverter, allowing it to be injected into the power grid [121]. DPV systems, which include solar panels and associated equipment, are increasingly being integrated into power grids at both the distribution and transmission levels due to their ability to generate clean, renewable energy and operate autonomously or in parallel with other energy sources [122]. Thus, DPV systems are connected at Point of Common Coupling (PCC) to power grids, contributing to the energy mix by injecting power directly into the system when sunlight is available.

PV systems are typically classified into two main categories: utility-scale PV farms

and DPV [123, 124]. Utility-scale systems are large installations that generate electricity on a commercial scale, feeding directly into the distribution or transmission network. On the other hand, DPV, as illustrated in Fig. 2.1, are smaller systems typically installed on rooftops or ground-mounted in residential, industrial, commercial, and farming areas. The use of building surfaces, such as walls or roofs, allows DPV systems to combine power generation with other building functions. This dual-purpose approach increases the overall utility of the infrastructure. Additionally, DPV can be really incorporated with other clean technologies, such as Electric Vehicle (EV) and HP [125].

As non-dispatchable energy sources, DPV systems generate power intermittently, influenced by panel orientation, irradiance, temperature, and other weather conditions and seasonal conditions. This presents challenges for grid operators in ensuring a reliable and continuous energy supply [126], especially in the context of the growing presence of DPV systems, which present challenges for grid operators with respect to managing variability and maintaining a reliable balance between generation and demand [127,128], raising concerns over visibility and control for utilities, as these systems contribute to grid complexity by creating bidirectional power flows and impacting voltage regulation [129].

To address the aforementioned issues, advanced monitoring and control mechanisms are needed to ensure optimal grid performance. These include sophisticated forecasting methods and energy storage solutions designed to enhance the reliability of DPV power by managing and mitigating its fluctuations [130]. However, solar energy's intermittent nature makes it difficult to consistently predict power output, complicating grid integration [131].

2.3 Heat Pump Demand

HP systems are energy-efficient alternatives to traditional heating and cooling systems. HP systems can be divided into two primary categories: ASHP [132], and GSHP [133]. Air-source systems transfer heat between indoor air and the outside atmosphere, while ground-source systems transfer heat to or from the ground to benefit from more stable underground temperatures. The difference between these systems allows for tailored

applications depending on geographic location and specific climate conditions. ASHP are generally more common in moderate climates, while GSHP systems offer enhanced efficiency in regions with significant temperature fluctuations. This flexibility in design contributes to the broader adoption of HP technology across diverse building types and geographic locations [134, 135].

Operating on the principles of thermodynamics, HPs can significantly reduce energy consumption by utilizing electricity primarily for moving heat rather than generating it directly [136]. The versatility of HP allows them to be integrated into various applications, including residential, commercial, and industrial settings. An HP system can function in coordination with DERs and Energy Storage Systems (ESSs) to optimize energy efficiency and manage thermal loads effectively [137].

The performance of HP can be impacted by external factors such as ambient temperature, building insulation, and system efficiency, which vary across different installations. One of the significant challenges HP systems face is the variability in power demand, particularly in residential or commercial buildings with fluctuating occupancy and external temperature changes [138]. As a result, the integration of predictive algorithms and demand-response mechanisms is critical to ensure that the system operates efficiently [139]. These algorithms allow the system to anticipate changes in heating or cooling demand, disaggregating power consumption patterns for more precise power use forecasting. For instance, a building with a HP system could reduce power usage during periods of low occupancy by automatically adjusting set temperatures, thereby improving overall energy management [140].

HP can operate in two primary modes, namely heating or cooling, depending on the seasonal demand and configuration [141]. Fig. 2.2 illustrates the basic working principle of a HP system used for heating and cooling purposes. The system consists of the following four key components: the evaporator, compressor, condenser, and expansion valve. These components are connected in a closed-loop system that transfers heat between the inside and outside environments. In heating mode, the HP extracts heat from the outdoor air (or ground, depending on the type) and transfers it inside the building. The refrigerant inside the system absorbs heat in the evaporator, where it evaporates into a gas. The refrigerant is then compressed in the compressor, increasing its temperature. The heated refrigerant flows into the condenser, where it releases heat

into the indoor environment, warming the space. The refrigerant cools down and is expanded through the expansion valve, returning to its low-pressure, low-temperature state, and the cycle repeats. In cooling mode, the HP works in reverse, absorbing heat from inside the building and releasing it outdoors, cooling the indoor environment.

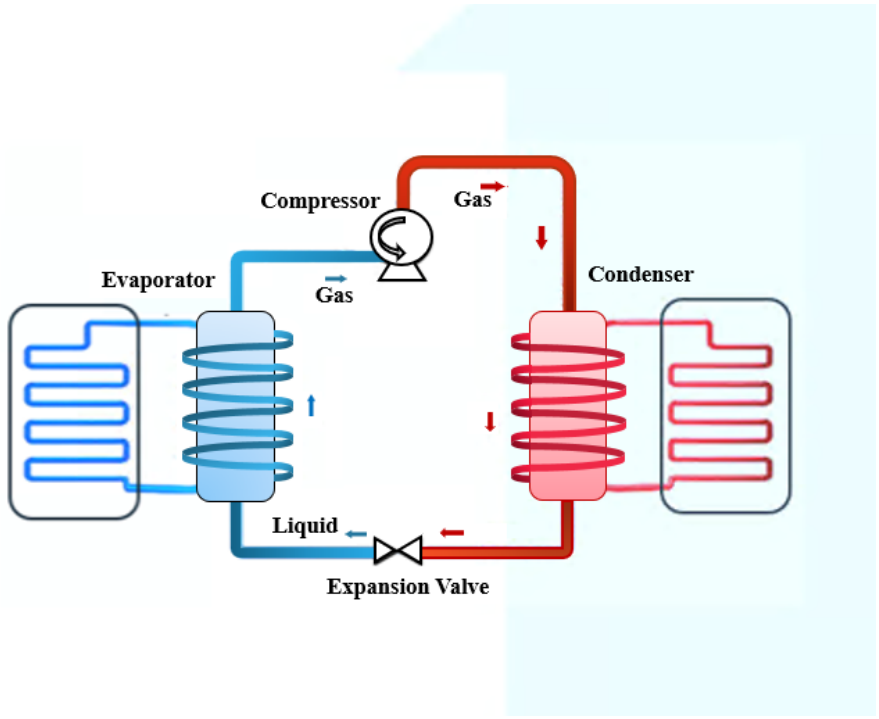

Figure 2.2: HP operation [141].

A key component within HP systems is the compressor, which plays a central role in the refrigeration cycle by pressurizing the refrigerant to raise its temperature. Advanced compressor technologies, such as variable-speed compressors, have been developed to improve the efficiency and flexibility of HPs [142]. Unlike traditional fixed-speed compressors that operate at a constant speed, variable-speed compressors can adjust their speed based on the heating or cooling demand, allowing for more precise temperature control and reduced energy consumption. Variable-speed compressors modulate the refrigerant flow rate, which enables HPs to operate efficiently across a range of temperatures and load conditions, enhancing comfort while minimizing power

usage. From an electrical system perspective, integrating variable-speed compressors allows for managing inrush currents and ensures compatibility with inverter-driven motors. These compressors can be part of ASHP and GSHP, where they contribute to the improved performance and adaptability of the system, particularly in fluctuating climates. By allowing the HP to operate more closely to optimal conditions, variable-speed compressor systems reduce wear and tear, extend the life of the equipment, and improve overall system efficiency.

From a control perspective, HP systems typically incorporate multiple control layers to manage energy transfer efficiently [143]. The primary control layer ensures that the HP reacts to local temperature demands and operates within safe limits. The secondary control level, often managed by a building's Energy Management System (EMS), optimizes the operational schedule of the HP in conjunction with other Heating, Ventilation, and HVAC systems, renewable energy sources, and energy storage units [144]. This control hierarchy helps balance energy demand and supply, ensuring the efficient use of resources [145].

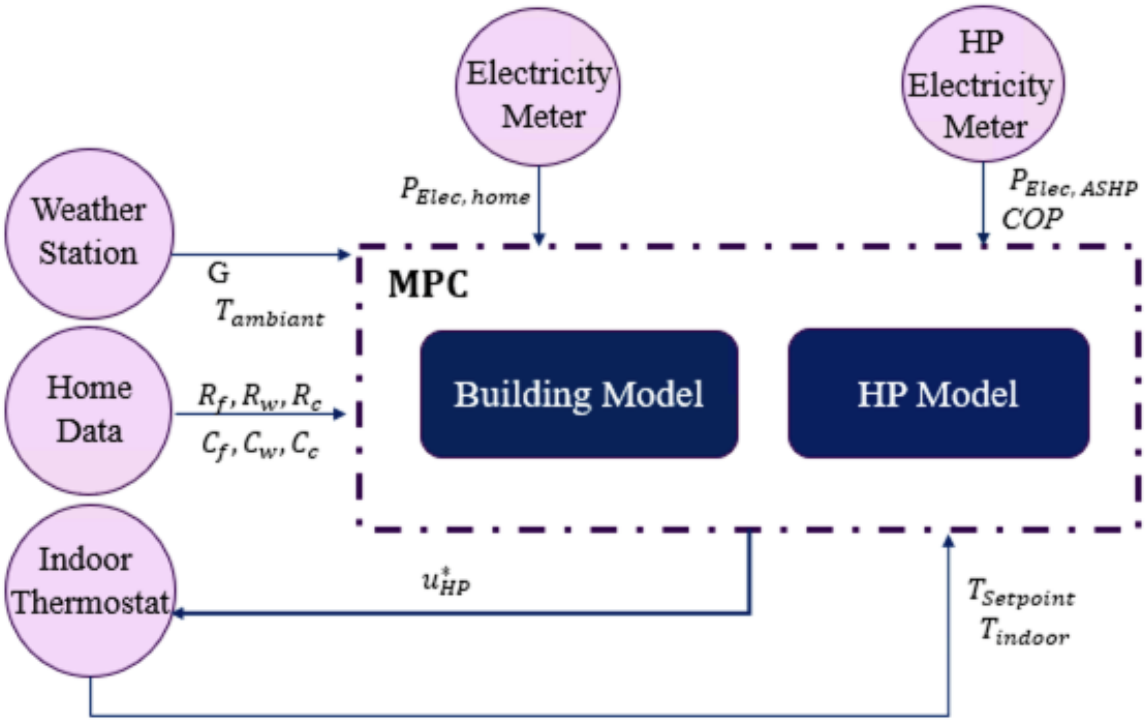

Figure 2.3: Simplified HP control model.

HPs display distinct operational patterns with alternating periods of activity and inactivity, driven by thermostat-based control, variable-speed technologies, and energy-saving strategies [31, 146]. The short-term load variations arise from cycling, defrost events, and user-defined schedules, resulting in temporal dependencies that shape the evolving demand profile. A simplified representation of the MPC-based control behavior for an HP system is illustrated in Fig. 2.3. In this framework, weather data, building characteristics, and indoor thermostat setpoints are used as inputs to the building and HP model. The controller processes temperature signals from both the home and the heat pump, and computes an optimal control action to ensure indoor comfort while improving energy efficiency. The interaction between temperature thresholds and system response governs the on/off operation of the HP.

In [147,148], HP performance is shown to be governed by thermodynamic principles, where the COP varies with indoor and outdoor temperatures, setpoints, and heating

schedules, directly affecting electricity consumption. Lower ambient temperatures increase heating demand, leading to more frequent cycling of the system [102, 149]. To represent HP operational behavior, physics-based models are commonly used; however, real systems exhibit transient dynamics that deviate from steady-state assumptions. In particular, HPs experience warm-up periods and control delays between thermostat signals and system response, introducing temporal variability in power demand. Overall, real-world operation often differs from manufacturer-based or steady-state models due to dynamic thermal behavior, control latency, building characteristics, and occupant-driven effects.

2.4 Geographical Information Systems Overview

GIS are powerful tools for generating, organizing, analyzing, and visualizing diverse datasets [150], playing a transformative role in spatial analysis and data visualization and enabling users to map and examine relationships within data, ultimately supporting more informed decision-making. A significant benefit of GIS lies in its capability to merge diverse datasets, including raster data from satellite imagery and vector data depicting geographic features and locations, layering them onto a map to offer a comprehensive perspective. This approach is important for informed decision-making across various fields such as environmental management, urban planning, and resource optimization [151–153]. GIS's power to analyze intricate patterns that are often hidden from conventional data representations is key to recognizing trends, evaluating risks, and forecasting outcomes, establishing its value as an essential tool for both researchers and industry professionals.

In the realm of renewable energy, GIS has become increasingly important for optimizing energy resource management, particularly in locating ideal sites for new installations. By providing geographical and environmental data, GIS tools can help identify the most suitable locations for solar farms, wind turbines, and other renewable energy projects [154,155]. Factors such as solar irradiance, wind speed, land slope, and proximity to existing infrastructure are integrated into GIS-based models to predict the viability and efficiency of renewable energy sites. This data-driven approach not only helps in maximizing energy production but also reduces costs and minimizes

environmental impacts by selecting locations that require less land modification and have minimal ecological disruption [156].

While satellite imagery and GIS have proven essential for analyzing and mapping various earth surface features, there remains a critical need for further advancements in automated detection and classification techniques. These tools have been invaluable in applications such as identifying solar DPV panels on rooftops using image-based ML/DL models [27]. Challenges persist due to environmental factors like cloud cover, seasonal variations, and fluctuations in image quality. The diversity of building architectures, differences in panel orientation, and varying installation conditions add complexity to accurate detection. Advancements in multi-temporal and multi-source data integration, such as combining satellite imagery with other data streams like LiDAR or in-situ measurements, are needed to enhance the robustness and reliability of detection models.

GIS datasets also provide detailed spatial information about building locations, land-use classification, and residential density, which can support the identification and sampling of representative households. By combining these spatial attributes with ML techniques, residential buildings can be selected while preserving some of the statistical characteristics of the study area. This approach enables scalable analysis when detailed household-level data are unavailable and helps construct representative samples for load modeling and energy demand studies [157].

2.5 Machine Learning/Deep Learning Techniques

ML and DL have revolutionized data-driven approaches across various fields by allowing systems to learn patterns, make predictions, and improve decision-making processes. ML algorithms, ranging from supervised to unsupervised and reinforcement learning techniques, are designed to identify patterns in datasets and create predictive models based on these patterns [158]. DL utilizes ANNs with multiple layers to handle large volumes of data and complex structures, enabling it to learn and generalize information effectively. The rise of DL has enabled significant advancements in areas where conventional ML techniques often struggle to manage data complexity and nonlinearity [159].

ML can be applied to different types of data depending on their structure and infor-

mation content. Time-series data are typically used for modeling temporal dynamics in applications such as energy forecasting and load estimation, where sequential models capture dependencies over time. Image-based data provide spatial information and are commonly processed using CNN for feature extraction and pattern recognition. Structured or tabular data, such as weather and system measurements, are often analyzed using classical ML methods to model nonlinear relationships between variables. In many applications, these data sources are combined to improve model performance by leveraging complementary temporal, spatial, and contextual information [160].

Data preprocessing is a critical step in ML, particularly for applications involving image and time-series data. For image data, preprocessing typically includes resizing, normalization, noise reduction, and augmentation techniques to improve model robustness and ensure consistent input dimensions. For time-series data, preprocessing involves handling missing values, smoothing noise, resampling to uniform time intervals, and normalization or scaling to stabilize training. In both cases, careful preprocessing improves feature quality, accelerates convergence, and enhances overall model performance [160].

Developing effective ML models requires careful feature engineering and appropriate model selection for both image and time-series data. For image data, feature engineering often relies on pretrained representations or features extracted using CNN, while for time-series data, it includes lag features, rolling statistics, and other temporal transformations to capture dependencies. Model selection depends on the data structure, where CNN-based models are typically used for spatial data, and models such as RNN, LSTM, or Transformer-based architectures are used for sequential data. Choosing an appropriate architecture is vital to effectively capture underlying patterns and ensure accurate predictions.

2.5.1 Model Development

ML and DL models typically involve three phases: training, validation, and testing. During the training phase, the model learns patterns and relationships from the dataset by adjusting its internal parameters to minimize prediction errors. The validation phase helps fine-tune the model by evaluating its performance on unseen data and adjusting

hyperparameters to prevent overfitting. Finally, the testing phase assesses the model's generalization capabilities on entirely separate data, ensuring its reliability in real-world scenarios. These processes rely on essential components such as feature selection, preprocessing, and model optimization to ensure accuracy and robustness [160].

Effective performance of ML models for both image and time-series applications requires careful hyperparameter tuning. In image-based models, key hyperparameters include learning rate, batch size, number of convolutional layers, kernel size, and dropout rate, all of which influence feature extraction and generalization performance. In time-series models, such as LSTM and other recurrent architectures, important hyperparameters include sequence length, number of hidden units, number of layers, learning rate, and batch size, which affect the model's ability to capture temporal dependencies [160].

The learning process in ANN is achieved through backpropagation, a method that iteratively adjusts weights to minimize the error between the predicted output and the actual output. This is done by calculating a loss function and propagating the error backward through the network using optimization algorithms like Stochastic Gradient Descent (SGD). ANN excels at capturing non-linear relationships in data and can handle a variety of tasks, from image recognition and natural language processing to time-series forecasting. The flexibility and scalability of ANN make them particularly effective in DL applications, where architectures like CNN and RNN are used to analyze spatial and temporal data, respectively [160].

2.5.2 Forecasting

Forecasting is the process of predicting future values or trends based on historical data and patterns. It is widely used across industries for applications such as energy demand prediction, market analysis, and weather forecasting. Forecasting techniques can be broadly categorized into statistical methods and ML approaches. Statistical methods, such as Auto Regressive Integrated Moving Average (ARIMA) and exponential smoothing, rely on mathematical models to capture trends and seasonality in time-series data. ML techniques, such as RF, SVM, and Gradient Boosting (GB), use data-driven approaches to identify complex patterns and nonlinear relationships in the

data. DL methods, including LSTM and CNN, have gained popularity for their ability to handle large datasets and capture temporal and spatial dependencies effectively. Bidirectional Long Short-Term Memory (BiLSTM) networks enhance the model's ability to capture both past and future dependencies in time-series data, further improving the accuracy of PV and HP disaggregation by leveraging contextual information from both directions [161].

Recent advancements in ML, including SVM, RF, and ensemble learning techniques, have shown promise in capturing the nonlinearities inherent in power forecasting and disaggregation tasks [162]. For DPV and HP disaggregation specifically, DL approaches such as LSTM networks and CNN have proven effective in handling the temporal and spatial dependencies of power data. LSTM, due to its ability to manage long-term dependencies, is especially suited for time-series forecasting, making it a powerful tool for predicting DPV generation and HP consumption based on weather data and historical load profiles [162, 163]. Similarly, CNN has been applied to analyze spatial features in power data, improving the accuracy of disaggregating power generation and consumption patterns of PV and HP from overall electricity usage in transmission networks [164].

2.5.3 Image Processing

In addition to time-series analysis, computer vision techniques have become increasingly important for extracting information from satellite and aerial imagery. Image processing workflows commonly employ tools such as the OpenCV library for preprocessing, feature extraction, and image enhancement [165]. Advanced DL models, including Mask R-CNN, enable pixel-level object detection and segmentation, facilitating the identification and quantification of rooftop DPV installations. The spatial information extracted from these methods can be integrated with electrical and other complementary data sources to improve accuracy in applications such as DPV capacity estimation, power generation forecasting, and distributed energy resource modeling [166].

Popular tools like TensorFlow, PyTorch, and Scikit-learn are often utilized to build and implement image processing models, providing efficient frameworks for managing

datasets, designing architectures, and performing computations. Additionally, hardware accelerators such as GPUs and TPUs are important for expediting the training of deep learning models, particularly those with complex architectures like CNN and LSTM, which require intensive computation.

2.6 Stochastic Analysis

Stochastic analysis is an essential tool for studying complex energy systems, particularly for capturing the variability of renewable generation and load demand [167]. It enables time-series data to be represented through statistical models, allowing the generation of multiple realistic scenarios for probabilistic evaluation. This approach supports the assessment of system performance, operational flexibility, and risk under diverse conditions, providing a structured framework for uncertainty quantification and decision-making in dynamic environments.

In the context of DPV and HP systems, load uncertainty represents the combined effect of temporal variability and the inherent lack of precise knowledge about demand and generation at each time instant. While variability is captured through the temporal resolution and sampling cadence of load data, uncertainty is influenced by the number and representativeness of samples available at each time step. In general, higher temporal resolution and a larger sample size improve the ability to capture diurnal and seasonal patterns as well as detail load behavior. For applications involving DPV and HP, consistent sampling between load, generation, and net-load data is essential to ensure meaningful comparison and analysis [65].

Load uncertainty in DPV and HP systems arises from the stochastic nature of customer demand and the limited availability of representative measurements. When the available historical data is limited, stochastic expansion techniques are applied to generate an extended set of load profiles by resampling from the observed data and representing them through interval-based non-parametric probability distributions. This allows the preservation of temporal variability and correlation while accounting for diversity across different customer behaviors. The resulting expanded dataset provides a more comprehensive representation of possible load conditions, which is essential for accurately modeling system behavior under uncertainty in PV and HP applications [65].

2.7 Synthetic Data

Synthetic data generation and stochastic analysis are widely used in energy system studies to address data limitations and uncertainty. Synthetic data methods create artificial datasets that preserve the statistical characteristics and variability of real measurements, enabling the exploration of diverse operating conditions. In parallel, stochastic analysis represents uncertainty in renewable generation and load demand using probabilistic models, allowing scenario generation for system evaluation and risk assessment [167–169]. Together, these approaches provide a structured framework for uncertainty quantification and support robust analysis and model validation in complex energy systems.

Time-series synthetic data generation focuses on producing sequential datasets that replicate the temporal behavior of system variables, with synthetic load profiles typically generated by varying physical and operational parameters to capture realistic demand patterns influenced by weather and user behavior [170]. Examples of synthetic data applications in power systems span both large- and small-scale systems. At the transmission level, synthetic grid models preserve power flow feasibility across realistic system footprints [171, 172]. At smaller scales, synthetic datasets are commonly used to model residential consumption patterns and renewable generation, providing representative profiles for households and local energy resources. Overall, most research on synthetic load profile generation has focused on household-level electricity demand due to the need for high-resolution and realistic datasets for modeling, forecasting, and evaluation of distributed energy systems [111].

Various methods have been proposed for synthetic load data generation, including physics-based, data-driven (e.g., ML and GANs), clustering-based, and hybrid approaches [107, 111, 113, 114, 173]. Physics-based methods rely on system modeling, while data-driven approaches learn patterns from historical data to generate realistic profiles. The quality of synthetic load data is typically evaluated using metrics such as load factors, load duration curves, and correlation measures to assess temporal behavior, variability, and statistical similarity with real data [170].

2.7.1 Synthetic PV Generation Profiles

Synthetic data generation for PV systems involves creating artificial but realistic time-series data, such as irradiance, temperature, and power output, to complement limited real-world measurements. It is widely used to represent solar variability in power system studies, particularly when high-resolution measurements are unavailable. Methods have been developed to generate high-resolution PV profiles from low-frequency data, including satellite-derived irradiance, while preserving key variability characteristics [174]. These approaches also enable spatially diverse profiles across different interconnection points, improving the representation of DPV effects and reducing errors in grid impact assessment [175].

With the rapid growth of global PV capacity, accurate estimation of PV generation has become increasingly important due to the complex interactions between system components, environmental conditions, and operational factors that are not fully captured by purely physical models [176]. Consequently, high-quality synthetic PV datasets are important for applications such as load disaggregation, enabling more reliable assessment, monitoring, and optimization of PV system performance under diverse operating conditions.

Synthetic PV generation data can be produced using three main approaches: physics-based modeling, statistical modeling, and data-driven techniques. Physics-based models rely on first-principles equations to simulate PV system behavior based on environmental inputs and system configurations [177], while data-driven methods, including statistical and ML techniques, generate synthetic profiles by learning patterns from historical data [178, 179].

Physics-based models simulate PV power output using mathematical formulations that incorporate irradiance, temperature, wind speed, and system characteristics such as module type, orientation, and shading. Widely used tools, such as PVsyst [180] and System Advisor Model (SAM) [181], implement these models to produce time-series power generation under different weather and operational conditions. These models provide physically consistent predictions and are especially useful for detailed assessments at the system or plant level [180, 181].

Statistical or stochastic methods create synthetic PV data by reproducing the prob-

abilistic characteristics of historical measurements. Techniques such as Markov processes [178], bootstrapping [182], or Gaussian Copulas [183] can generate daily or hourly irradiance and temperature profiles that preserve the statistical distribution and variability of observed data.

ML approaches leverage deep generative models to produce realistic PV time series that closely resemble measured data. GANs have been widely used to generate high-resolution PV power profiles by learning the underlying distribution of historical observations and replicating their temporal variability [179]. In parallel, variational autoencoders provide a probabilistic framework for learning latent representations of PV data, enabling the generation of diverse synthetic samples that preserve key statistical characteristics of the original dataset [179]. Clustering-based approaches, such as k-means, have also been widely used to construct representative load profiles by grouping similar consumption patterns and generating synthetic samples from these clusters [107]. These data-driven approaches are particularly effective in capturing complex, nonlinear relationships between environmental variables and PV output, thereby enhancing the realism and applicability of synthetic datasets for grid simulation and solar energy analysis.

Despite the robustness of synthetic data generation models, uncertainties in PV power predictions may arise from modeling errors, inaccurate input conditions, and environmental factors such as temperature and solar spectral distribution [184, 185]. Moreover, numerical weather prediction and Artificial Intelligence (AI)-based weather models used as inputs can introduce additional discrepancies due to spatial and temporal resolution limitations, as well as data assimilation challenges [186–189]. While standard numerical models typically account for factors such as shading, tilt angle, and soiling, less-explored variables, humidity and wind speed, should be considered, since these also influence DPV system performance [190–192]. Several studies have explored advanced and hybrid modeling approaches, such as combining PVlib with spectral correction models, to better align simulated PV generation with real-world observations [193, 194].

Validation of synthetic DPV data is a critical step to ensure that the generated profiles accurately reflect real-world behavior and can be reliably used in energy system studies. A common approach involves assessing statistical similarity by comparing key

properties of real and synthetic datasets, such as probability density functions (pdf), cumulative distribution functions (cdf), and autocorrelation structures, to verify that temporal variability and distributional characteristics are preserved [181,182]. In some studies, quantitative performance metrics, including Kullback–Leibler divergence and Hellinger distance, are used to measure the similarity between probability distributions and evaluate the fidelity of generated data [195,196]. Together, these validation strategies provide a comprehensive framework for assessing the quality, reliability, and practical applicability of synthetic DPV datasets.

2.7.2 Synthetic Heat Pump Load Profiles

HP power consumption is influenced by a wide range of factors, including COP, compressor speed, comfort settings, control delays, system location, HP type and capacity, as well as building characteristics such as insulation and thermal properties [197]. In addition, environmental conditions, including ambient and indoor temperatures and humidity, play a significant role in shaping the operational behavior of HPs [198]. Considering these factors, synthetic data generation must incorporate both physical dependencies and stochastic variations to accurately reflect real-world operating conditions and capture the key drivers of HP demand.

Synthetic HP load profiles can be generated by systematically varying the physical and operational parameters of different HP models, enabling the representation of diverse operating conditions. These profiles can be developed using either simulation-based approaches [94], which rely on physics-informed models, or data-driven and ML models [199] that learn patterns from historical data. Regardless of the approach, synthetic datasets often reproduce characteristic temporal behaviors of HP demand, including two distinct daily peaks: a higher peak in the morning (6:00–9:00), and a slightly lower peak in the evening (16:00–21:00), reflecting typical occupancy patterns and heating requirements [31].

Simulation-based approaches are widely used to generate synthetic HP demand data, particularly when detailed physical representation of system behavior is required. Tools such as TRNSYS are commonly applied for modeling HP performance at the building level, providing high-resolution insights into thermal dynamics and energy

consumption, although their application becomes less practical for large-scale residential populations due to computational complexity [94]. To address this limitation, simulation frameworks can be extended to include multiple unit types and building configurations, enabling probabilistic scenario analysis across diverse HP systems. In cases where empirical data are scarce, synthetic profiles can be generated by combining a single validated HP dataset from a case study with typical meteorological year weather data. This physics-informed modeling approach allows the creation of diverse and realistic load scenarios, while baseline assumptions for HP behavior are derived from existing literature to ensure consistency and reliability.

Data-driven and ML approaches provide an alternative method for generating synthetic HP load profiles by leveraging patterns extracted from historical data [199]. One common methodology involves the use of clustering techniques, such as the k-means algorithm, to group similar HP load profiles into representative clusters. Based on an underlying dataset, k clusters are identified along with their associated load patterns, capturing typical consumption behaviors. To generate synthetic profiles for a target region, daily temperature profiles are mapped to the most relevant clusters, and for each day, a HP load profile is randomly sampled from the corresponding cluster set [107]. This approach enables the generation of realistic and diverse demand profiles while preserving the statistical characteristics and variability observed in real-world data.

Synthetic HP load profiles have a wide range of applications across energy system analysis and optimization. In grid simulation studies, they are used to assess the impact of high HP penetration on LV network demand, helping to identify potential constraints and infrastructure requirements [200]. In energy management, synthetic data enables the testing and validation of control strategies, such as HP with thermal ESSs, to support load shifting and demand-side flexibility [201]. At the building level, these profiles are useful for evaluating the performance and efficiency of different HP types under varying weather and operating conditions [202]. Additionally, synthetic HP data can play an important role in load disaggregation tasks, where it supports the identification and separation of HP consumption from aggregated demand signals. Overall, these applications highlight the importance of synthetic data as a versatile tool for analysis, optimization, and decision-making in modern energy systems.

2.8 Summary

This chapter provided a comprehensive overview of the key background topics supporting the proposed research. It first discussed DPV generation, covering its fundamental principles, technologies, and the increasing integration of DPV systems into modern power grids. It then reviewed HP systems, emphasizing their role in energy-efficient heating and cooling, their characterization and control behavior, and their interaction with renewable energy sources. The chapter also examined the use of GIS in power system analysis, highlighting its applications in monitoring, visualization, and spatial analysis, particularly for DPV detection and building characterization in HP-related studies. Furthermore, an overview of ML and DL was presented, focusing on data preparation, model selection, and their application to time-series and image-based data for forecasting, detection, and disaggregation tasks in DPV and HP systems. Finally, stochastic analysis and synthetic data approaches were discussed, along with their associated challenges, for adequately estimating PV generation and HP load profiles.

Chapter 3

Disaggregation of PV Generation at the Transmission System Level

Nomenclature

Indices

ω	Scenarios
H	Hours
s	RES type
Y	Years

Parameters

α	Power output temperature coefficient for solar panels [pu/°C]
τ	Temperature of the photovoltaic cell [°C]
$\tau_{\mathbf{std}}$	Temperature of the solar cell under standard testing conditions [°C]
φ	Performance reduction factor of solar panels [pu]
$\widehat{L}$	Estimated natural active power consumption [MW]

$\widehat{PV}$	Estimated PV power generation [MW]
$G_{\mathbf{std}}$	Solar irradiance at standard conditions [kW/m^2]
$G_{Y,H}$	Global solar irradiance [kW/m^2]
$I_{Y,H}$	Total installed capacity of solar panels [kW]
m	Test dataset size
N	Net load profile [MW]
n	Training dataset size

Variables/Functions

σ	Sigmoid activation function [pu]
b	Biases [pu]
C	Confidence scores for test [pu]
c_t	Cell state [pu]
F, g	Activation functions [pu]
f_t	Forget gate [pu]
h_t	Hidden state [pu]
i_t	Input gate [pu]
o_t	Output gate [pu]
P_s	Power produced by photovoltaic panels [kW]
r_i	Confidence scores for training [pu]
s_j	Confidence scores for test [pu]

t	Time step [pu]
W	Random weights [pu]
x	Input state [pu]
y	Output state [pu]

3.1 Introduction

In systems with numerous unmonitored PV installations spread along a feeder, as illustrated in Fig. 3.1, disaggregating PV power is especially beneficial for system operators. Therefore, this chapter introduces a novel approach for disaggregating PV generation from net-load measurements recorded at the transmission system level. The proposed technique is applied to actual data from an existing transmission line feeder to identify PV generation from net demand measurements. The developed methodology incorporates GIS for detecting PV panels based on an algorithm that provides an accurate estimate of solar PV capacity. These estimations are validated against actual data from a local utility, showing a close match between the two. This information is then utilized in reliable software tools to simulate PV power generation in the studied region, which is then used to estimate and disaggregate the generated power from net-load data by applying multiple ML and DL models.

The proposed techniques are applied to obtain aggregated DPV generation from net load data provided by the IESO for the Waterloo region in Ontario. The results demonstrate that, with the proposed approach, it is feasible to adequately disaggregate PV power generation from transmission feeder net-load measurements with minimal or no additional sensor infrastructure.

3.2 General Approach

Feeder PV-load disaggregation at HV/MV substations involves separating the total solar PV generation in the feeder from the overall active power net-load measurements

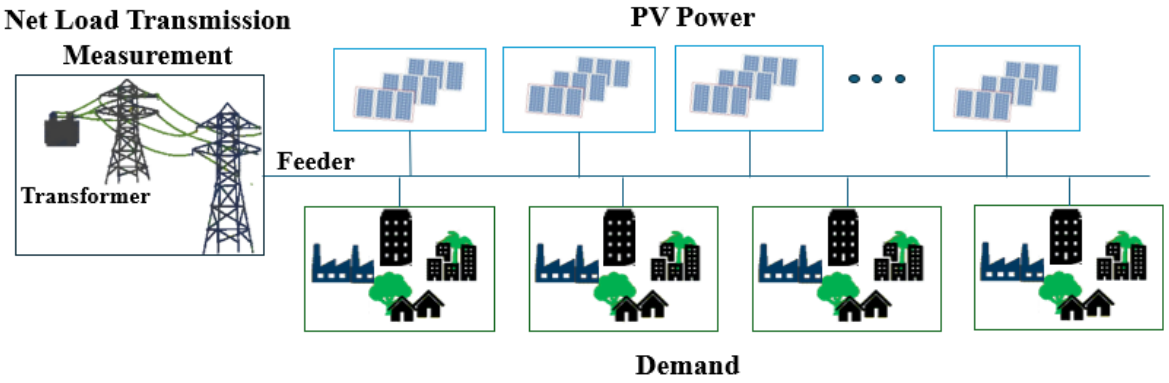

Figure 3.1: PV generation identification at the transmission system level from net-load measurements in power grid feeders.

at the HV/MV substation. This methodology utilizes historical transmission-level data of net-load power measurements, along with accessible meteorological data, to assess PV generation from installed PV capacity estimates through the disaggregation of load profiles and solar power generation data.

At the transmission system level, there is typically no data available providing information on PV installed capacity below certain thresholds (e.g., 5 MW in Ontario, Canada [203]), with small PV panels dispersed across a wide service area associated with an HV/MV substation, featuring diverse configurations such as tilt angles and azimuths. To address this issue, estimates are needed of the PV capacity connected to the transmission system substation transformers in the region of interest, as illustrated, for example, in Fig. 3.2. This can be accomplished, as mentioned in Chapter 2, using GIS and image DL-based techniques to detect and quantify the number of PV panels, allowing for an assessment of the overall capacity of micro-generation PV systems integrated into the distribution network serviced by HV/MV substations.

To estimate the PV generation based on the estimated installed PV capacity, synthetic PV power profiles can be generated using simulation methods as discussed in chapter 2. Despite variations in the tilt angles and orientation of the PV panels, these generally align with the region's latitude to maximize energy harvest [49]. Therefore, a virtual equivalent PV station can be assumed to estimate the aggregate output of all solar PV installations connected to the transmission system substation, based on the

total estimated PV panel capacity and an assumed tilt angle and orientation, along with irradiation and weather data. This allows obtaining an aggregated PV output profile using an existing simulation tool. Based on this synthetic PV profile, supervised ML/DL models can be applied to disaggregate demand and PV profiles from net-load metered data

The overall proposed procedure is depicted in Fig. 3.3, which is divided into the following four main phases, explained in detail in the following section:

1. Estimation of the equivalent PV capacity and other relevant parameters based on GIS and simulation tools to produce synthetic PV generation aggregated profiles for forecasting purposes.

2. Gathering relevant data and performing a correlation analysis to determine pertinent features for PV generation forecasting.

3. Forecasting of aggregated PV generation based on synthetic PV output profiles and identified relevant features

4. Disaggregation of net-load power measurements to estimate PV power generation and load demand.

3.3 Solar PV Output Estimation

To estimate the PV generation capacity within the transmission system of a region, satellite imagery combined with sophisticated DL techniques can be used, as previously mentioned. Thus, image segmentation can be employed to precisely identify and delineate objects within an image. This process includes state-of-the-art object recognition techniques for locating and classifying objects with bounding boxes and semantic segmentation for pixel-level categorization [160, 204], which is particularly effective for detecting PV panels. Various segmentation models are available, each optimized for different types of imagery, study objectives, and data availability. Hence, a mapping approach is used here that leverages pre-trained Deep Neural Network (DNN) for object detection, with human annotations for validation to ensure accuracy.

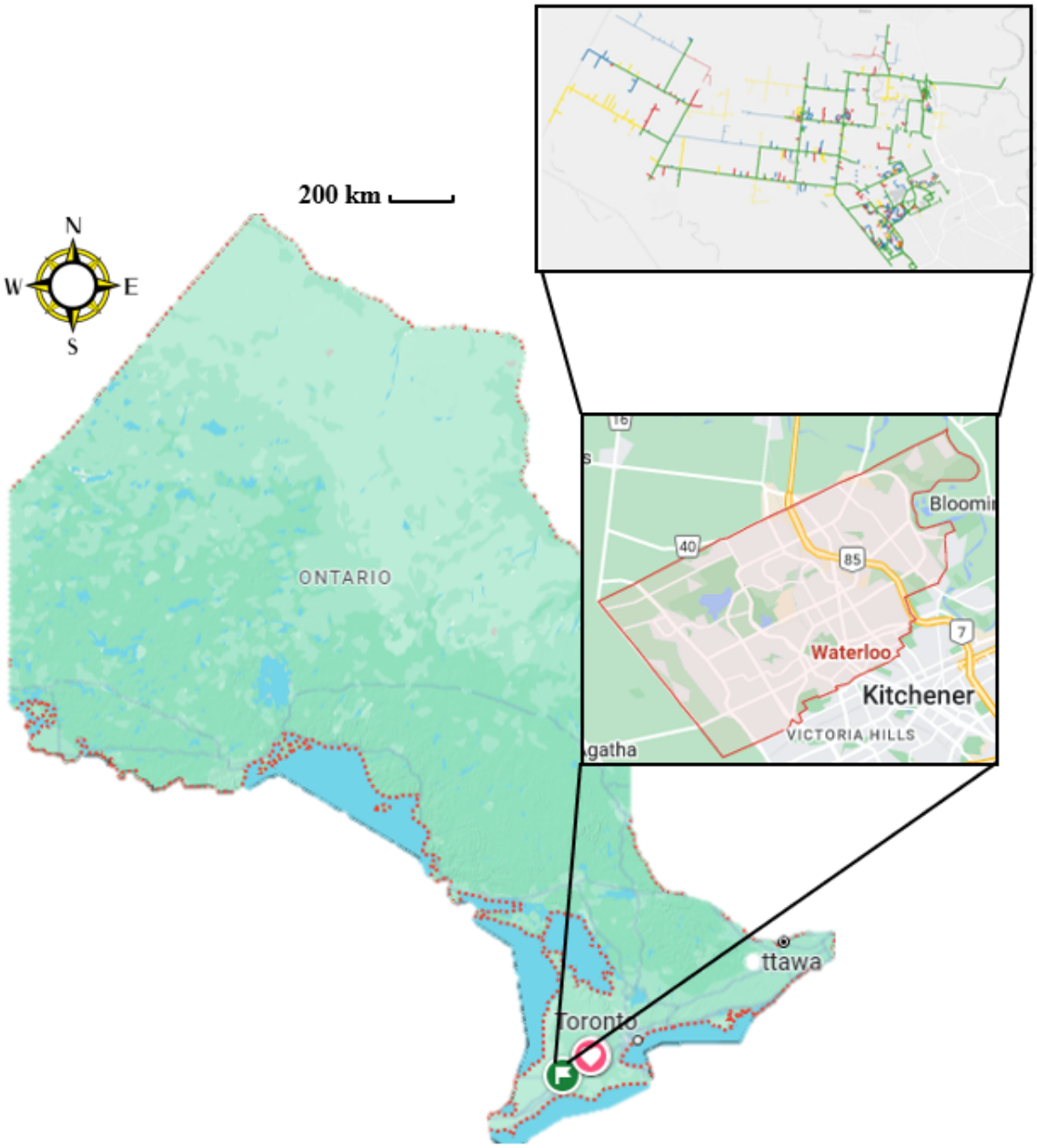

Figure 3.2: Waterloo region in Ontario, Canada.

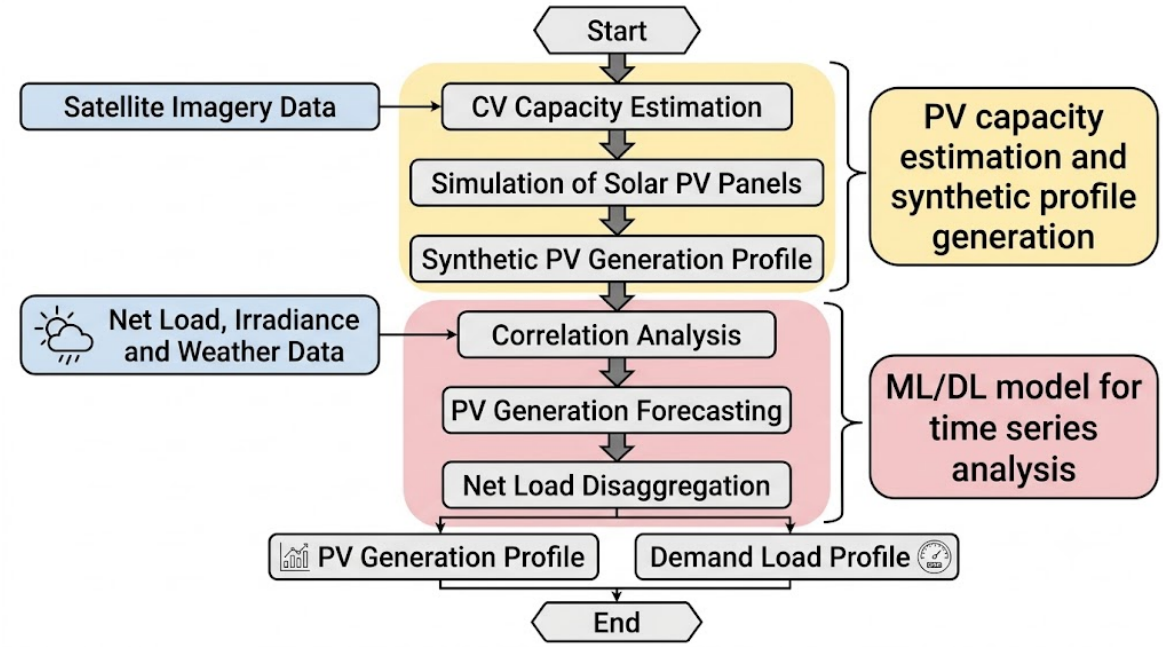

Figure 3.3: Overview of the proposed PV generation and demand disaggregation approach.

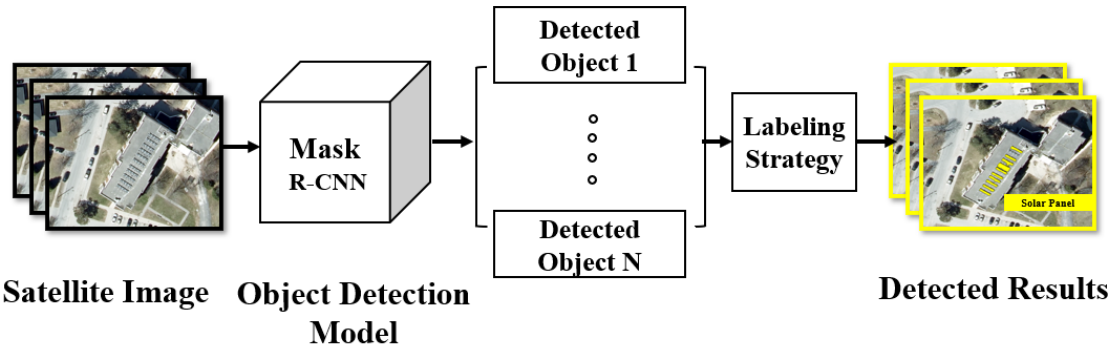

Figure 3.4: Mask R-CNN architecture for detecting and segmenting PV solar panels.

For object detection, the DNN-based Mask R-CNN algorithm in [160, 204] is used here as the pre-trained object detection model. As illustrated in Fig. 3.4, Mask R-CNN is a specialized DNN designed to process grid-like data, such as images represented as a two-dimensional pixel array. It processes the data in two phases to predict object classes and their bounding boxes. In the initial phase, two NNs, namely, the backbone and the "Region Proposal Network", suggest potential object bounding boxes. In the subsequent phase, features are extracted from each proposed box, followed by classification and segmentation mask prediction for each region of interest. Hence, based on satellite images for the region of interest, a pre-trained Mask R-CNN panel segmentation model can be used to identify PV panels in the region. The raw prediction output provides a list of bounding boxes with the following confidence scores, C^i_{train} and C^j_{test} [205]:

$$\begin{aligned} \{C^i_{\text{train}} = (r^i_1, r^i_2, r^i_3, \ldots) \mid i = 1, 2, \ldots, n\} \\ \{C^j_{\text{test}} = (s^j_1, s^j_2, s^j_3, \ldots) \mid j = 1, 2, \ldots, m\} \end{aligned} \tag{3.1}$$

where, as per the nomenclature section, n and m represent the number of training and testing image tasks, respectively, and r^i_k and s^j_k correspond to the confidence scores between 0 and 1 for training and testing, respectively, of prediction object k. To assess the accuracy of the results, manual annotations of all solar PV arrays in the aerial images were conducted to validate and enhance the results of the algorithmic

detections with the help of human annotations.

The identification of solar PV systems is influenced by a variety of factors that pose significant challenges, as expected with DL-based models when applied to complex, real-world pictures on a large scale. Thus, the following key difficulties that need to be considered in this process are:

- False Positives: Solar PV systems are susceptible to misclassification due to their resemblance to various other objects. In the current study, such misclassifications include shadows from nearby structures, dark-colored roofing materials, reflective surfaces on roofs, water pools, skylights, vehicle windshields, building edges, and car roofs. Some representative examples of these instances are illustrated in Fig. 3.5. This issue can be effectively addressed with human annotations.

- False Negatives: Identifying solar PV systems can be challenging, even for experienced annotators, particularly when black panels are installed on dark rooftops or when image resolution is insufficient. In instances where manual annotation is difficult, as in the case of small or irregularly shaped PV installations, model predictions also tend to be prone to errors, resulting in reduced classification or segmentation performance, making detection more complex. Environmental factors such as snow cover and panel soiling can also obscure visibility, further increasing the likelihood of missed detections [27]. This issue can be minimized by being more careful during the human annotation process, but it cannot be fully eliminated and is hence a potential source of error.

- Consistency of Imagery Datasets: Overhead imagery is captured from specific angles and times of day. As a result, images within the same dataset may exhibit differences in shadow presence and size, visibility of vertical walls, or other features that vary with the camera angle. These inconsistencies can be addressed by ensuring that a sufficiently large set of images is annotated. However, in some cases, the significance of the differences across images is unclear within the dataset [27], making these errors difficult to detect.

The power output of the detected PV panels $P_{s_{Y,H}}$ can be calculated as a function of hourly incident solar irradiance, PV cell temperature, and a derating factor that

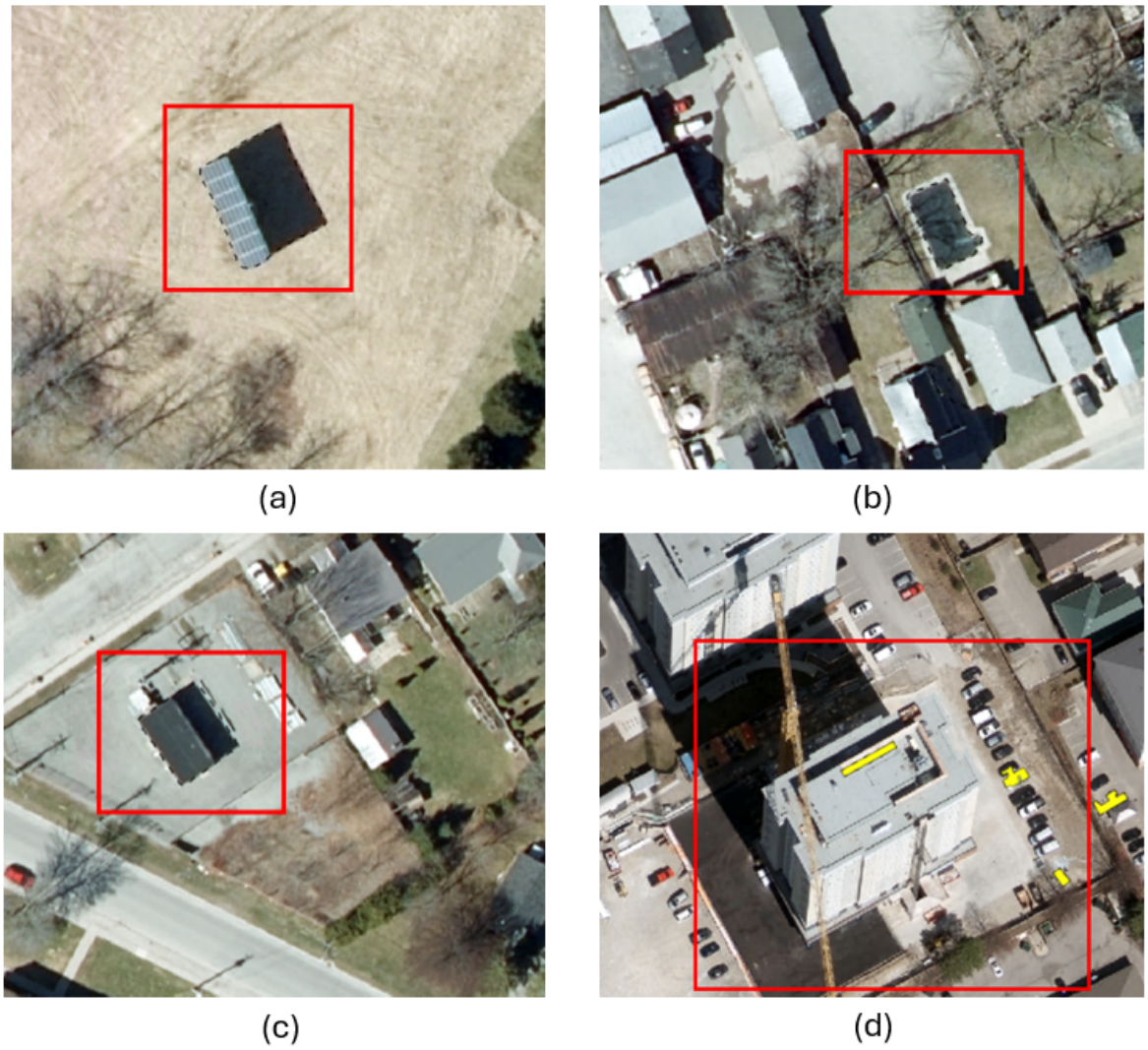

Figure 3.5: Example of false positive segmentation of solar PV panels: (a) shadows from surrounding structures, (b) water pool, (c) dark-colored roofing materials, (d) skylights and car roofs.

considers issues such as dust accumulation, wire losses, and other deviations from optimal performance, under standard test conditions (stc), as follows [49]:

$$P_{s_{Y,H}} = \varphi I_{Y,H} \left(\frac{G_{Y,H}}{G_{\text{stc}}} \right) [1 + \alpha(\tau_{Y,H} - \tau_{\text{stc}})] \quad \forall Y, H \tag{3.2}$$

where φ is the derating factor of solar panels; $I_{Y,H}$ is the total installed capacity of solar panels; $G_{Y,H}$ is the incident solar irradiance at a specific time and location; G_{stc} is the standard test conditions irradiance; α is the temperature coefficient of power for solar panels; $\tau_{Y,H}$ is the actual solar cell temperature; τ_{stc} is the solar cell temperature at standard test conditions; Y is the year; and H is the hour of the prediction. This formula is integrated into the practical and reliable SAM open-access tool for generating PV output data developed by the National Renewable Energy Laboratory (NREL) [206], which uses real solar irradiance and weather data to accurately simulate PV output. The synthetic dataset generated by SAM not only includes the PV output $P_{s_{Y,H}}$, but also DNI, DHI, ambient air temperature, calculated GHI, wind speed, and dew point, which can then be used for PV forecasting purposes.

3.4 Solar and Load Power Disaggregation

The goal of the solar and load disaggregation method is to distinguish between net load and solar power. This can be accomplished using a supervised learning model that requires net-load measurements and PV generation data during the training phase. These data are considered to be collected from the HV/MV substation of interest, which includes numerous unmonitored residential PV systems. Based on the estimated equivalent capacity and power of the installed PV system, a comprehensive method is proposed next to disaggregate solar generation and load demand.

To accurately separate $\widehat{PV}$ forecasted generation from the estimated demand $\widehat{N}$, the net-load profile $L = \widehat{N} - \widehat{PV}$ can be used. For this purpose, the approach depicted in Fig. 3.6 is applied using ML/DL techniques for PV profile forecasting. This disaggregation method for net-load component disaggregation leverages net-load data from the HV/MV substation, synthetic PV data, and meteorological information used for forecasting solar PV generation. The forecasting can be accomplished through the

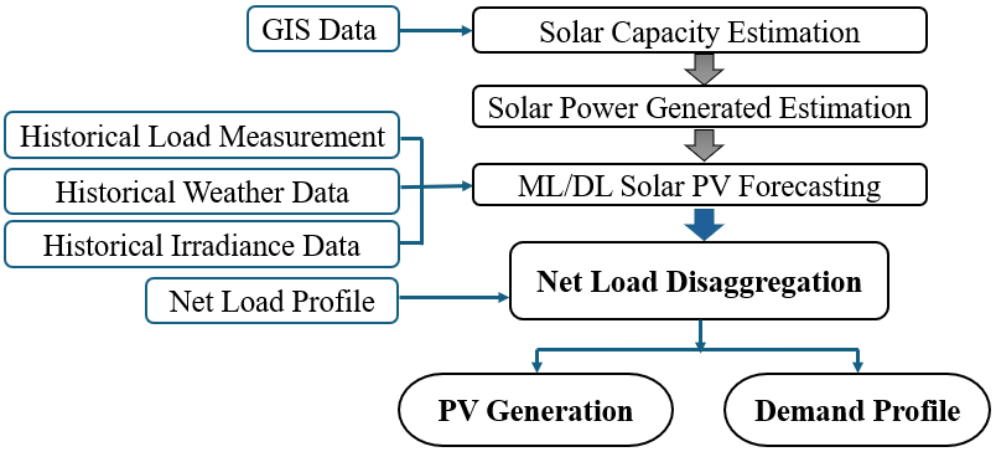

Figure 3.6: Proposed approach for disaggregating net-load components.

application of ML/DL time series algorithms, including LSTM, CNN-LSTM, BiLSTM, SVM, K-Nearest Neighbors (KNN), and Regression methods.

3.5 Machine Learning Models

Linear Regression, KNN, and SVM are benchmark ML techniques used here, as explained next. These have been extensively employed for both time series forecasting and disaggregation tasks [15, 41, 47, 160].

3.5.1 Regression Model

Linear Regression is a simple yet powerful statistical method that models the relationship between a dependent variable and one or more independent variables by fitting a linear equation to the observed data. In the context of time series forecasting, Linear Regression can be employed to predict future values based on past trends, offering a straightforward approach to understanding and predicting time-dependent data. It is computationally efficient, but it cannot capture nonlinear patterns [207].

3.5.2 KNN Model

KNN is a non-parametric, instance-based learning algorithm that predicts the output based on the majority vote of its nearest neighbors in the feature space. It is particularly useful for classification and regression tasks, including time series forecasting, by utilizing historical data points to predict future values. This algorithm bypasses complex equation solving by leveraging raw data and the correlation between the target point and its nearest neighbors. In the current study, KNN is utilized to identify historical time series features that resemble future PV generation, making it particularly effective for preprocessing time series data [208].

The KNN training process is based on measuring how similar or different two data points are in a multi-dimensional space in terms of a Euclidean distance norm. The nearest neighbors are then selected based on their similarity, ensuring that predictions are grounded in closely related past observations [209]. The initial values of the KNN model hyperparameters can be chosen based on typical values found in the existing literature.

3.5.3 SVM Model

SVM is a supervised learning model used for both classification and regression. In time series applications, SVM works by finding the optimal hyperplane that maximizes the margin between different data points, ensuring robust predictions by minimizing error. SVM is particularly effective in handling nonlinear data through the use of Kernel functions.

For PV power forecasting, SVM regression is utilized here to model the relationship between input features, such as weather parameters (temperature, irradiance, wind speed, etc.), and the output, i.e., generated PV power. The goal in SVM regression is to find a predictive function that closely matches actual power output [210]:

When dealing with nonlinear dependencies, SVM employs Kernel functions to transform the input data into a higher-dimensional space where patterns become easier to separate. Popular Kernels include polynomial, Gaussian Radial Basis Function (RBF), and hyperbolic tangent [211]. This ability to map complex relationships makes SVM particularly effective for forecasting PV power, which is influenced by fluctuating and

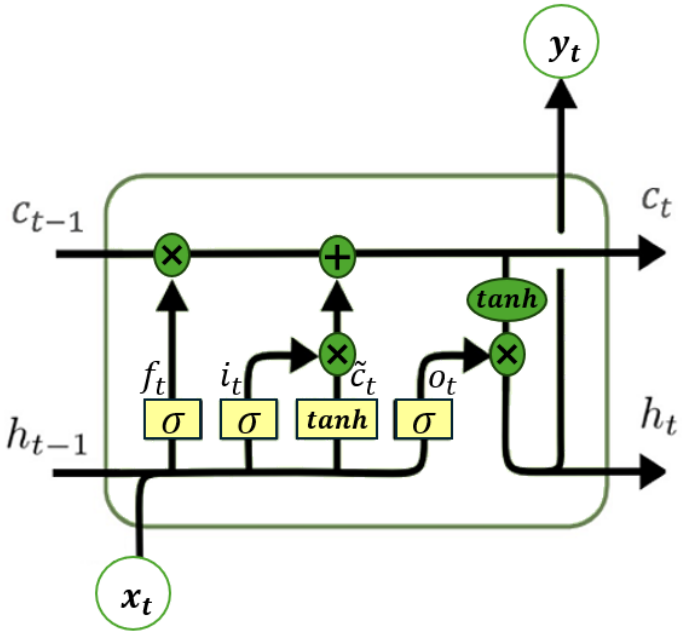

Figure 3.7: Structure of LSTM cell with input x_t and output y_t [160].

interdependent environmental factors.

3.6 Deep Learning Models

3.6.1 LSTM Model

LSTM is a type of RNN designed to overcome the vanishing and exploding gradient issues that standard RNNs experience during training, thereby enhancing their ability to handle long-term dependencies in sequential data. LSTMs utilize a unique architecture featuring memory cells and gates to store, update, and retrieve information over extended time intervals. The LSTM's ability to store and retrieve long-term memory is crucial for modeling complex time-dependent patterns, such as those found in PV power generation [160].

As illustrated in Fig. 3.7, an LSTM block consists of several essential components: x represents the input state, y denotes the output state, t is the present time step, and

σ stands for the sigmoid activation function. The core elements include the input gate i_t, cell state $\tilde{c}_t$, forget gate f_t, hidden state h_t, and output gate o_t. The structure and functionality of an LSTM cell can be defined as follows for random weights W_f, W_i, W_c, and W_o and biases b_f, b_i, b_c, and b_o [160]:

$$f_t = \sigma\left(W_f[h_{t-1}, x_t]^{\mathrm{T}} + b_f\right) \tag{3.3}$$

$$i_t = \sigma\left(W_i[h_{t-1}, x_t]^{\mathrm{T}} + b_i\right) \tag{3.4}$$

$$\tilde{c}_t = \tanh\left(W_c[h_{t-1}, x_t]^{\mathrm{T}} + b_c\right) \tag{3.5}$$

$$c_t = f_t \odot c_{t-1} + i_t \odot \tilde{c}_t \tag{3.6}$$

$$o_t = \sigma\left(W_o[h_{t-1}, x_t]^{\mathrm{T}} + b_o\right) \tag{3.7}$$

$$h_t = o_t \odot \tanh(c_t) \tag{3.8}$$

The σ and `tanh` activation functions are used to enable selective memory updates and transformations. Additionally, key hyperparameters such as the number of neurons, learning rate, and dropout rate are fine-tuned to optimize the model's performance and avoid underfitting or overfitting [160].

3.6.2 CNN-LSTM Model

CNN-LSTM is a new hybrid approach that combines the strengths of CNNs and LSTM networks to enhance the accuracy of time series forecasting [41, 160]. CNN layers are employed to automatically extract local patterns and nonlinear relationships from the input data, which is particularly beneficial for capturing complex, multi-dimensional features in photovoltaic generation patterns. The extracted features are then passed to the LSTM layers, which are well-suited for modeling temporal dependencies and learning long-term relationships in the data. One-Dimensional CNNs (1D-CNNs) are particularly useful for processing sequential data such as time series or natural language, where the Kernel (or filter) moves along the input data in one dimension, as shown in Fig. 3.8. This allows for the capture of local dependencies and extraction of features across the sequence, making it well-suited for applications where data points are temporally or spatially ordered, such as PV power generation time series [212].

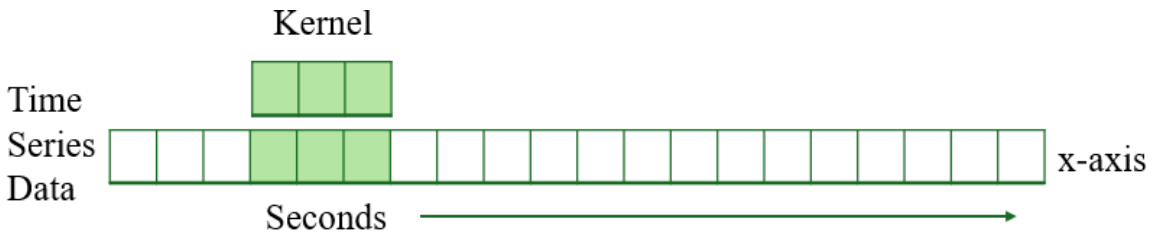

Figure 3.8: 1D-CNN computational process.

The CNN model is based on a DL architecture commonly used for processing sequential data, which extracts important features from the input data by applying convolutional layers followed by pooling layers. In the context of PV power generation, a CNN can be used to classify weather conditions based on input patterns. The CNN architecture typically involves convolution layers with `Rectified Linear Unit (ReLU)` activation functions and fully connected layers to map extracted features to the output labels [212].

The CNN-LSTM model applied here uses CNN for weather classification, and based on the classified weather condition, an LSTM model is selected to forecast PV power generation. This hybrid approach allows the model to handle different weather conditions separately, reducing the complexity and variability of data fitting. The overall structure of the CNN-LSTM hybrid model facilitates capturing nonlinear relationships and temporal dependencies, offering better forecasting accuracy than a standalone LSTM model. The use of a CNN for feature extraction and LSTM for sequential forecasting, as shown in Fig. 3.9, allows the hybrid model to significantly reduce forecasting error, providing a more reliable prediction of PV power generation.

Compared to a standard LSTM model, the CNN-LSTM model demonstrates a superior ability to capture local trends and nonlinear relationships between diverse features and PV generation patterns. This results in fewer forecast errors and a closer match between actual and predicted values. By leveraging the combined advantages of CNN and LSTM, the CNN-LSTM model provides more accurate forecasts, making it a valuable tool for improving prediction and energy management.

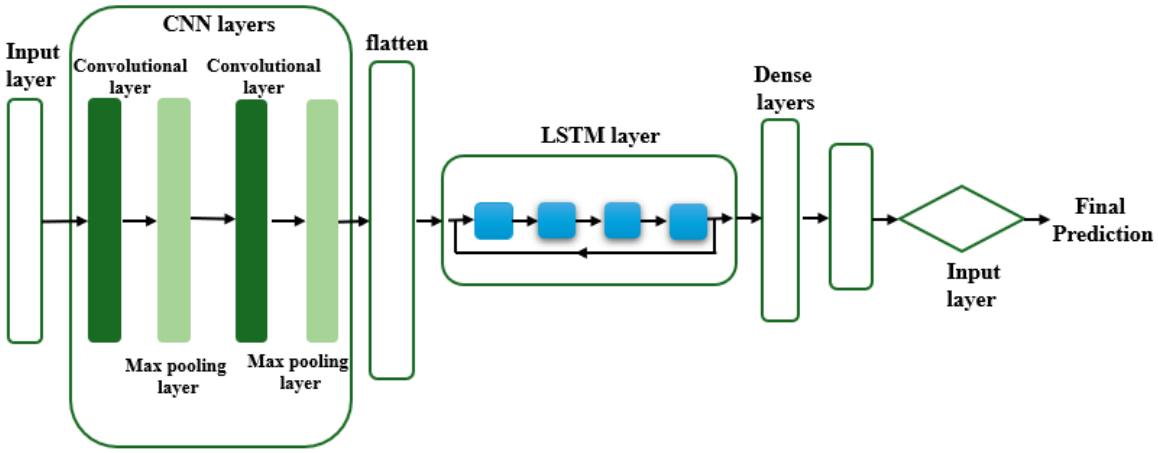

Figure 3.9: CNN-LSTM hybrid model.

3.6.3 BiLSTM Model

The BiLSTM model in this study is designed to efficiently process time series data by leveraging bidirectional temporal contexts. A sliding window technique can be employed during training to segment the input sequence, enabling the model to extract meaningful temporal features.

Fig. 3.10 shows the structure of BiLSTM. While standard LSTM captures information from previous time steps through a backward-propagation path, BiLSTM enhances this capability by adding a forward-propagation path. This forward LSTM layer processes data in the reverse direction, enabling the model to consider both past and future information simultaneously. As a result, the output layer of BiLSTM integrates these bidirectional contexts, enabling the hidden cells to utilize comprehensive temporal information during model training.

Modern BiLSTM models incorporate a sliding window technique applied to the input sequence [213]. The LSTM block structure forms the core of the BiLSTM model proposed here. In these models, the computational cost of the forward and backward layers is equivalent. However, the direction of hidden state propagation is reversed in the forward layer, allowing the model to capture both past and future time-dependent information. The mathematical formulation for the forward and backward LSTM layers

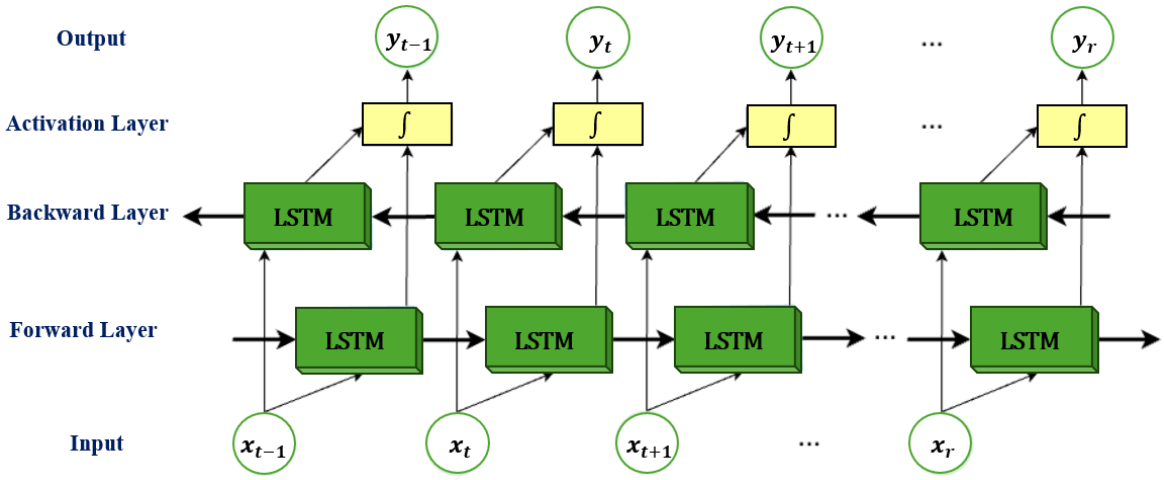

Figure 3.10: Structure of BiLSTM cell with time series inputs x_t and outputs y_t [213].

of the BiLSTM network can be expressed as follows [214]:

$$h_f = F(W_{f1}\ x_f + W_{f2}\ h_{t-1}) \tag{3.9}$$

$$h_b = F(W_{b1}\ x_t + W_{b2}\ h_{t+1}) \tag{3.10}$$

where h_f and h_b are the outputs of the forward and backward LSTM layers, respectively, as depicted in Fig. 3.10, and F is an activation function such as σ or `tanh`. The final output of the BiLSTM model is then computed by combining these outputs as follows [214]:

$$y_i = g(W_{o1}\ h_f + W_{o2}\ h_b) \tag{3.11}$$

where g is another activation function.

To improve performance, the input data can be normalized, and the sliding window length can be tailored to the specific characteristics of the time series data. The optimal window size can then be determined by analyzing the data's periodicity, temporal dependencies, and the inherent patterns within the time series. By adjusting the window length to suit the underlying structure of the data, the model can extract more meaningful temporal features and improve predictive accuracy [213].

Correlation analysis is needed to identify historical weather data and other relevant feature values that are critical for accurate prediction. Based on this analysis, the most significant features can be selected as inputs for the various ML/DL forecasting techniques, evaluating their respective error. By obtaining the PV power generation profile through these models, the aggregated demand load profile can be calculated. The disaggregated profiles, i.e., N and $\widehat{PV}$ profiles, can then be utilized for proper system operation.

3.7 Results and Discussion

3.7.1 Data Sets

Transmission Level Measurement

The first dataset used consisted of the transmission-level net-load data supplied by the IESO, which corresponded to two HV/MV transformers in the Waterloo Region, illustrated in Fig. 3.2, with a transformer power rating of 108 MW. These data span the period from January 2018 to December 2021 and include measurements recorded with 1 min granularity, which were aggregated to the 15 min interval used here.

GIS Data

The second dataset for the PV panel detection task is images that span a total area of 240 km^2 in the Waterloo Region. The images used here, which are not publicly available, were provided by the Geospatial Center at the University of Waterloo. All imagery corresponded to aerial photography in April 2021, including images from the Landsat 8 satellite. Large satellite images, ranging from 1 km^2 pixels, were cropped to create patches suitable for semantic image segmentation, as shown, for example, in Fig. 3.11, with solar PV panels annotated in yellow. The implementation of the pre-trained Mask R-CNN approach was carried out using Python's ArcGIS Pro API applied to the available high-resolution imagery of the region of interest, and a pre-trained model using a large dataset of color aerial imagery from Fresno, CA, USA [215].

PV Dataset

A synthetic PV data generation method was implemented using the SAM software [216]. Fig. 3.12 illustrates the PV power output values and the likelihood obtained for hours and months across the different years of study.

Meteorological Data

The 30-minute meteorological datasets used were obtained from the NREL [206] for the Waterloo Region. The dataset includes variables such as temperature, irradiance, wind speed, dew point, and others, which were used to identify relevant correlations for solar generation forecasting, revealing how variations in meteorological conditions influence solar energy output.

Temporal Features

These consist of 15 min intervals for the 24 h a day, the months of the year, the day of the week, and years. The synthetic PV data depicted in Fig. 3.12 revealed that both the hour and month significantly affect the PV output.

Data Preprocessing

The data obtained from various repositories had to undergo preprocessing before being used for forecasting and disaggregation. This preparation involved several steps, including data cleaning, synchronization, and vectorizing (one-hot encoding) to produce a clean and well-structured dataset. The raw data contained high-frequency noise, missing entries, incorrect labels, and duplicate records. Missing values were addressed by appropriate imputation methods, such as averaging.

3.7.2 Feature Extraction and Correlation Analysis

It is important to synchronize the data since they were collected at different sampling rates: 1 minute for load data, 30 minutes for weather data, and 15 minutes for irradiance data. In this study, all datasets were synchronized using their respective timestamps and resampled to a uniform 15-minute interval.

As previously mentioned, the proposed model utilizing supervised learning requires data for both net load (input vector) and estimated PV generation (label) from the



Figure 3.11: Solar PV panels segmentation in the Waterloo region.

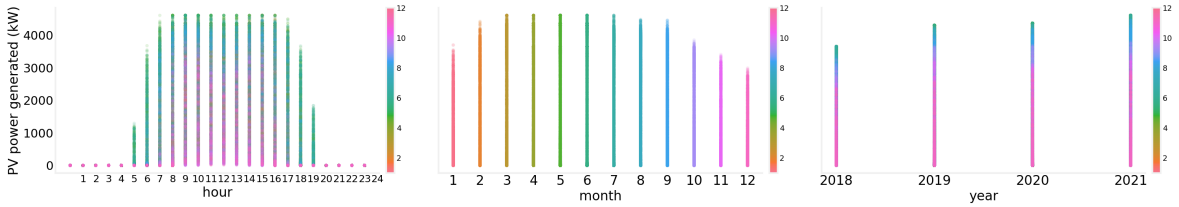

Figure 3.12: Simulated PV power output from SAM software with the colors signifying the probability of the PV output values, with red for more likely values and green-blue for least likely.

feeder for the training process. The dataset is partitioned into 75% for training, 10% for validation, and 15% for testing. Training dataset was used to fit the model parameters, while the validation set provided feedback for model performance during hyperparameter tuning. The test set, reserved for final evaluation, ensured an unbiased assessment of the models' generalizability. Moreover, categorical variables were transformed into numerical values through one-hot encoding [217, 218], which created a new binary feature for each category, allowing categorical data to be represented in a format suitable for numerical analysis and model training.

Dimensionality reduction, also known as feature projection, was utilized to transform data into a new subspace, retaining essential information and reducing noise and redundant variables to accurately represent the input signal and improve load identification by isolating valuable information in a smaller or similarly sized subspace [219]. Fig. 3.13 and Fig. 3.14 depict the relation between PV power generation and net load versus solar irradiance and ambient temperature for four days in May and December 2020, illustrating the nonlinear relation between solar irradiance and PV as per (3.2), derived from the PV synthetic data.

Fig. 3.15 illustrates the Pearson correlation coefficients between solar energy generation and various features for forecasting. A positive correlation is obtained when the coefficient exceeds 0.3, showing that temperature, GHI, DNI, DHI, and dew point have a significant impact on PV power generation. Furthermore, temporal factors such as time of day, day of the week, and month of the year are also important contributors. These pre-processed features were provided to the DL and benchmark ML models to ensure consistency across all models and standardize the input data. This guaranteed a fair and meaningful performance comparison between the two model types.

3.7.3 Mask R-CNN PV Detection

In semantic segmentation, the primary objective is to assess the accuracy of predicted and labeled masks. However, in object detection, the Intersection over $Union$ (IoU) metric is often more meaningful than accuracy, especially in cases where small objects are present [220]. This metric evaluates the overlap between predicted and ground truth masks. Since PV panels occupy only a small fraction of the image, accuracy may

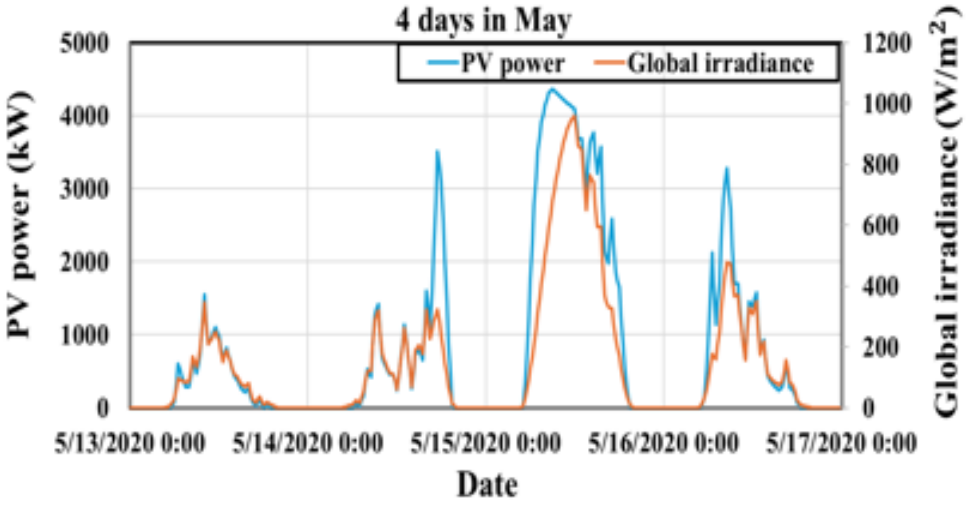

(a)

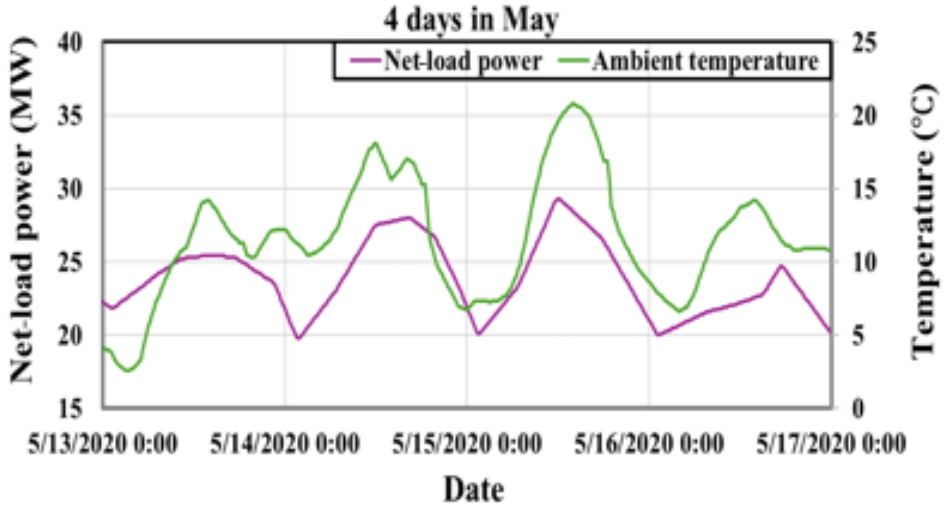

(b)

Figure 3.13: Time series for four days showing (a) PV power generation versus solar irradiance and (b) net-load versus ambient temperature for May 2020.

remain high even if many panels are missed. In such cases, the following IoU metric provides a more reliable evaluation of model performance [221]:

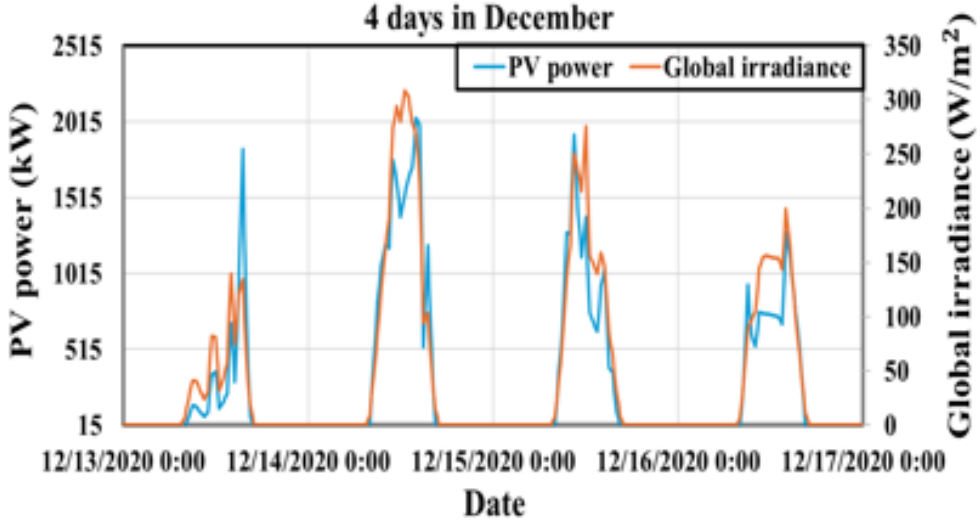

(a)

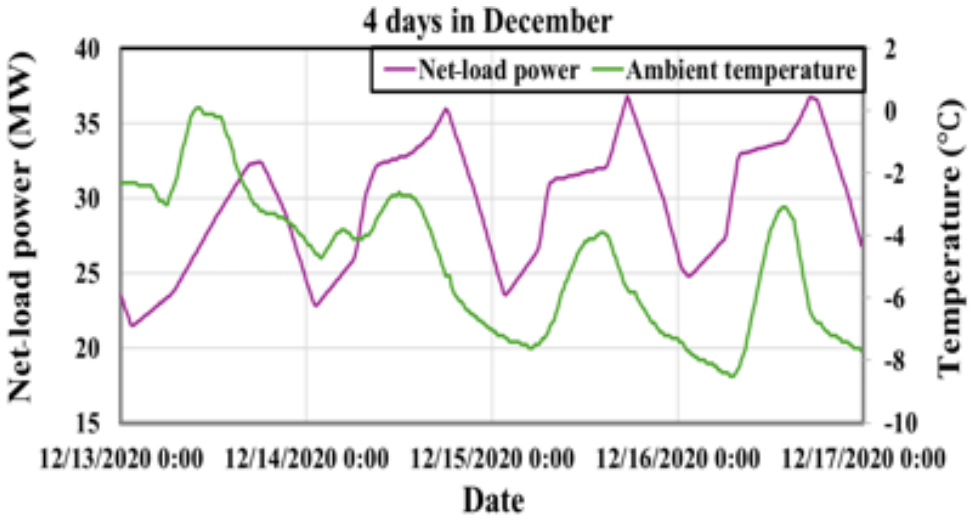

(b)

Figure 3.14: Time series for four days showing (a) PV power generation versus solar irradiance and (b) net-load versus ambient temperature for December 2020.

$$IoU = \frac{Area of Overlap}{Area of Union} = \frac{|A \cap B|}{|A \cup B|} \tag{3.12}$$



Figure 3.15: Correlation metrics between solar power output and various factors in May 2020.

The proposed methods attained a performance range of 65%-70%, as determined by this metric.

In some instances, the IoU metric does not provide insights into the completeness of the model, in which case this can be complemented with additional metrics, including $Accuracy$, $Precision$, $Recall$, and $F1Score$. Thus, $Accuracy$ can also be used to assess the DL model's performance with respect to human annotation, which is defined as follows [58]:

$$Accuracy = \frac{TP}{TP + TN + FP + FN} \tag{3.13}$$

where TP, TN, FP, and FN represent, respectively, the total number of true positives (correctly detected PV panels), true negatives (non-PV objects correctly classified as non-PV), false positives (non-PV objects incorrectly classified as PV panels), and false negatives (actual PV panels not detected by the model). In the PV detection task, these parameters are measured based on PV panel area in square meters. The model's reliability can also be assessed using the $Precision$ metric, which is computed as the ratio of correctly predicted PV panels (TP) to the total number of predicted positives as follows [58]:

$$Precision = \frac{TP}{TP + FP} \tag{3.14}$$

This is used to determine how often a positive prediction is correct. Finally, $Recall$, which measures the completeness of the model, can be used to assess the proportion of labeled PV panel pixels that are correctly identified as follows [58]:

$$Recall = \frac{TP}{TP + FN} \tag{3.15}$$

These metrics allow a comprehensive evaluation of the model performance and are widely utilized in semantic segmentation tasks. However, to balance both $Precision$ and $Recall$, the following $F1Score$ can also be used as the Harmonic Mean of these two metrics [222]:

Table 3.1: Performance Metrics for Mask-RCNN Model Evaluation

Metric	**Value**
IoU	65%
$Accuracy$	99%
$Precision$	80.6%
$Recall$	65.9%
$F1score$	72.5%

$$F1score = 2 \times \frac{Precision \times Recall}{Precision + Recall} \tag{3.16}$$

Table 3.1 summarizes the performance results of the proposed model for an area of 240 km^2 in the Waterloo Region.

3.7.4 PV Capacity Estimation

The estimation of PV power generation was conducted using GIS tools and DL image-based techniques applied to high-resolution satellite imagery to identify PV panels. Manual annotations of PV panels were conducted thrice to ensure consistency. In rare instances, the algorithm detected features that were initially overlooked during manual annotation. This back-and-forth process allowed the reliable identification of the PV panels in the region of interest. To validate the capacity estimates, data from Enova Power Corp. provided information on the maximum average capacity of solar panel installations in the Waterloo Region, including both ground-mounted and rooftop PV systems from 2018 to 2021. This information is summarized in Table 3.2, illustrating how the total solar capacity has increased significantly over the years, with 2021 representing a 32.69% increase compared to 2018. Thus, in 2021, the total solar panel capacity was recorded at 4570 kW, with the GIS-based estimated capacity closely matching it at approximately 4560 kW. Due to the unavailability of image data for the years 2018, 2019, and 2020, Enova's data were used as the capacity forecast.

Table 3.2: Actual Installed PV Capacity at Relevant HV/MV Transformer.

Year	2018	2019	2020	2021
Total Capacity (kW)	3444	4240	4270	4570

This assumption was made with the expectation that the GIS-based estimates would produce reliable capacity forecasts.

3.7.5 Hyperparameters Settings

To achieve optimal performance in the proposed model, it is critical to carefully tune hyperparameters. The hyperparameters of the BiLSTM model, such as the number of neurons, activation functions, and learning rates, were fine-tuned based on a review of similar articles and iterative experimentation in the relevant literature. Thus, for the LSTM-based model, 128 nodes were selected to address potential issues such as overfitting and underfitting [223]. Furthermore, early stopping was implemented to halt training when the validation loss did not plateau, effectively preventing overfitting and reducing unnecessary computational overhead. Selecting the appropriate number of nodes is important, as a higher number can lead to overfitting, with the model memorizing the training data but failing to generalize to unseen data, while a lower number may result in underfitting, with the model lacking the needed complexity to capture key patterns in the data. In this model, each node serves as a computational unit that processes inputs through a transfer function and connects them to outputs via weighted connections.

The Adam optimizer was used for training all LSTM-based models, as it is a well-established optimization algorithm for DNNs. It leverages a weighted average to monitor the relative prediction error of the loss function and is based on the SGD process [224]. A key advantage of Adam is its ability to mitigate the effects of outliers while requiring only first-order gradients, making it computationally efficient. One notable feature of Adam is its calculation of both momentum and the second moment of the gradient using exponentially weighted moving averages, which contributes to its robust convergence [225, 226].

An important hyperparameter in this study is the dense layer integrated into each

Table 3.3: Hyperparameter Settings for LSTM, CNN-LSTM, and BiLSTM Models

Hyperparameter	**LSTM**	**CNN-LSTM**	**BiLSTM**
Epoch	20, 30, 40	20, 30, 40	20, 30, 40
Batch size	100	100	100
Number of units	128	128	128
Dropout rate	0.2	N/A	N/A
Kernel size	N/A	1	1st=1, 2nd=2
MaxPooling size	N/A	1	N/A
Padding	N/A	Valid	Causal
Activation function	`tanh`	`ReLU`	`ReLU`
Dense layer units	1	1	1
Train data	75% dataset	75% dataset	75% dataset
Validation data	10% dataset	10% dataset	10% dataset
Test data	15% dataset	15% dataset	15% dataset
Optimizer	Adam	Adam	Adam
Learning rate	0.001	0.001	0.001

model. This configuration was chosen to balance computational efficiency and model performance, ensuring an optimal runtime without compromising accuracy. Additionally, a learning rate of 0.001 was selected for all LSTM-based models, as this value has been shown to yield optimal results across various studies. The dense layer was strategically configured to ensure consistency and adaptability across different models.

Table 3.3 presents the key hyperparameters used in the LSTM, CNN-LSTM, and BiLSTM models. While certain hyperparameter values, such as the learning rate, are shared across all models, other parameters are unique to the specific architecture. For example, the `ReLU` activation function is used in the CNN-LSTM and BiLSTM models, whereas the LSTM model employs the `tanh` activation function. Additionally,

the CNN-LSTM incorporated a Kernel size of 1, while the BiLSTM utilized two Kernel sizes, 1 and 2, to capture hierarchical temporal patterns effectively.

The dropout rate hyperparameter employed in LSTM was carefully chosen to improve model generalization, since this is commonly used to mitigate overfitting by randomly setting a portion of the network's weights to zero during training, ensuring better generalization for unseen data. The padding strategy was also adapted to the specific model structure, using "Valid" Padding for the CNN-LSTM model and "Causal" Padding for the BiLSTM model. These adjustments were made to enhance each model's predictive accuracy and robustness. Additionally, the inclusion of Max-Pooling in the CNN-LSTM model further strengthened its ability to extract spatial features from input data, a feature not utilized by the LSTM and BiLSTM models.

As seen in Table 3.4, in addition to the LSTM-based models, several benchmark ML techniques were also considered, each differing significantly in structure and implementation. Unlike LSTM models, which rely on sequential data processing and recurrent layers, these models leverage simpler mathematical and statistical approaches for analysis and prediction. However, due to their lack of consideration for temporal dependencies in the data, these models may not be as effective in comparison to the LSTM algorithm, which accounts for the complexity of sequential patterns [227].

To ensure a fair comparison, lag features for the SVM, KNN, and Linear Regression models were included. The hyperparameters for these models were carefully selected to optimize their performance according to the characteristics of the dataset. For Linear Regression, no additional hyperparameters were required, as this technique is based on a closed-form solution that minimizes the mean squared error between predicted and actual values, thus being a baseline model for regression tasks. The KNN algorithm was configured with 140 neighbors, which is based on similar values found in the existing literature plus a trial-and-error process, specifying the number of nearest data points considered when making predictions. The default leaf size of 30 was used, as it strikes a balance between computational complexity and performance of the search tree structure. For SVM, the RBF Kernel was employed, as it is well-suited for capturing nonlinear relationships in the data, with the Kernel hyperparameter defining the transformation of input data into a higher-dimensional space, enabling linear separability. The C parameter, which regulates the trade-off between maximizing

Table 3.4: Hyperparameter Settings for Linear Regression, KNN, and SVM Models

Techniques	**Hyperparameter**	**Value**
Linear Regression	None	N/A
	Lag count	3
KNN	N_neighbors	140
	Leaf size	Default 30
	Power parameter p	Default 2
	Lag count	3
SVM	Kernel	Radial Basis Function (RBF)
	C	1
	Degree	3
	Lag count	3

the margin and minimizing classification error, was set to 1. The Degree was fixed at 3, which is a value specific to polynomial Kernels, but it does not directly affect the RBF Kernel. The Gamma parameter was set to "Scale" to adjust the influence of each individual training example, allowing the model to better capture the distribution of the data.

The aforementioned benchmark models served as a base to evaluate the LSTM-based DL models, providing a baseline and alternative perspectives of the data. Although the hyperparameters for these models are simpler than those of the LSTM-based models, their proper configuration remains important for achieving optimal performance.

3.7.6 Forecasting Error Metrics

As outlined in Section 3.5, this study employs six ML/DL techniques, i.e., LSTM, CNN-LSTM, BiLSTM, SVM, KNN, and Regression, for forecasting and disaggregation. The

evaluation criteria for these techniques are based on the following five key performance indicators [228]:

$$RMSE = \sqrt{\frac{\sum_{i=1}^{n}(y_i - x_i)^2}{n}} \tag{3.17}$$

$$MAE = \frac{\sum_{i=1}^{n}|y_i - x_i|}{n} \tag{3.18}$$

$$R^2 = 1 - \frac{\sum_{i=1}^{n}(y_i - x_i)^2}{\sum_{i=1}^{n}(y_i - \bar{y})^2} \tag{3.19}$$

$$SD = \sqrt{\frac{\sum_{i=1}^{n}(x_i - \bar{x})^2}{n}} \tag{3.20}$$

$$PA = \frac{\sum_{i=1}^{n}(x_i - \bar{x})(y_i - \bar{y})}{\sqrt{\sum(x_i - \bar{x})^2(y_i - \bar{y})^2}} \tag{3.21}$$

where y_i denotes the estimated PV value, $\bar{y} = \sum_{i=1}^{n} y_i/n$ represents the average mean of the estimated PV values, x_i is the predicted output, $\bar{x} = \sum_{i=1}^{n} x_i/n$ corresponds to the average mean of the predicted output, and n is the number of data points considered [213].

3.7.7 Application and Comparison

The estimation outcomes for PV generation and load demand disaggregation are depicted for May 2021 in Fig. 3.16, with similar results for July and December 2021 shown in Figs. 3.17 and 3.18, respectively. PV synthetic data from 2018, 2019, and 2020 were used for designing the ML/DL models, while estimated PV output power for 2021 was utilized as a reference for comparison purposes. The results for the Regression, KNN, SVM, LSTM, CNN-LSTM, and BiLSTM models are depicted in these figures, which show that the proposed BiLSTM method produced the best results in general, as discussed next based on the calculated performance indicators.

Table 3.5 compares performance indicators for 2021. To ensure a fair evaluation, the error metrics excluded time samples where PV generation is zero, thus preventing overestimation in the reported results. Among the Regression, KNN, and SVM mod-

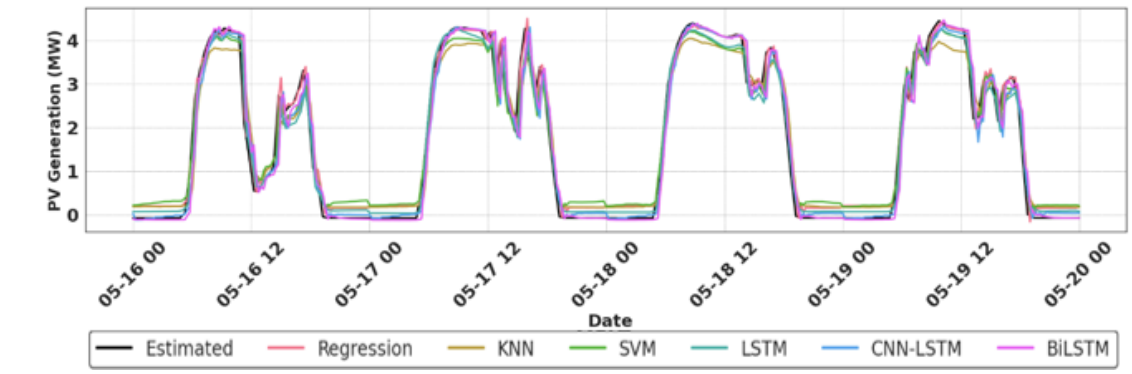

(a)

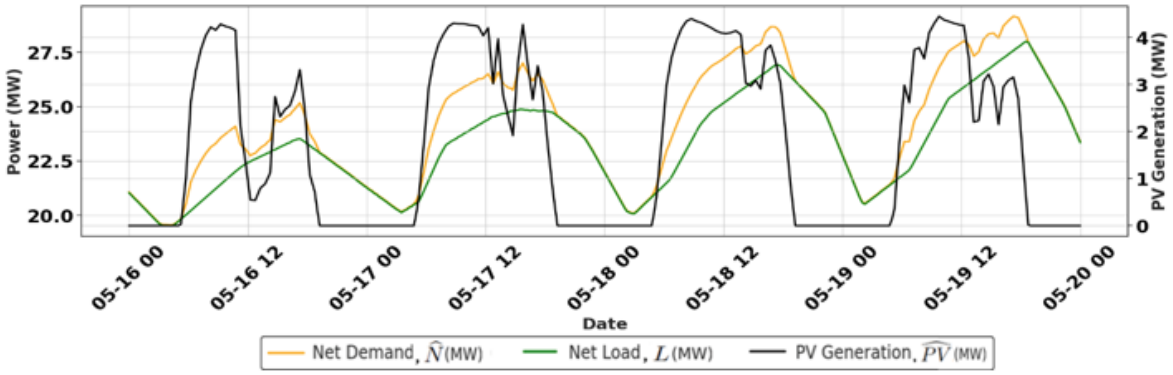

(b)

Figure 3.16: Measured and disaggregated powers for May 2021: (a) PV generation forecast and (b) BiLSTM disaggregation results.

els, which are not DL techniques, the Regression and SVM algorithms deliver the best $RMSE$, due to KNN's reliance on a single hyperparameter, i.e., the number of nearest neighbors, which is inadequate for accurately modeling the complex input-output relationships in predictive tasks. Furthermore, KNN is prone to overfitting due to its limited hyperparameters and lack of regularization mechanisms.

Observe in Table 3.5 that all models closely approximate the estimated PV output for 2021. However, the proposed BiLSTM DL model consistently provides accurate estimations across various weather conditions, underscoring its enhanced performance relative to existing methods.

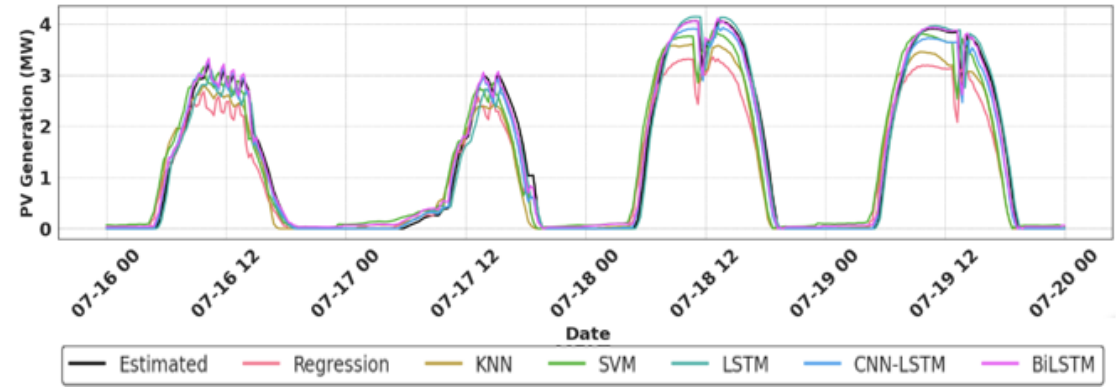

(a)

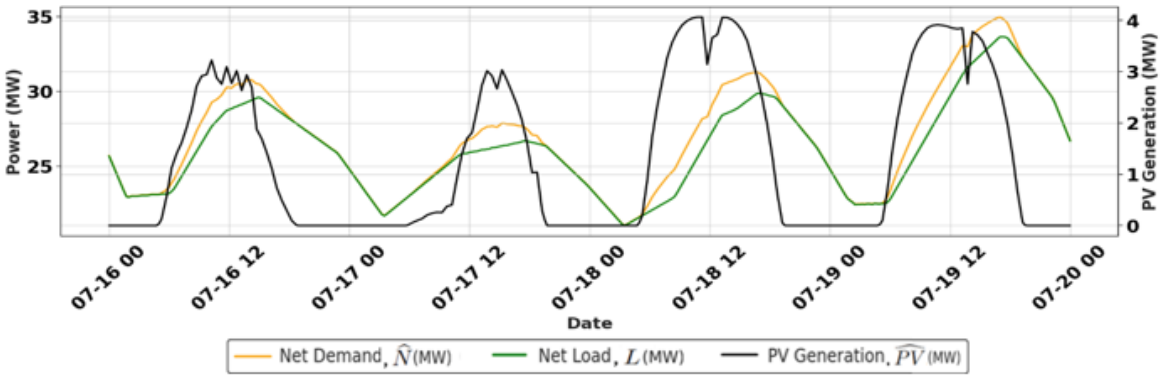

(b)

Figure 3.17: Measured and disaggregated powers for July 2021: (a) PV generation forecast and (b) BiLSTM disaggregation results.

The CNN-LSTM model exhibits superior capability for identifying local patterns and nonlinear correlations between various features and electrical load compared to the LSTM model. This results in lower forecasting error for the CNN-LSTM method, which achieves better alignment between the estimated and predicted PV generation, as illustrated in Table 3.5 and Fig. 3.16 to Fig. 3.18.

To better compare the performance of the DL and non.DL models, a rolling time window analysis was applied to the obtained metrics to assess the differences between the algorithms over time. Thus, Fig. 3.19 to Fig. 3.21 display the performance measurements, specifically Mean Absolute Error (MAE) and Root Mean Squared Error

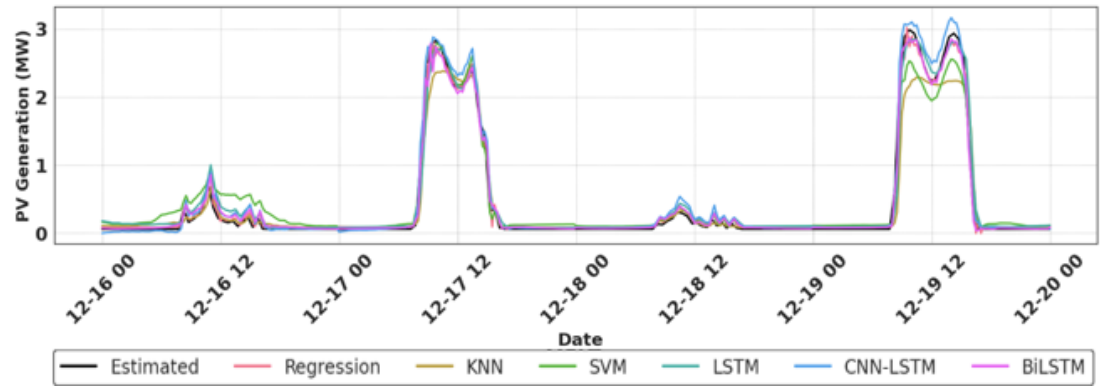

(a)

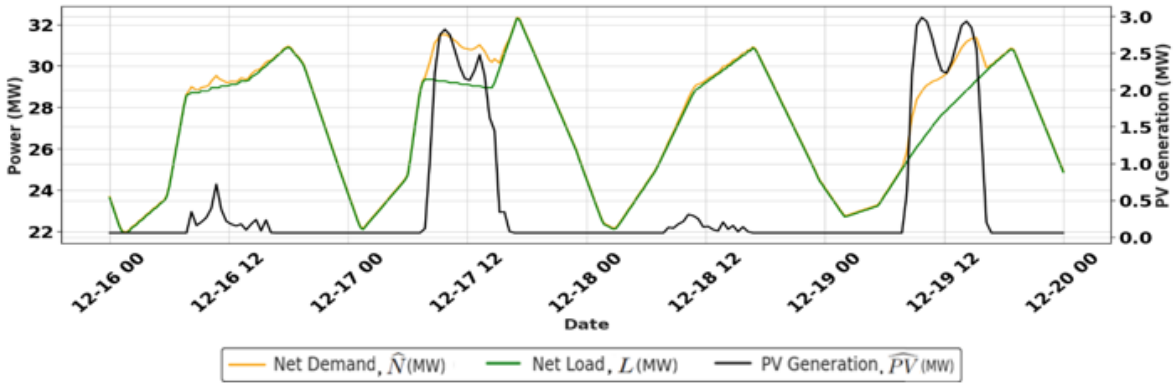

(b)

Figure 3.18: Measured and disaggregated powers for December 2021: (a) PV generation forecast and (b) BiLSTM disaggregation results.

(RMSE), for both ML and DL algorithms, with lower RMSEs and MAEs indicating better predictive accuracy and model results. For a fair evaluation, time samples when there is no PV generation were excluded to prevent skewing the results. Observe that, for all models, error values increase during peak PV generation at around noon, which suggests that the highest prediction errors are likely due to rapid fluctuations in irradiance and temperature variations at peak solar generation. Note that the most significant prediction error differences between the DL and non-DL algorithms occur in May, which corresponds to high solar activity and variability, while lower error differences are observed in December, which has the lowest peak PV power generation

Table 3.5: Quantitative Comparison of ML/DL Models for PV Generation Forecasting

Period	**Error**	**Regression**	**KNN**	**SVM**	**LSTM**	**CNN-LSTM**	**BiLSTM**
May, 2021	MAE [MW]	0.17	0.38	0.25	0.26	0.18	0.13
	RMSE [MW]	0.27	0.47	0.32	0.36	0.27	0.23
	R^2 [p.u.]	0.95	0.87	0.94	0.93	0.97	0.97
	SD [MW]	1.33	1.33	1.33	1.40	1.66	1.67
	PA [p.u.]	0.97	0.94	0.97	0.96	0.98	0.99
July, 2021	MAE [MW]	0.10	0.35	0.18	0.16	0.16	0.09
	RMSE [MW]	0.17	0.42	0.24	0.23	0.21	0.16
	R^2 [p.u.]	0.98	0.89	0.96	0.96	0.98	0.96
	SD [MW]	1.28	1.28	1.28	1.31	1.62	1.28
	PA [p.u.]	0.99	0.97	0.98	0.98	0.99	0.98
Dec, 2021	MAE [MW]	0.09	0.16	0.11	0.06	0.09	0.01
	RMSE [MW]	0.16	0.28	0.17	0.12	0.16	0.12
	R^2 [p.u.]	0.96	0.89	0.95	0.98	0.96	0.98
	SD [MW]	0.88	0.88	0.88	0.87	0.88	0.88
	PA [p.u.]	0.98	0.95	0.98	0.99	0.98	0.99

due to reduced sunlight.

Among the non-DL models, observed that KNN exhibits the highest error in Fig. 3.19 to Fig. 3.21, highlighting its limitations in capturing complex temporal dependencies. In contrast, the Regression model demonstrates better performance, followed by SVM, as both benefit from their ability to map nonlinear relationships more effectively. On the other hand, note that the DL models, particularly BiLSTM and CNN-LSTM, consistently show lower RMSE and MAE values, thus indicating superior performance. The BiLSTM model yields the most accurate predictions, with its values closely matching actual observations. This can be attributed to its bidirectional processing capability, which allows it to learn patterns from both past and future time steps, enhancing predictive accuracy. Similarly, CNN-LSTM leverages convolutional layers to extract spatial-temporal features before passing them through its LSTM layers, improving its

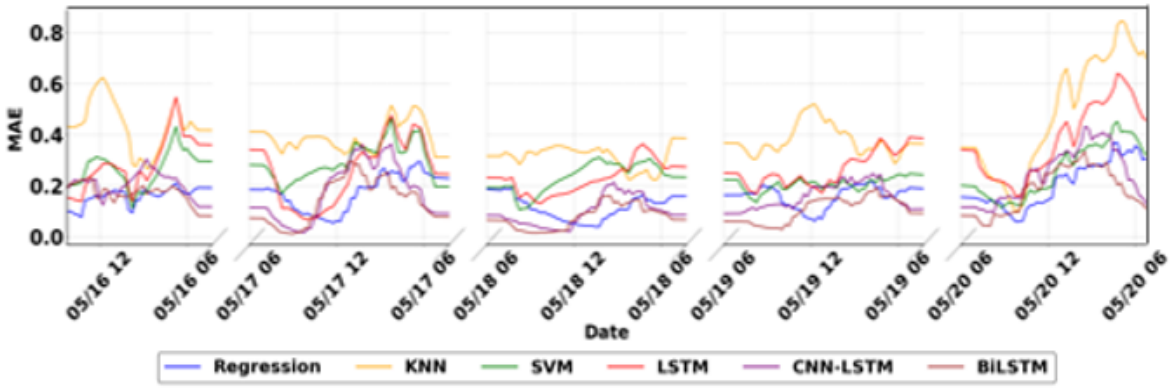

(a)

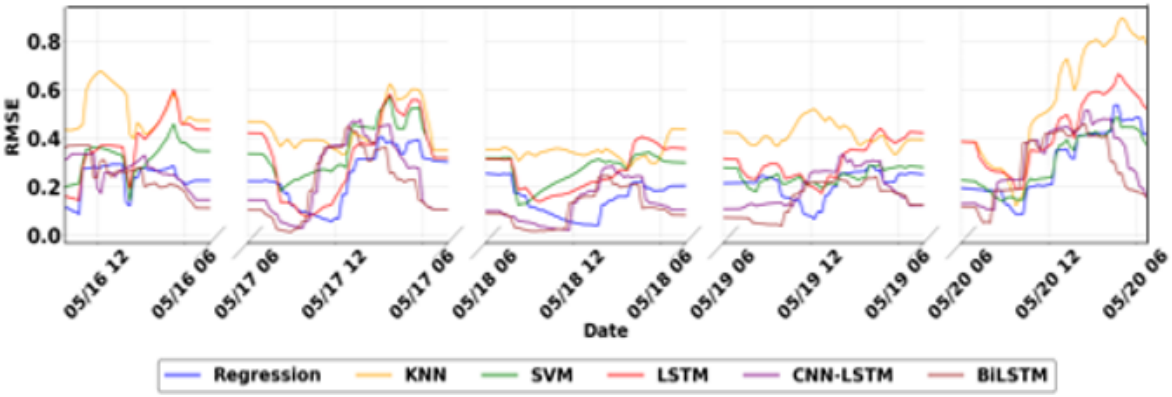

(b)

Figure 3.19: Rolling window performance metric analysis for different algorithms over the specified date range in May 2021: (a) MAE and (b) RMSE.

ability to generalize across different time periods.

The various proposed identification techniques can be further compared using the RMSE and MAE distributions illustrated in the boxplots depicted in Fig. 3.22 and Fig. 3.23, which allow comparing the medians and variability for the different months previously discussed, providing details of the data's distribution characteristics for different seasonal conditions. The boxes represent the range between the first (25% percentile) and third (75% percentile) data quartiles, while the whiskers show the range between minimum and maximum data points, with the open circles reflecting data

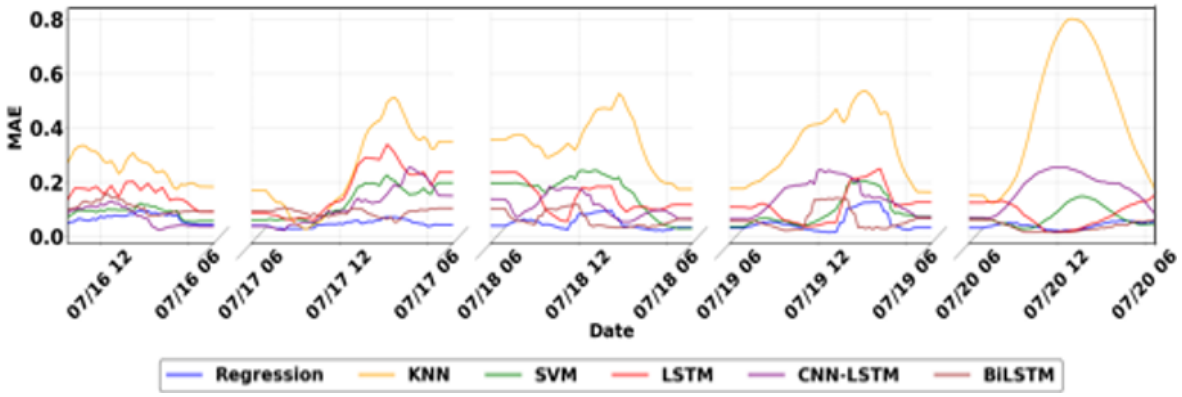

(a)

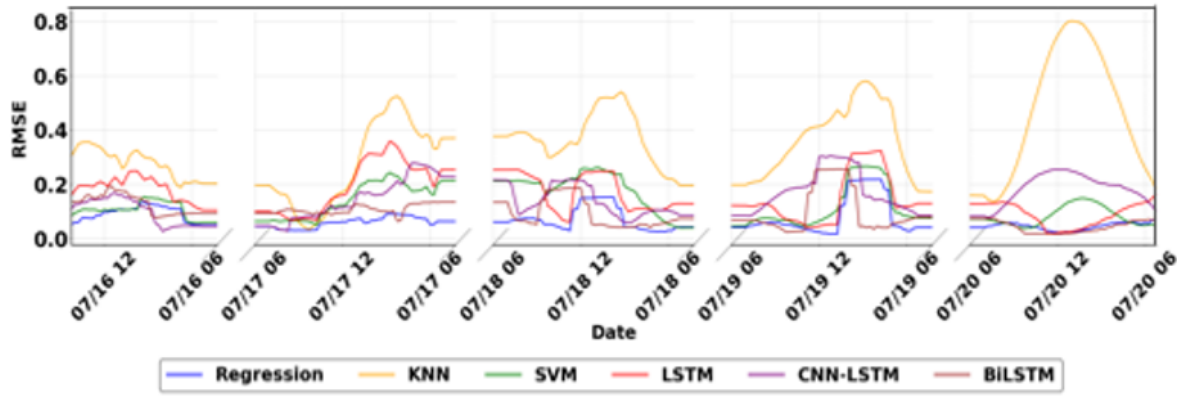

(b)

Figure 3.20: Rolling window performance metric analysis for different algorithms over the specified date range in July 2021: (a) MAE and (b) RMSE.

outliers beyond 1.5 times the shown Interquartile Ranges (IQRs). Observe that the median RMSE and MAE values for all models are the highest in May, due to greater variability of solar power generation during this period. The IQRs are not consistent across months for each algorithm, with May generally showing the widest IQRs, especially for the Regression, LSTM, CNN-LSTM, and BiLSTM models, indicating higher dispersion and sensitivity during peak solar generation. In contrast, July tends to have the lowest overall spread due to the highest radiation days and temperatures of the year, as expected. Note that for the KNN and SVM models, December shows broader

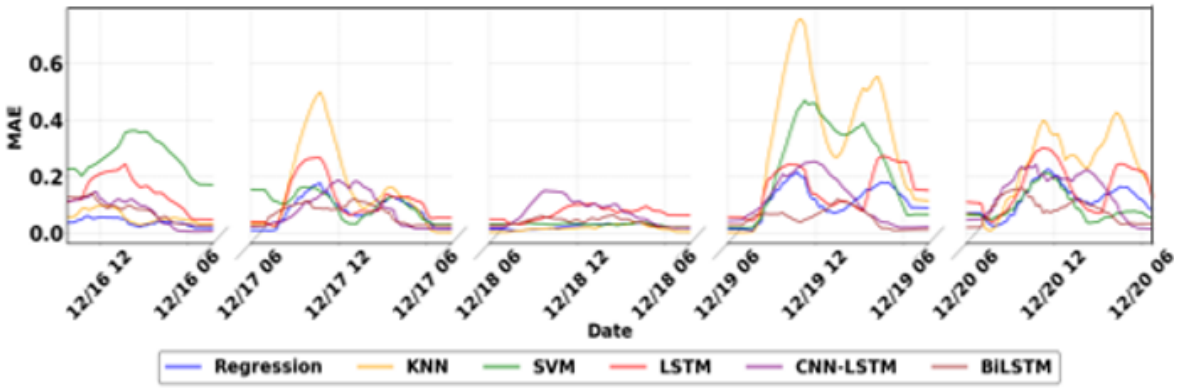

(a)

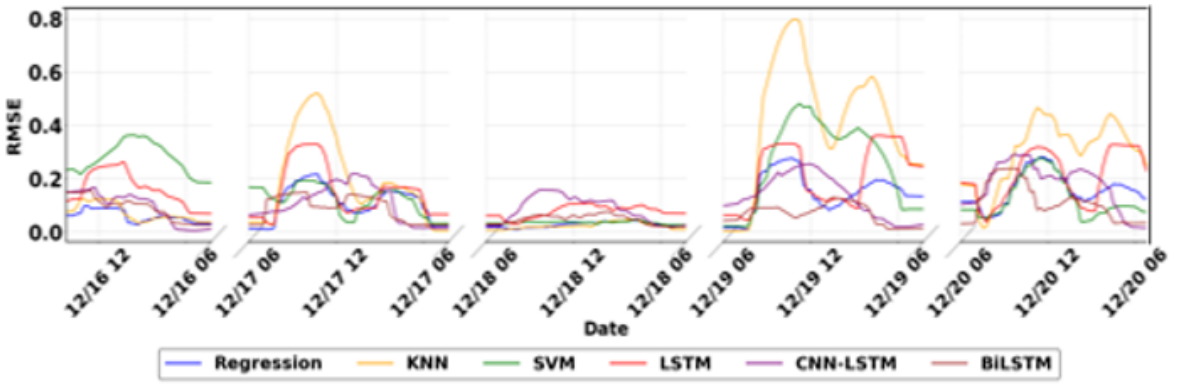

(b)

Figure 3.21: Rolling window performance metric analysis for different algorithms over the specified date range of December 2021: (a) MAE and (b) RMSE.

IQRs, with KNN displaying the highest IQRs among all algorithms and months, thus reflecting its higher prediction errors previously highlighted.

The demonstrated superiority of DL algorithms over non-DL techniques confirms the effectiveness of incorporating temporal feature extraction and sequential learning mechanisms. By leveraging memory-based architectures, DL models can better capture long-term dependencies, making them more resilient to variations in PV generation patterns. These results highlight the advantage of using DL approaches for improved solar power prediction.

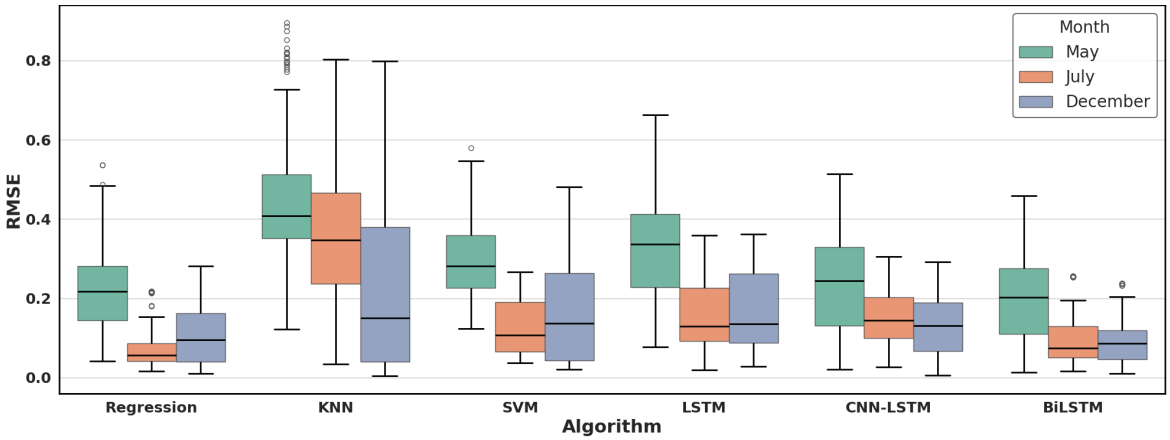

Figure 3.22: RMSE boxplots across models and months.

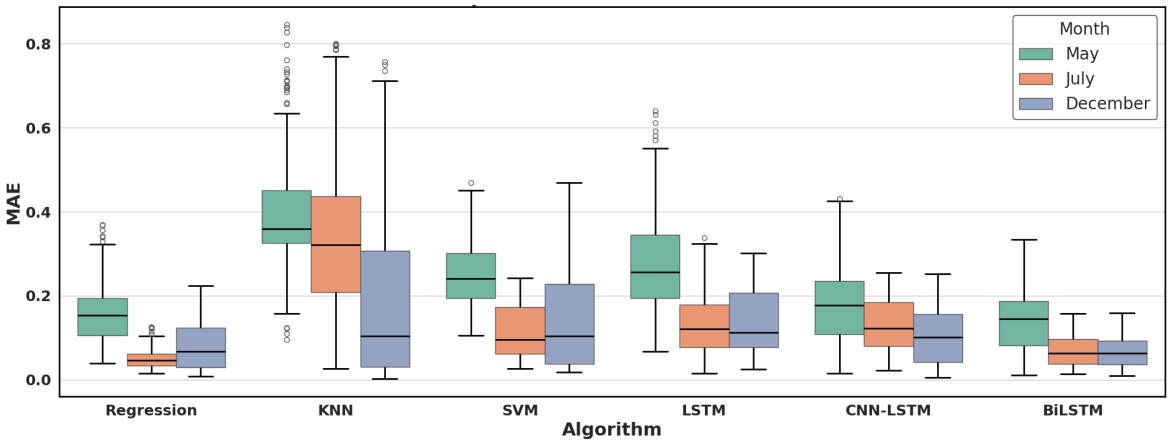

Figure 3.23: MAE boxplots across models and months.

3.8 Summary

This chapter introduced ML/DL based approaches for disaggregating PV power generation from net-load measurements, specifically separating the contributions of small PV systems from actual demand load. The proposed approach considered a range of data inputs, including net-load measurements, meteorological and irradiance data, satellite imagery, and temporal information. A Mask R-CNN model was first employed to detect solar PV panels from high-resolution satellite images, enabling accurate estimation of solar capacity and PV power generation. The results for the case study in the Waterloo region in Ontario, Canada, demonstrated that the identified PV capacity achieved an accuracy of approximately 98%. The synthetic PV data generated using a reliable software tool was then used for effective net-load disaggregation. The BiLSTM algorithm was shown to have superior precision with respect to estimated PV generation compared to several other ML/DL approaches. Overall, the results show that the proposed method should be useful for various feeder applications, offering robust performance for practical use.

Chapter 4

Modeling of Heat Pumps for Smart Residential Applications

Nomenclature

Parameters

G	Solar irradiance [W/m^2]
x	ML-model input parameters
y	ML-model output parameters

Variables/Functions

P_{HP}	Averaged electrical power consumption [W]
σ	Sigmoid activation function [pu]
$\tilde{C}_t$	Cell candidate [pu]
$\widehat{T}_i$	Estimated indoor temperature [°C]
C_t	Cell state [pu]
f_t	Forget gate [pu]

i_t	Input gate [pu]
o_t	Output gate [pu]
T_a	Ambient outdoor temperature [°C]
T_i	Indoor air temperature [°C]

4.1 Introduction

This chapter presents a data-driven framework for modeling the power and energy consumption of a central air-source HP in a Canadian home during winter, when HP electricity demand is significantly higher, based on actual measurements. The proposed approach employs supervised ML techniques, specifically ANN and LSTM networks, to model HP electricity consumption using inputs such as power demand measurements, outdoor temperature, temporal variables, and solar radiation. The developed models are evaluated against a physics-based model described in detail in [229,230] to evaluate the performance of the proposed data-driven models. The results obtained from actual measurements in a household in Milton, Ontario, Canada, demonstrate the superior performance of the proposed LSTM model, outperforming both the ANN and physics-based models, enabling accurate residential HP power and energy modeling to facilitate the deployment of demand-side flexibility in smart grids.

4.2 Machine Learning Models

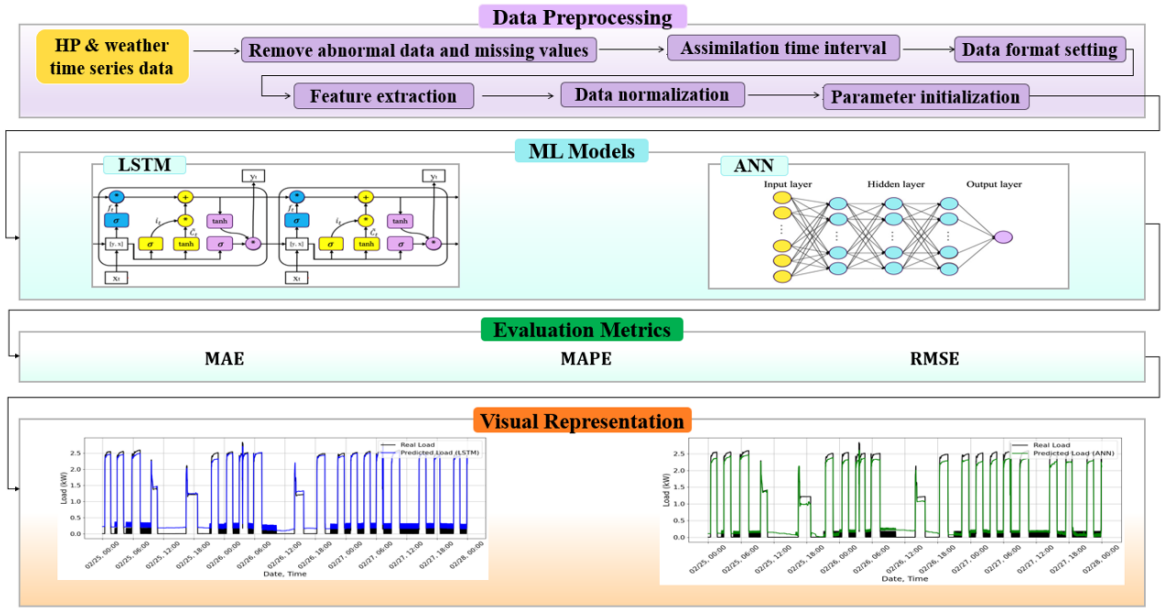

Figure 4.1: Framework for ML-based model for HPs.

Fig. 4.1 shows the block diagram of the proposed HP ML modeling framework, outlining the sequential flow of input features through each model's architecture and their integration within the overall workflow. As depicted, the process begins with the Data preprocessing stage, where raw HP and weather time-series data undergo cleaning, time-interval assimilation, formatting, feature extraction, normalization, and parameter initialization. The preprocessed features are then passed to the ML models layer, which utilizes LSTM and ANN architectures for load forecasting, as explained next. Model performance is assessed using standard Evaluation Metrics, including MAE, Mean Absolute Percentage Error (MAPE), and RMSE, before being rendered in the Visual Representation block to compare actual versus predicted load profiles.

4.2.1 ANN Model

ANNs are data-driven models capable of learning complex relationships between inputs and outputs without requiring explicit physical assumptions. In this study, a Multi-Layer Perceptron (MLP) architecture is used to model HP power consumption based on input features. The network consists of an input layer that receives environmental and operational variables, a hidden layer for capturing nonlinear interactions, and an output layer that captures the HP power consumption. The connections between nodes are defined by weights that are adjusted during training. Selecting the appropriate number of hidden layers and neurons is essential to balance the model's capacity to learn patterns from training data while maintaining generalization for unseen inputs [93].

The training process can be carried out using the backpropagation algorithm, which iteratively updates the weights to minimize the difference between modeled and actual outputs. The performance function, typically based on Mean Squared Error (MSE), guides the adjustment of weights and biases through gradient descent. The model is typically trained using a portion of the historical data, with validation and testing sets used to assess model accuracy. Once trained, the ANN is able to capture HP consumption based on available environmental and thermal inputs. Its ability to directly learn from data makes it suitable for applications where system dynamics are difficult to model explicitly or where real-time modeling is required [231].

4.2.2 LSTM Model

LSTM networks are specialized types of RNNs designed to model sequential data while mitigating the vanishing gradient problem. Unlike traditional RNNs, LSTM networks maintain a more stable memory through gated mechanisms, enabling them to learn temporal dependencies over longer sequences. In this study, the LSTM model is employed for short-term load modeling, leveraging existing data to capture HP power consumption with one-minute resolution [232].

Each LSTM unit, as shown in Fig. 4.2, contains the following four interacting components: a forget gate f_t, an input gate i_t, the cell candidate $\tilde{C}_t$, and an output gate o_t. These gates regulate the flow of information and maintain a controlled memory cell C_t across time steps. The forget gate f_t determines which parts of the previous cell

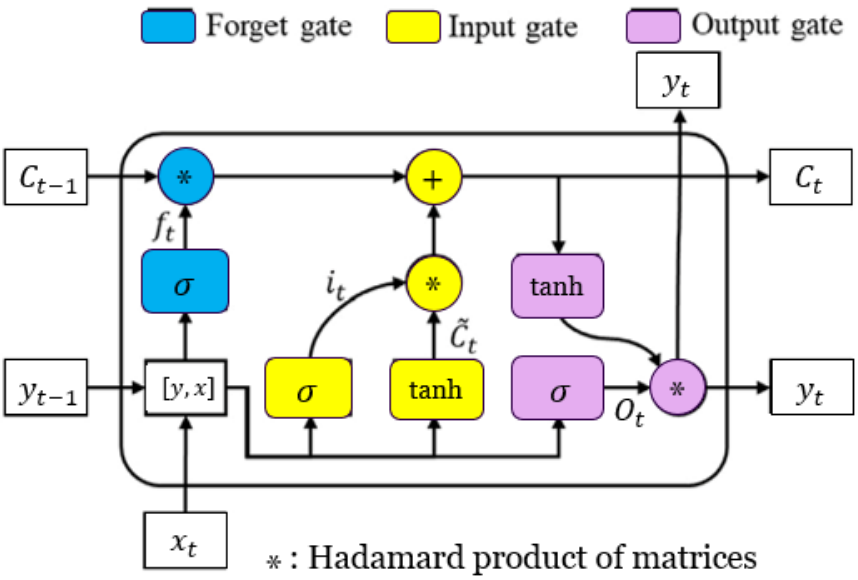

Figure 4.2: Structure of an LSTM cell.

state C_{t-1} to discard, while the input gate i_t identifies the new information to store. The cell candidate $\tilde{C}_t$ generates potential updates to the cell state, and the output gate o_t defines how much of the cell state contributes to the output at each step.

The LSTM model processes time series data by updating these gates at each time step, using both current inputs and hidden states from the previous step. This structure allows the network to capture both short- and long-term dependencies in power consumption patterns. For training, sequences are formed using sliding windows of past observations, so that the network learns to associate these sequences with the corresponding load values. The trained model can then be generalized to model electricity consumption based on incoming real-time data [166].

4.2.3 Evaluation Metrics

To assess the performance of the models, several widely used statistical error metrics were employed in this study, which include MAE, MAPE, and RMSE [229]. These evaluation criteria were selected for their effectiveness in measuring both the magnitude and scale of errors.



Figure 4.3: Case study of a detached house in Milton, Ontario, Canada, equipped with a Mitsubishi Zuba HP [233].

4.3 Results and Discussion

4.3.1 Household and Heat Pump Description

The case study considers a 232 m^2 Canadian single-family home in Milton, Ontario, depicted in Fig. 4.3, with standard insulation and modern energy-efficient construction. The thermostat controlling the HP is located in the living room, where the indoor temperature was measured.

The installed Mitsubishi Zuba Central HP (PVA-A36AA7/PUZ-HA36NKA) shown in Fig. 4.3 is a variable-speed unit designed for cold climates [233]. It provides a heating capacity of 9.7 kW at 8°C (with an operating range of 5.4–10.6 kW), 8.4 kW at −8°C, and 7.1 kW at −25°C, with corresponding COP values of 3.92, 3.2, and 3.0, respectively. The unit operates at 208/230 V, uses R-410A refrigerant, and has an electrical power draw ranging from 1.0 to 4.895 kW. In addition, a 10 kW auxiliary electric heater supports operation under extreme cold conditions.

A physics-based model of the studied residential HP system, developed based on the

same experimental setup and dataset, is used here for comparison purposes. The model combines a lumped Thermal Equivalent Circuit (TEC) representation of the building with a temperature-dependent HP COP model to estimate the thermal dynamics and electrical energy consumption of the system. The modeling parameters were identified through nonlinear optimization using measured indoor temperature data. A complete description of the model formulation, parameter identification procedure, and validation is available in [230], which is used here for evaluating the proposed ML models.

4.3.2 Data Collection and Preprocessing

High-resolution monitoring was conducted over almost 70 winter days (Dec. 20, 2024 to Jan. 20, 2025, and Jan. 24 to Mar. 1, 2025), with outdoor temperatures ranging from $-17°C$ to $10°C$. The dataset includes 1 min HP electrical power measurements from a dedicated meter and 1 min indoor temperature recordings at the thermostat location. Ambient temperature and solar irradiance were obtained from [234], and thermal radiation estimates were derived from [235].

High-quality data-driven models require comprehensive datasets with complete temporal and operational parameters. For this study, the dataset incorporates five primary data categories, namely, environmental conditions, temporal markers, interior thermal measurements, household HP information, and energy consumption records, as illustrated in Fig. 4.4. The data acquisition and preparation methodology proceeds through the following sequential stages:

Acquisition of Directly Measurable Parameters

The environmental and temporal parameters can be sourced from established monitoring systems. Meteorological observations spanning the measured days can be obtained from regional weather monitoring stations, including ambient temperature, dew point, relative humidity, global horizontal radiation, and diffuse horizontal radiation, recorded at short intervals (5 min).

Indoor Thermal Parameters and Load Data

Operational data for the house can be acquired through direct metering under real-world conditions.

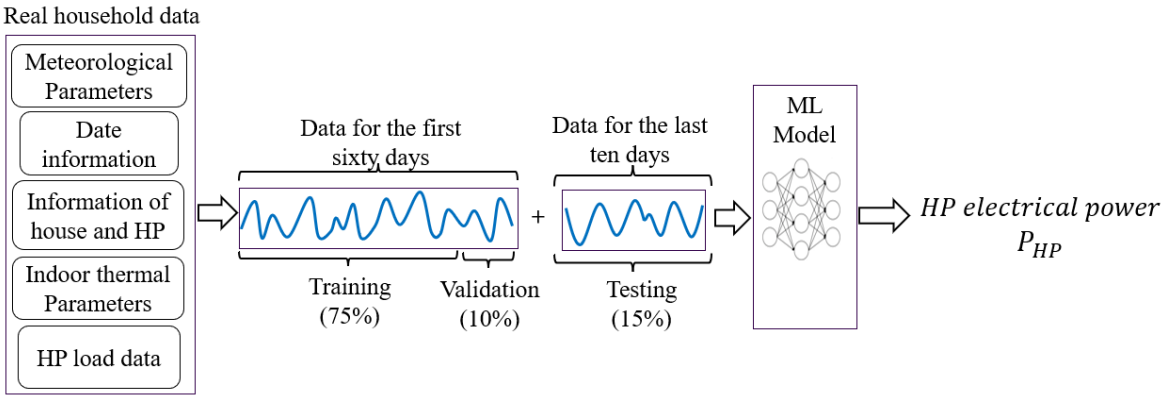

Figure 4.4: Overview of the datasets utilized.

Dataset Preparation

The temporal sequence data can be partitioned for model development, with a typical 75% allocated for training, 10% for validation, and the remaining 15% reserved for testing. All parameters require temporal synchronization and normalization procedures to enhance convergence stability and prevent parameter overfitting during the regularization process.

Feature Extraction

Effective HP load models require temporal features, in particular hour of the day, day of the week, and seasonality, to capture cyclical consumption patterns [236]. Environmental variables, especially ambient temperature and solar radiation, are also critical, as they directly influence heating and cooling demands. Moreover, selecting features that have a strong correlation with HP load, particularly indoor temperature, can improve modeling accuracy. Thus, these features were used here to develop the ML models described next.

4.3.3 Hyperparameters

To ensure a fair and consistent comparison, the LSTM and ANN models were configured using a uniform training strategy. The architecture and training configurations for the obtained models are summarized in Table 4.1. The LSTM model architecture

Table 4.1: Hyperparameters of LSTM and ANN Models

Parameter	**LSTM Model**	**ANN Model**
Architecture	LSTM (128) Dropout (0.2) Dense (1)	Dense (64, ReLU) Dropout (0.2) Dense (1)
Optimizer	Adam (lr* = 0.005)	Adam (default lr*)
Batch Size	1000	1000
Epochs	30	30
Early Stopping	Patience (5) min_delta (0)	Patience (5)
Loss Function	MSE	MSE
Validation Data	Yes	Yes

*lr: learning rate

comprises a single LSTM layer with 128 units, followed by a dropout layer with a rate of 0.2, and a final dense output layer with one neuron. The ANN model includes a dense hidden layer with 64 neurons activated by the ReLU function, followed by a dropout layer with a rate of 0.2, and a dense output layer with one neuron. Both models were trained using the Adam optimizer, with a learning rate of 0.005 for the LSTM and the default learning rate for the ANN. A batch size of 1000 was selected, and the training process was conducted for up to 30 epochs. Early stopping was employed to prevent overfitting, with a patience of 5 epochs and a minimum delta of 0 for the LSTM model. These parameters are based on [166], which were tuned through trial and error. The MSE was used as the loss function for both models. Validation data are used during training to monitor generalization performance.

4.3.4 Application and Comparison

Fig. 4.5 compares the ML-based and physics-based models for selected cold winter days, along with outdoor and indoor temperature profiles. Observe that, as confirmed

Table 4.2: Energy Modeling of Proposed Models

Model	**Window**	**Energy [kWh]**	**MAE [kWh]**	**RMSE [kWh]**	**MAPE [%]**
LSTM	24 hours	37.28	0.3416	0.3870	1.88
LSTM	1 week	209.00	1.7760	1.9820	1.97
ANN	24 hours	35.78	0.5822	0.6648	3.64
ANN	1 week	199.09	1.7260	2.2660	1.97
Physics-based	24 hours	33.90	1.1486	1.5547	8.10
Physics-based	1 week	237.71	13.9370	18.3670	12.41

by the errors presented in Table 4.2, the physics-based model reasonably captures overall energy use and general load trends, and provides insight into thermal and control processes, but does not accurately reproduce short-term demand variations. On the other hand, the LSTM-based ML model delivers superior accuracy, modeling the temporal dependencies and internal building dynamics that make it particularly effective for capturing HP load across varying weather patterns.

Table 4.3 summarizes the data-driven modeling performance of all models across various input window sizes ranging from 1 hour to 1 week for a few cold days at the end of February 2025. The results demonstrate that the LSTM generally outperforms the ANN and physics-based models across most time windows and evaluation metrics. Note that for the shortest window of 1 hour, the LSTM model significantly outperforms the ANN and physics-based models. As the input window increases, the performance of both ML-based models tends to decrease; however, the LSTM maintains superior accuracy throughout. For the 24-hour window, the LSTM achieves the lowest MAE and RMSE among all models, indicating that it is the best-performing approach, while the ANN yields slightly higher errors. While ANN reaches its best MAPE for a 6-hour window, the LSTM achieves a lower MAPE for a 1-week window. Notably, the LSTM's RMSE remains stable and low across all window sizes, further underscoring its strong

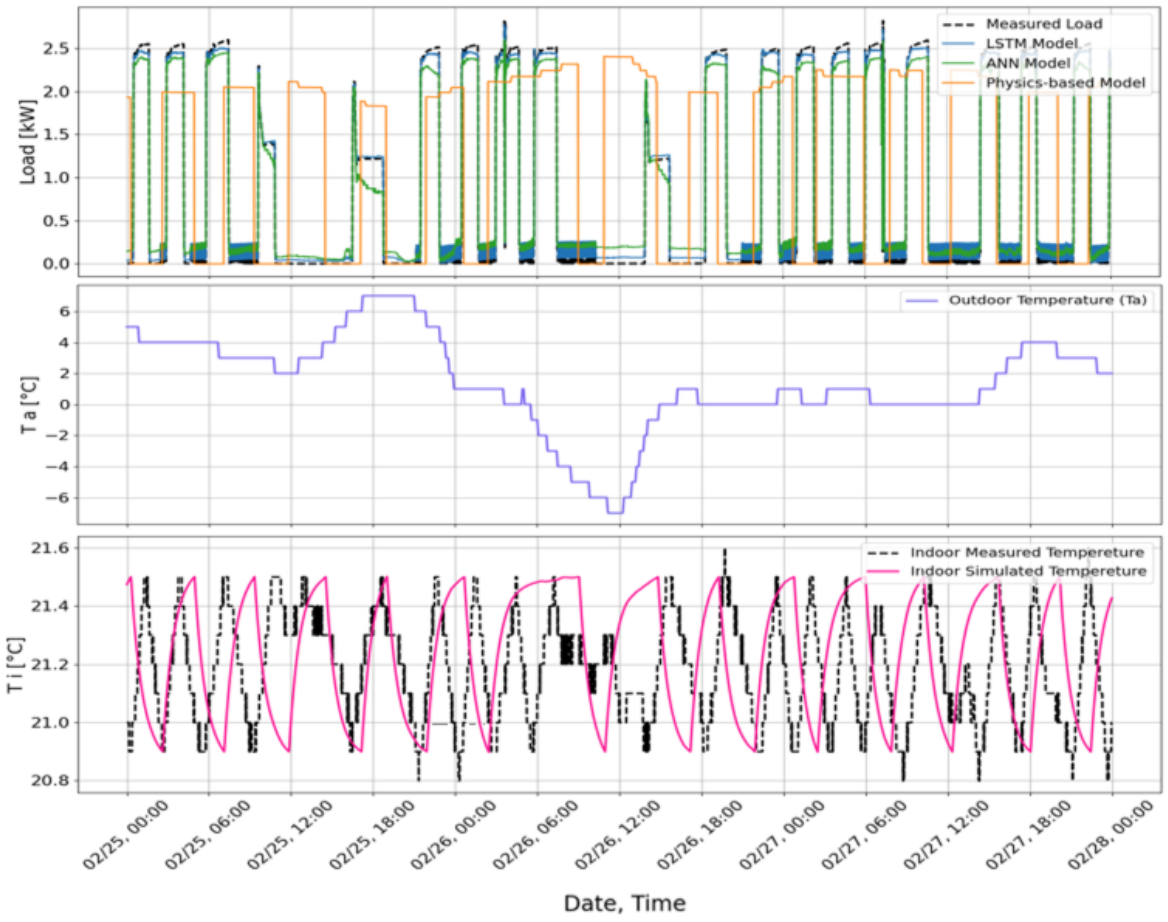

Figure 4.5: Measured vs. LSTM, ANN, and physics-based load estimates, outdoor temperature T_a and indoor temperature T_i for some cold days at the end of February 2025.

Table 4.3: Power Estimation Errors for the Proposed Models

Model	**Window**	**MAE [kW]**	**RMSE [kW]**	**MAPE [%]**
LSTM	1 hour	0.0155	0.0206	2.04
LSTM	6 hours	0.0430	0.0541	13.76
LSTM	24 hours	0.0485	0.0575	13.11
LSTM	1 week	0.0480	0.0545	12.73
ANN	1 hour	0.1555	0.1615	7.03
ANN	6 hours	0.1384	0.1519	12.32
ANN	24 hours	0.1282	0.1452	13.56
ANN	1 week	0.1358	0.1565	14.53
Physics-based	1 hour	0.2618	0.4817	49.56
Physics-based	6 hours	0.7533	1.2623	177.37
Physics-based	24 hours	1.1758	1.6233	222.16
Physics-based	1 week	1.2306	1.5994	280.98

generalization capabilities and adaptability to different temporal contexts.

As shown in Table 4.3, the physics-based model shows larger errors, particularly over short time scales, due to limited representation of fast load fluctuations and simplified HP dynamics and control behavior. However, it maintains reasonable agreement over longer periods and provides strong interpretability through explicit thermodynamic and system parameters, supporting scenario analysis and system-level understanding despite lower short-term accuracy than ML approaches.

4.4 Summary

This chapter proposed an ML-modeling framework based on ANN and LSTM techniques to estimate power and energy consumption of a central air-source HP in residential applications using actual indoor temperature and demand data. The presented supervised ML models were compared with an existing physics-based model, demonstrating that the developed ML model can properly capture complex cold-climate heating patterns with high short-term accuracy. Overall, the results of applying the proposed approach to a residential HP in Canada during the winter season highlight that the presented LSTM model is best suited for high-resolution short-term representation of HP power consumption.

Chapter 5

Heat Pump Load Disaggregation for Transmission System Applications

Nomenclature

Indices

$i \in \mathcal{P}$	Index for the set of units or devices
t	Time index (hour of operation)

Parameters

$c_{p,\text{air}}$	Specific heat capacity of air [kWh/kg·K]
$\dot{m}_{\text{air}}$	Air mass flow rate [kg/h]
P_i	Power of unit i [kW]

Variables/Functions

ΔT	Temperature rise [K]
x_i	Statistical weighting factor
$\epsilon_t^{\mathbf{HP}}$	Error term in HP load estimation [kW]
$P_{th}^{\mathbf{HP}}$	Thermal output of the HP [kW]
$P_e^{\mathbf{HP}}$	Electrical input of the HP [kW]
$P_t^{\mathbf{HP}}$	Deterministic estimate of the HP load profile [kW]
P_t^{Net}	Transmission net load [kW]
$\widehat{P}_t^{\mathbf{HP}}$	Estimated HP load at hour t [kW]
$\widehat{P}_t^{\mathrm{D}}$	Estimated demand at time t [kW]
$\widehat{P}_{\mathrm{Aggr},t}^{\mathrm{HP}}$	Synthesized aggregated HP load profile at time t [kW]
$\widehat{P}_{i,t}^{\mathrm{HP}}$	Individual stochastic HP load profile of unit i [kW]
$\widehat{P}_{\mathrm{Forc},t}^{\mathrm{HP}}$	Forecasted HP load [kW]

5.1 Introduction

HP load profiles in various regions around the world are essential for evaluating the performance of clean technologies and the impact of operational strategies on large-scale transmission systems. Traditionally, these profiles are either unavailable or, in rare cases, based on field measurements and load surveys, which are both case-dependent and resource-intensive. Hence, this study proposes a practical methodology for system operators to extract aggregated residential HP demand embedded in transmission-level net-load measurements with limited additional meter data. To establish baseline HP

profiles and capacity, publicly available statistics, GIS data, typical house characteristics, ML models, and statistical techniques are proposed here. Thus, in this study, probabilistic synthetic load profiles are generated using a combination of physics-based simulations and data-driven techniques based on a real HP dataset. An ML framework is then employed for load forecasting HP disaggregation applications, showing that the synthetic profiles effectively capture temperature-dependent behavior and reasonably approximate expected HP behavior. Finally, these profiles are used for load disaggregation at the transmission system level using actual data from a HV/MV substation in Milton, Ontario, Canada, to demonstrate the practical relevance for the proposed techniques for the IESO of Ontario.

5.2 Methodology

This section outlines the proposed methodology for HP load modeling and disaggregation using transmission-level measurements. In feeders with numerous unmonitored HP units, as illustrated in Fig. 5.1, accurately disaggregating HP demand provides valuable insights for system planning. Thus, the present study focuses on estimating aggregated residential HP consumption from HV/MV transmission feeder measurements, considering that multiple distributed HPs are connected to the transmission system.

A detailed overview of the proposed stochastic synthetic HP load generation and disaggregation methodology is provided in Fig. 5.2, beginning with the collection of input data, including multi-year meteorological data in Step 0. Steps 1 and 2 involve developing a simulation model for individual HPs over multiple years, based on real HP load data and meteorological inputs. Steps 3 and 4 focus on identifying residential building characteristics using GIS data and estimating heating capacities for different building types, which are used for HP load characterization in Step 5. Based on these inputs, stochastic synthetic HP load profiles can be generated in Step 6 for multiple households and aggregated in Step 7, based on weighting factors and correlated features at the HV/MV transformer level, extracted from available documentation regarding HP deployment in the region of interest. Using publicly available regional statistics, such as population and the number of houses of the various types identified in Steps

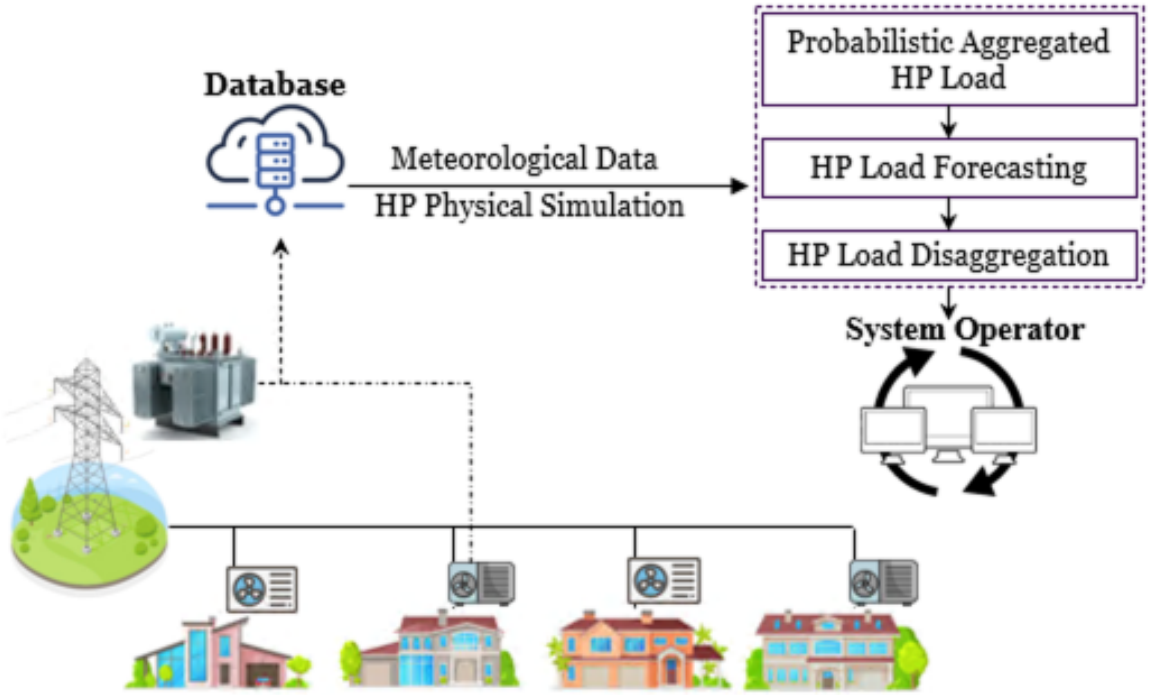

Figure 5.1: HP load identification at the transmission system level from net-load measurements.

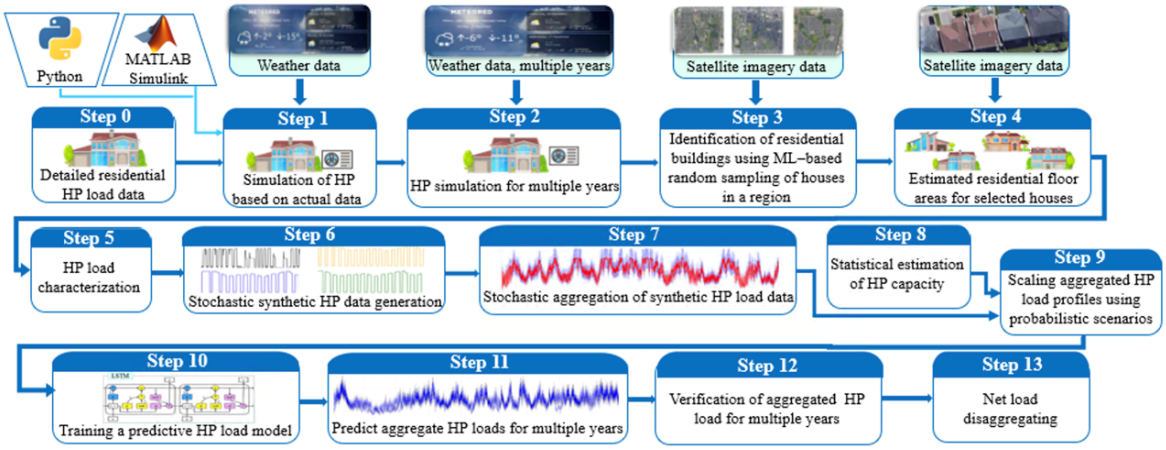

Figure 5.2: Generation of stochastic synthetic HP load data.

3 and 4, the HP capacity for a given region can be estimated in Step 8, which is then used in Step 9 to scale up the synthetic load profiles generated in Step 7 to obtain the total aggregated synthetic HP load. An ML model is then trained on the aggregated HP load profiles in Step 9 to enable prediction of HP demand over multiple years in Steps 10 and 11, which is followed by verification of the results in Step 12. Finally, the result of this prediction can be used for net load disaggregation in Step 13. Each of the aforementioned steps is described in detail next.

5.2.1 Heat Pump Modeling and Synthetic Load Generation

This section presents the methodology used to generate synthetic HP load profiles based on an actual measured dataset. Ideally, comprehensive numerical simulations would rely on a large and diverse collection of HP operational data. However, obtaining load measurements from all HP owners is rarely feasible, and the availability of publicly accessible datasets suitable for expanding the numerical experiments is limited. Hence, the generation of stochastic synthetic HP load data is proposed here.

The proposed synthetic HP load generation, corresponding to Steps 1 and 2 in Fig. 5.2, is predicated on a physics-based modeling approach, discussed in detail in [230], which considers the HP thermodynamic behavior, control dynamics, and operational constraints that accurately capture the performance of HP systems. The

model used incorporates temperature-dependent efficiency, thermal system characteristics, cycling behavior, and operational behavior, enabling realistic simulation of both steady-state and transient responses, including transitional effects that cause deviations from ideal steady-state assumptions and significantly influence short-term power demand. By accounting for these dynamics, the model can be used to provide a reliable prediction of expected HP electricity consumption under varying environmental and load conditions, forming a robust foundation for load disaggregation and capacity estimation studies.

In Step 3, to make synthetic HP load profiles more realistic for the studied region and to capture variability in building characteristics and operational conditions, it is necessary to identify regional building attributes, including house types, floor areas, and other relevant features, which enable more accurate parameter adjustments for HP load profile generation. This is accomplished using GIS data to randomly select residential buildings using an ML-based image processing approach. In Step 4, the same GIS data can be employed to estimate the floor areas of the selected houses. The synthetic HP data generation in Step 6 is then based on the HP load characterization performed in Step 5.

A detailed overview of the proposed synthetic HP load modeling framework is illustrated in Fig. 5.3, which begins with the preprocessing of single HP load and weather data, allowing the simulation and validation of a single HP model for multiple years. Thus, key features that influence HP performance can be extracted by conducting a correlation analysis of important characteristics used for synthetic HP simulation and validation based on previous studies [116, 237]. This yields key influencing features, namely HP brand and model, that are closely related to building characteristics, weather conditions, thermostat setpoints, and COP, which are the primary features affecting HP operational behavior and load profiles. Of the latter, the most significant parameter defining HP load is the COP [230], which establishes the following relationship between thermal output and electrical input:

$$\mathrm{COP} = \frac{P_{th}^{\mathrm{HP}}}{P_{e}^{\mathrm{HP}}} \tag{5.1}$$

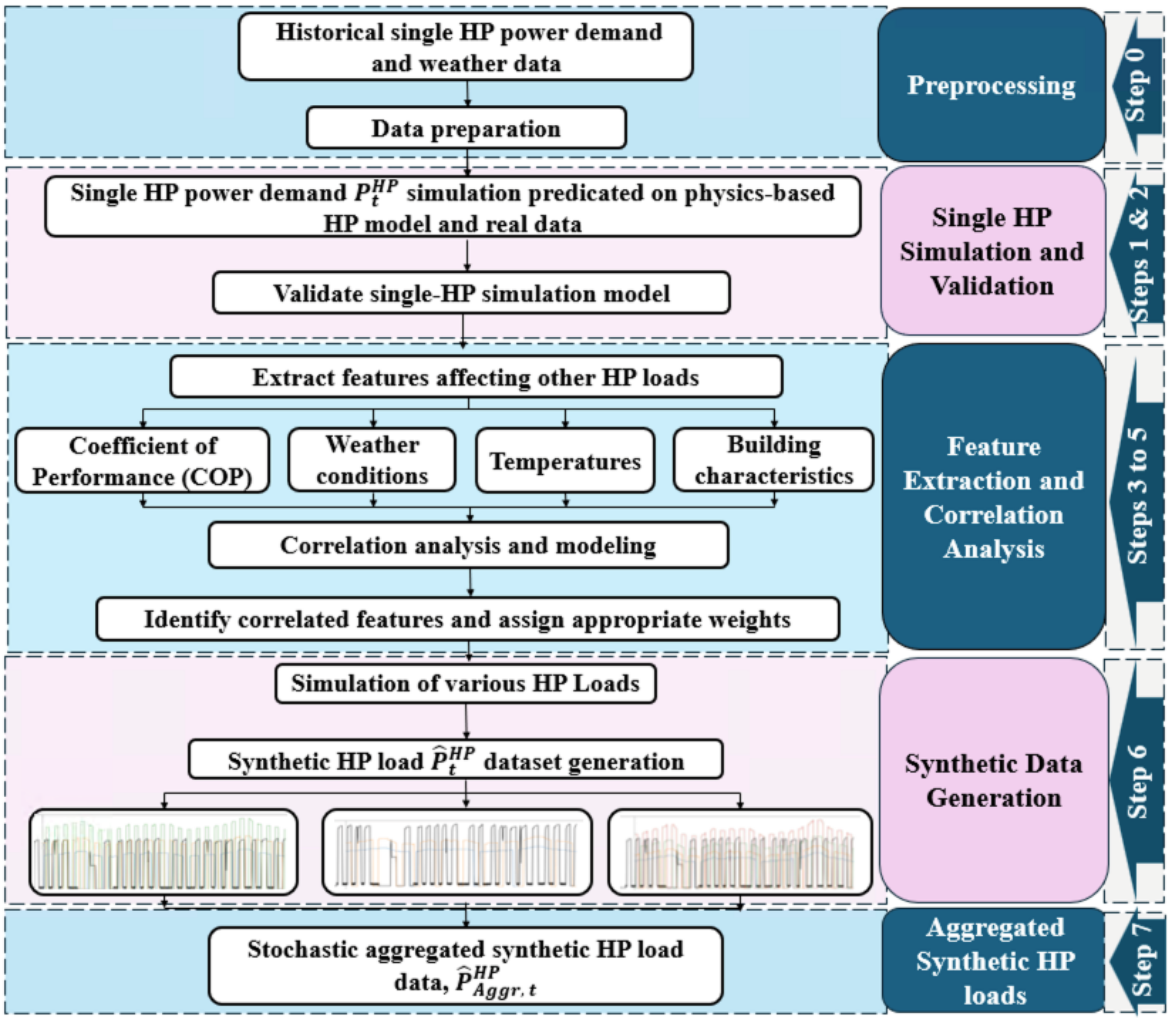

Figure 5.3: Detailed overview of proposed physics-based HP synthetic data generation.

$$\Delta T = \frac{P_{th}^{\mathrm{HP}}}{c_{p,air}\,\dot{m}_{air}} \tag{5.2}$$

where P_e^{HP} is the electrical input HP power in kW, P_{th}^{HP} is the HP thermal output in kW, ΔT is the temperature rise in K, $\dot{m}_{air}$ is the air mass flow rate in kg/s, and $c_{p,air}$ is the specific heat capacity of air in kJ/kg·K. Studies show that even for the same HP

model in similar houses and conditions, COP values may vary, resulting in a probability range for COP and its effect on performance [238]. The COP of similar HPs can then be represented as a scatter plot around a temperature-dependent average line, enabling the generation of probabilistic COP values for these HPs [116]. Considering that distributed HP systems are installed in diverse residential environments with different configurations, the COP can be modeled as a function of temperature time series and the specific HP model number and brand, which are related to the HPs capacity and design.

Based on the aforementioned framework, an expanded synthetic HP dataset can be constructed through stochastic expansion techniques to increase the effective sample size for simulation and analysis, representing multiple HP configurations [239]. Thus, a probabilistic model that represents the estimated synthetic HP load $\widehat{P}_t^{\mathrm{HP}}$, which explicitly accounts for uncertainty, can be defined as follows:

$$\widehat{P}_t^{\mathrm{HP}} = P_t^{\mathrm{HP}} + \epsilon_t^{\mathrm{HP}} \tag{5.3}$$

where P_t^{HP} represents the deterministic estimate of the HP load profile, and ϵ_t^{HP} denotes the stochastic deviation arising from modeling uncertainty and variability in operational behavior. This process relies on a probabilistic modeling framework that enables the generation of diverse HP models and operating conditions by combining probabilistic parameter variation with random sampling. This approach produces synthetic datasets representing different HP units while capturing differences in building characteristics and operational conditions to address the limited size of the available HP dataset.

As shown in Fig. 5.3, Step 7 involves HP stochastic load aggregation, which is formulated as a weighted sum of stochastic synthetic individual HP load models. In this case, assigning appropriate weights to each probabilistic HP load enables the aggregated HP load to capture the combined contributions of diverse HP configurations operating under varying conditions and uncertainties. A variance-based selection criterion ensures sufficient coverage of the underlying uncertainty space. The aggregation yields a set of candidate HP load scenarios which account for uncertainties in residential floor area, HP brand and model, thermostat setpoints, and probabilistic COP behavior.

The aggregated stochastic load profile can thus be defined as a convex combination of these candidate scenarios, as follows:

$$\widehat{P}^{\mathrm{HP}}_{\mathrm{Aggr},t} = \sum_{i \in \mathcal{P}} x_i \, \widehat{P}^{\mathrm{HP}}_{i,t} \tag{5.4}$$

where $\widehat{P}^{\mathrm{HP}}_{\mathrm{Aggr},t}$ represents the synthesized aggregated HP load profile at time t, $\widehat{P}^{\mathrm{HP}}_{i,t}$ denotes an individual stochastic HP load profile, and $x_i \in [0, 1]$ is the associated weighting factor, which statistically represent, for the region of interest, the house types, brands and models of deployed HPs, temperature set points, and COP stochastic values within a chosen range, as previously explained, assuming uniform probability, and based on market and behavior studies. The weighting vector x determines the contribution of each scenario to the final aggregated profile [239]. This variance-oriented approach promotes diversity in the generated profiles, enabling representation of both extreme and intermediate HP demand levels while preserving computational tractability under limited data availability.

5.2.2 Heat Pump Demand Disaggregation

As previously discussed, the goal of the HP and load disaggregation is to identify the HP load in an available aggregated load profile. In this context, accurate HP load modeling plays a key role in predicting the power consumption patterns of heating and cooling systems. In this paper, HP load modeling was used to generate synthetic HP demand profiles, as detailed in Section 5.2.1, to improve the accuracy of the aggregated HP load profile at HV/MV substations.

The proposed disaggregation approach is illustrated in Fig. 5.4, based on the stochastic aggregated HP load profiles generated in Step 7, which are used together with an estimation of the installed HP capacity in Step 8 for the study region to determine the total HP aggregated load in Step 9. To accomplish this, the equivalent aggregated HP capacity needs to be estimated in Step 8, using publicly available statistics, since no direct data are available on the installed HP capacity in the study area. These public datasets provide information on the number of installed HP units in the region of interest and allow tracking of their adoption and growth over time, including

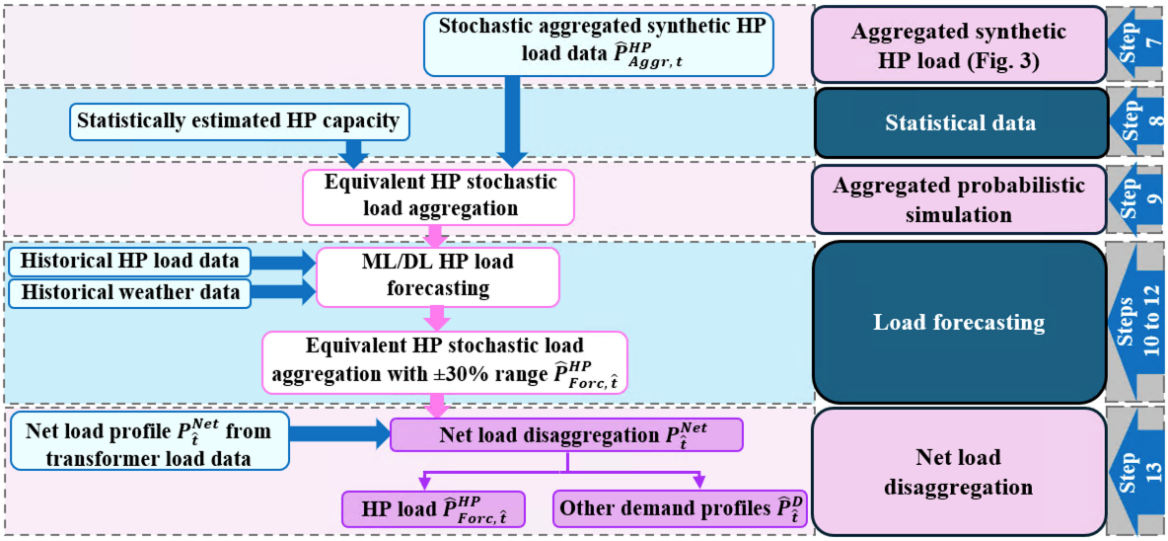

Figure 5.4: Proposed approach for disaggregating net-load components.

statistics on regional HP penetration rates and the distribution of household types in the region. Thus, in Step 9, the equivalent HP stochastic load aggregation is obtained through a scaling process, which multiplies the load profile obtained in Step 7 by a constant factor derived from the statistically estimated HP capacity in Step 8 for a specific year.

Steps 10, 11, and 12 focus on forecasting and verifying the aggregated HP load for time $\widehat{t}$ at which the HV/MV transmission load measurement $P^{\text{Net}}_{\widehat{t}}$ was taken. This can be accomplished using ML/DL time series algorithms, such as LSTM networks, to estimate aggregated HP demand for future years using historical aggregated HP load and weather data, which yields a forecasted HP load $\widehat{P}^{\text{HP}}_{\text{Forc},\widehat{t}}$ at a given time $\widehat{t}$. A ±30% wide range is considered to account for stochastic deviations arising from modeling uncertainty. Since no real data are available for validation, statistical methods such as probability density function (pdf) analysis and correlation analysis are used for verification, which characterize the distribution and variability of the aggregated HP load. The load can then be disaggregated in Step 13 as follows:

$$\widehat{P}^{\text{D}}_{\widehat{t}} = P^{\text{Net}}_{\widehat{t}} - \widehat{P}^{\text{HP}}_{\text{Forc},\widehat{t}} \tag{5.5}$$

where $\widehat{P}^{\mathrm{D}}_{\widehat{t}}$ is obtained from the measured net demand $P^{\mathrm{Net}}_{\widehat{t}}$ and the forecasted HP load $\widehat{P}^{\mathrm{HP}}_{\mathrm{Forc},\widehat{t}}$.

5.3 Results, Validation and Verification

5.3.1 Data Description and Processing

Proper preparation of data inputs is essential to ensure adequate results. The input components of the proposed methodology define the required sampling resolution, time-series coverage, and statistical representativeness. These inputs are preprocessed within the input modeling stage to generate probabilistic synthetic profiles of HP load consumption. The framework considers the following multiple HP conditions and key influencing factors:

Transmission-Level Measurement

The first dataset consists of transmission-level net-load data provided by the IESO, corresponding to four HV/MV transformers in Milton, ON, Canada, shown in Fig. 5.5, and related grid layout data to identify the region of interest [240]. The dataset contains electricity measurements in MW with a 1 min sampling interval, spanning the period from January 2022 to December 2025. These measurements provide information on aggregate load behavior at the transmission level, which is essential for HP load disaggregation and analysis.

HP Data

This dataset consists of measurements from an HP located in Milton, ON. The unit is a Zuba model PUZ-HA36NKA, with a nominal heating capacity of 38,000 BTU/h and a cooling capacity of 33,000 BTU/h. The minimum and maximum heating capacities range from 18,600 BTU/h to 40,000 BTU/h [241] for a 232 m^2 residential house. Detection of residential HPs is generally more effective during winter, when space-heating demand dominates [104]; thus, using data for December to March improves the identification of HP load signatures and reduces the dataset size required for reliable detection. In this study, the dataset covered the period from January 2025 to March 2025, with electricity consumption recorded in kWh with 1 min resolution.

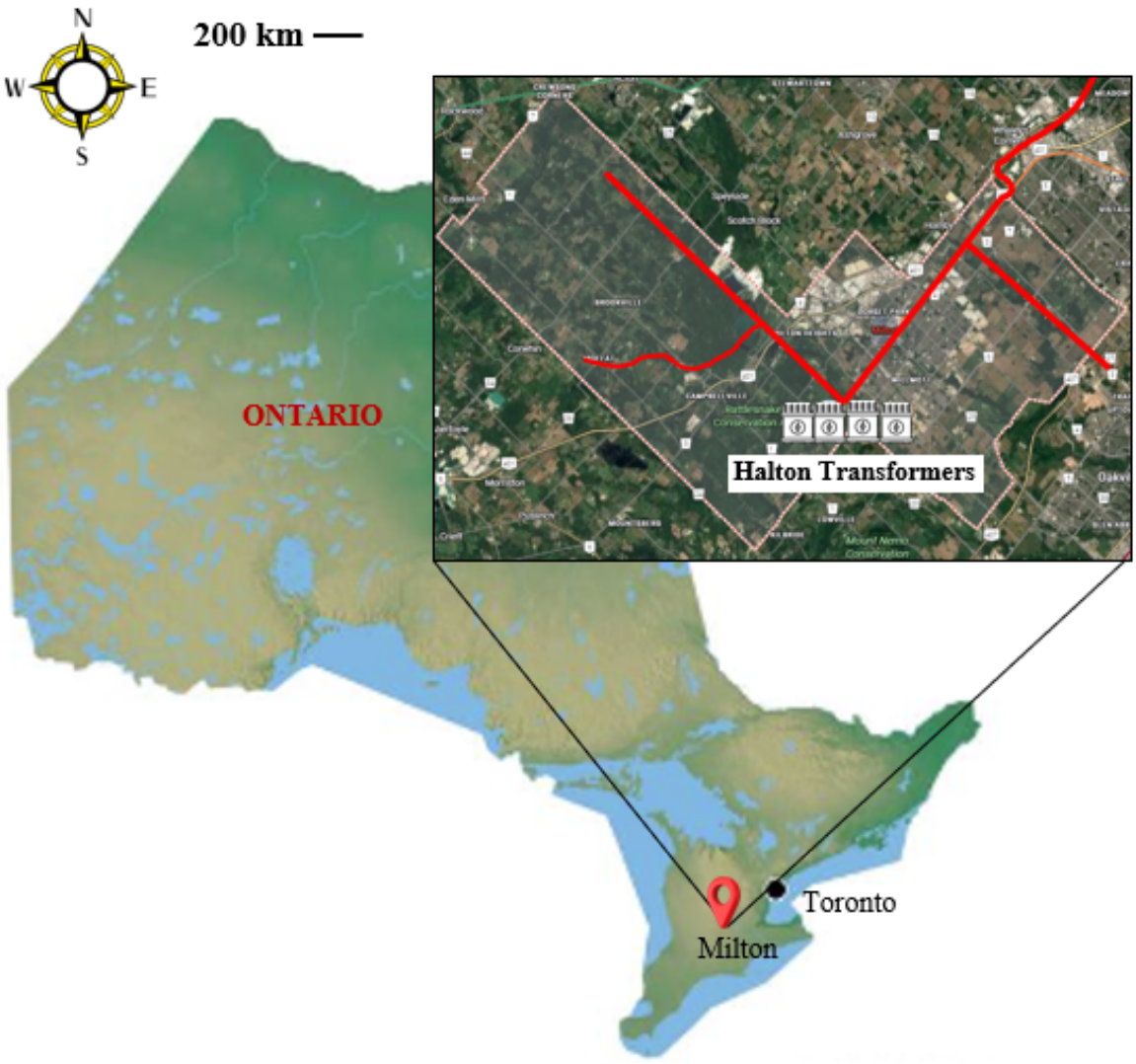

Figure 5.5: Milton region in Ontario, Canada.

Indoor Temperature Data

Indoor temperature measurements were gathered using standard temperature meters installed within the household with 1 min resolution. These measurements provide key input for modeling HP heating cycles and energy consumption.

Temporal Features

HPs operate in heating and cooling cycles that result in regular periods of on and off operation [31]. Leveraging temporal information, such as the time of day, day of the week, and day of the year, can enhance the contextualization of models by capturing these cyclical behaviors and improving the accuracy of HP load predictions.

Meteorological Data

The heat demand of a building typically increases as the ambient temperature decreases. Therefore, outdoor temperature and solar radiation are used as key inputs for HP load simulations, with 5 min resolution for the Milton region from the relevant weather stations [242], resampled to a 1 min resolution using linear interpolation.

GIS Data

GIS-based data provide a practical means of estimating household characteristics for the region of interest, such as typical house types and average floor areas, that are often unavailable to grid operators. Since dwelling area is closely related to thermal energy demand, particularly in Canada, space heating dominates residential consumption, which allows the identification and modeling of HP usage. In this study, GIS data and satellite imagery from Google Maps were used to characterize and size residential buildings in the Milton area of interest and to provide spatial context for HP load modeling.

HP Capacity Data

Public data statistics provide a practical and reliable approach for estimating the number of installed HPs within the studied region and for tracking their adoption and growth over time [243, 244]. This approach is particularly useful, considering that direct access to detailed technical information about individual households is rarely available. In this study, publicly available statistics related to HP installations in Ontario between 2022 and 2025 were used to approximate regional HP penetration. These data, together with information on household types in the Milton region [245], were used to estimate the aggregated HP capacity and inform the probabilistic modeling framework.

HP Market and Technology Data

Available market statistics on leading manufacturers, commonly installed brands, and representative models were used to inform realistic assumptions regarding HP system performance and capacity ranges [246]. Incorporating this information ensures that synthetic load modeling reflects prevailing market conditions, enhancing the accuracy and representativeness of aggregated HP load profiles in the region of interest.

Data Collection and Preprocessing

Time-series data were synchronized to a 1 min resolution. Preprocessing steps include normalization, noise filtering, and feature extraction to ensure accurate and reliable results.

5.3.2 Synthetic Heat Pump Load Generation

As shown in Fig. 5.3, Steps 1 and 2 of the synthetic data generation process are based on HP simulation and validation. Hence, a physical simulation framework was first developed for a residential building, based on building characteristics, and its associated HP model using a 2025 real dataset. The simulation model was then used to generate an HP load profile for 2022 within the Milton region based on historical meteorological data. Fig. 5.6 presents the simulated HP electrical load profiles for January to March 2022 and 2025.

The synthetic load profiles for the HP considered are followed by the identification and extraction of key features that influence system performance in Steps 3 to 5, which are then used to drive the simulation of representative load profiles. Various features can be incorporated into the load profile generation process, including HP brand and model, specifications related to building characteristics, thermostat setpoints, a probabilistic COP representation, date and time, temperature, and irradiance levels.

Since detailed information on HP capacity, brand, and model was not available, market research was used for the region of interest. Thus, it was concluded that Mitsubishi Zuba and Carrier are among the most widely used HP brands in Canada [246], and hence these two brands were selected for modeling. Since Mitsubishi Zuba is the market leader, it was assumed that 60% of HP units are Mitsubishi Zuba and

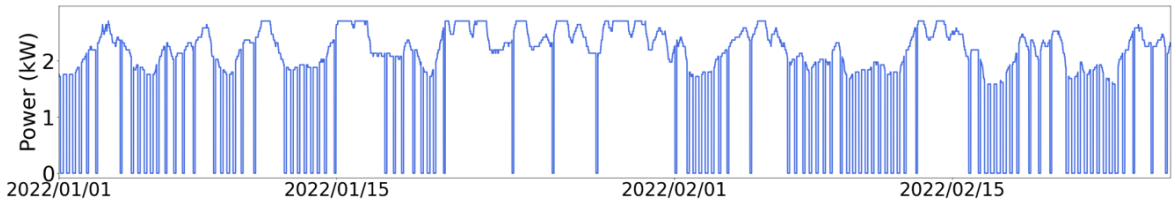

(a)

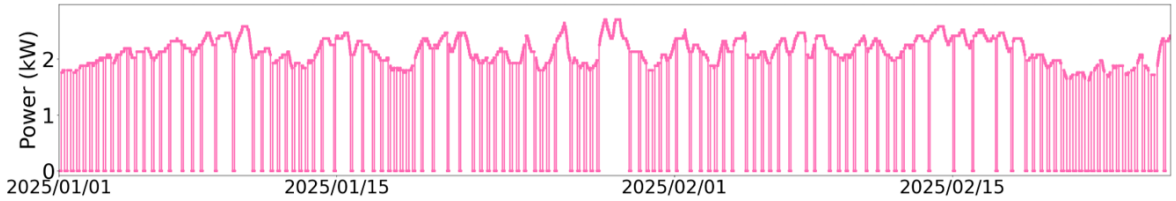

(b)

Figure 5.6: Simulated HP electrical load for January to March in (a) 2022 and (b) 2025.

40% are Carrier. Heating performance and capacity data for each brand and model, which can be estimated from the house sizes, were obtained from the manufacturers' technical catalogs [241, 247].

Since there is no available information identifying which specific houses are equipped with HPs to determine their capacities, satellite imagery data were utilized to analyze housing types and sizes in the Milton region. To minimize bias, a random sampling approach was applied using ML techniques and the OpenCV library [165]. In this context, the study area was divided into 11 representative blocks, with four houses randomly selected from each block to analyze housing types and estimate residential building sizes, and thus associated HP brands and models. Fig. 5.7 shows a representative block illustrating the random house selection process, where the red marks indicate the randomly selected houses. The resulting data were used to derive probabilistic estimates of typical housing types and sizes in Milton, which were then employed to estimate residential heating loads for the HP model and brand selection, resulting in 4 different HP Mitsubishi Zuba models and 3 different HP Carrier models, i.e., a total of 7 HP types, with different heating capacity, as determined by the building charac-



Figure 5.7: Milton area for random house size selection.

Table 5.1: Probability of Thermostat Setpoints [237]

Set Point [°C]	20	21	22	23	24
Probability	25%	30%	20%	15%	10%

teristics. Houses with floor areas exceeding the practical heating capacity of a single commercially available HP were excluded from the analysis. Based on the random sampling results, 36 out of the 44 selected houses were identified as suitable candidates for HP installation, with heating demands that could be adequately met by various single units of the 7 different HP types selected.

The third feature influencing HP power consumption is the thermostat set point, which affects the number of on/off cycles. A study analyzing heating set point preferences among Canadian households provides detailed insights for this parameter [237]. Based on this reference, assumptions for different set points were incorporated into the simulation. Table 5.1 shows the range of set points from 20°C to 24°C for Canada, along with the associated probabilities.

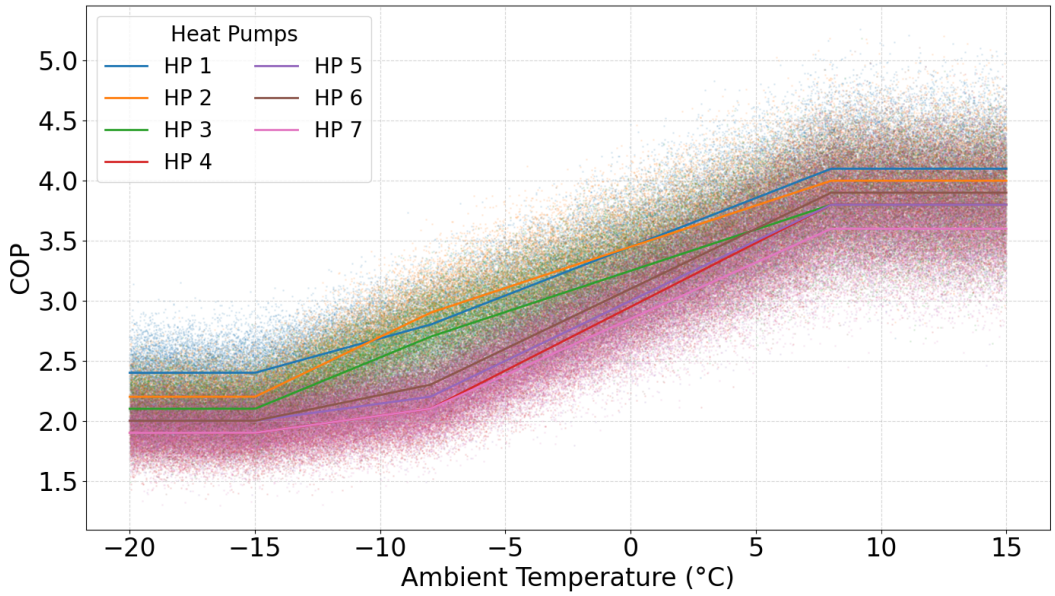

Figure 5.8: Nominal and probabilistic COP values for the 7 HP types used, assuming a ±8% variability and normal pdf.

The probabilistic COP model used is based on the temperature and HP brand, which allows the simulation of synthetic load profiles. Fig. 5.8 shows the nominal and probabilistic COP values for the 7 HP types selected, based on an assumed variability range of ±8%, as per [116], since the performance of each HP does not exactly follow the average COP, varying as a function of outdoor temperature, which results in scatter COP values around a nominal value, assuming a normal pdf. The nominal COP values were obtained from the manufacturers' catalogs and are shown as average lines in the figure.

As per (5.4), the final aggregated HP load is expressed as a convex combination of individual stochastic profiles. In this formulation, each generated profile contributes to the aggregated load through an associated weighting factor, enabling the model to capture the combined effects of variations in house characteristics, HP brands and models, thermostat setpoints, and COP uncertainties. This approach ensures adequate uncertainty coverage while preserving scenario diversity. Fig. 5.9 illustrates the probabilistic framework used in Step 7 to generate synthetic HP load profiles for the 36 randomly

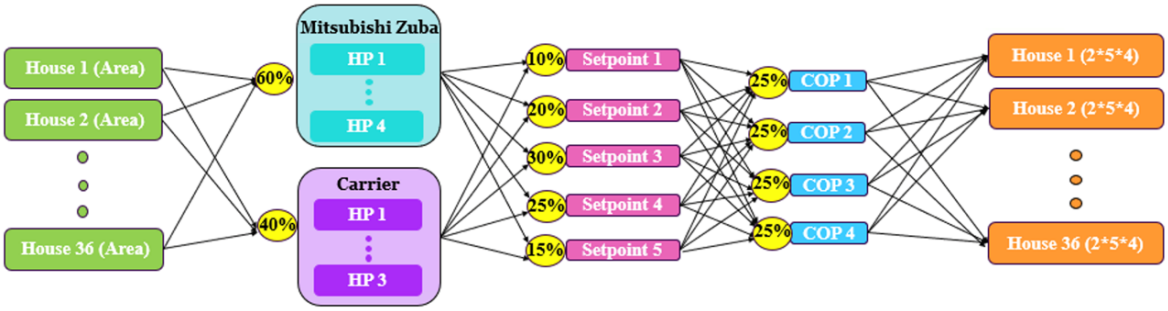

Figure 5.9: Probability scenarios employed to generate synthetic HP load profiles based on standard stochastic analysis.

selected houses based on GIS data. By incorporating multiple stochastic factors and probabilistic inputs, and based on basic stochastic analysis principles, diverse HP load profiles can be generated by randomly sampling across combinations of HP brand and model types, COP scatter behavior, and temperature setpoints. Thus, weighted probabilities to reflect market share and user preference distributions, with multiple probabilistic realizations for the 36 houses with various models of the 2 HP brands, 5 setpoints, and 4 COP values for each HP type, randomly chosen from Fig. 5.8, yielded a total of 1440 synthetic HP load profiles. This process effectively expands the scenario space and adequately captures uncertainties in system configuration and user behavior. These load profiles are then aggregated to represent the overall HP load across all cases, which is then simply scaled up in Step 9 to match the total HP capacity identified in Step 8 for the region of interest, as explained next.

5.3.3 Heat Pump Capacity Estimation

As indicated, since HP characteristics vary significantly across households due to differences in HP size, building characteristics, and operating conditions, regional capacity estimation must rely on aggregated statistics and reasonable assumptions. Thus, based on [243], by the end of 2020, approximately 329,000 HPs had been installed in single-detached homes across Ontario. Between 2020 and July 2024, an additional 58,531 HPs were installed under federal incentive programs. This results in a total of 102,960 installations by July 2025, which is an increase of approximately 76% from July 2024

to July 2025 [244].

According to the 2021 Canadian Census, there were about 2,944,200 single-detached houses in Ontario, accounting for 53.6% of the province's 5,491,200 occupied private dwellings [245]. In Milton, Ontario, the 2021 Census reported 22,701 single-detached homes, representing 56.7% of the city's 40,035 occupied private dwellings [245], which is approximately 0.77% of Ontario's single-detached homes. Based on this percentage and the number of HPs installed in Ontario, it can be concluded that there were 2,540 HPs installed in Milton by 2020. Then, applying the same proportional allocation to post-2020 installations, it can be estimated that there were 450 additional installations between 2020 and July 2024, and 340 further installations between July 2024 and July 2025. Hence, based on these public statistics, the total number of installed HPs in Milton can be estimated to be approximately 2,770 units in 2022 and about 3,100 units by February 2025. These estimates provide a reasonable basis for aggregated HP capacity modeling in the absence of detailed installation-level data, which is used in Step 9 to scale up the aggregated synthetic HP load obtained in Step 7. Hence, the scaling factor for the generated 1,440 synthetic HP aggregated load profile can be determined to be 1.92, i.e., 2,770/1,440, and 2.15 for 2025.

5.3.4 Machine Learning Model

ML techniques can play a key role in extracting HPs load signatures, enabling accurate spatial and temporal predictions of aggregated HP behavior, particularly during peak hours. Since different ML models can be applied for this purpose, an LSTM model was selected here to estimate the HP aggregated load for future years, due to its ability to capture temporal dependencies in time-series data. Thus, the aggregated probabilistic HP load profile for the region obtained in Step 9 for 2022 is then used as the dataset for training and evaluation of the selected LSTM model to estimate the 2025 HP aggregated load in Steps 10 and 11.

Fig. 5.10 illustrates the workflow of the prediction model, using the LSTM model based on pretraining aggregated 2022 dataset. This model was then fine-tuned using limited 2025 data, which required adding a network layer trained on this dataset. This approach enables the model to leverage previously learned features with minimal new data, resulting in an adequate prediction of the aggregated HP load for 2025. Fig. 5.11

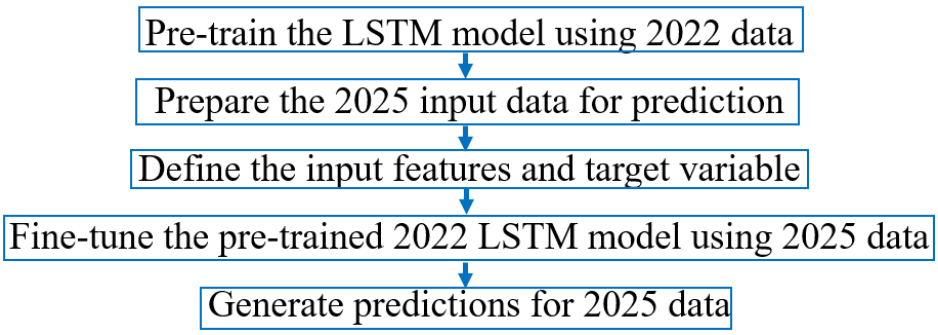

Figure 5.10: LSTM pre-training and fine-tuning workflow for aggregated HP load forecasting.

presents the HP load profiles for 2022 used for training the LSTM model, and the resulting 2025 prediction. A ±30% range of uncertainty is applied for both years to represent significant variability in the data used.

5.3.5 Verification

Since the resulting aggregated load for 2022 is influenced by multiple stochastic variables, it is treated as a random variable. Therefore, in Step 12, to verify the generated aggregated HP load profile, the pdf of the aggregated load was computed to characterize its distribution and capture the variability and uncertainty in HP demand. Fig. 5.12 shows the pdf of the HP load data for 2022, covering the period from January 01, 2022, to March 25, 2022. The pdf was estimated to be a Kernel Density Estimation (KDE) function, which provides a smooth approximation of the underlying distribution from the sample data. A 60% Highest Density Interval (HDI) is further estimated from the KDE to represent the main uncertainty range of the aggregated load. This pdf exhibits two distinct peaks, one around 6 MW and another at about 10 MW. These peaks can be interpreted as reflecting the daily cycle of HP usage, with the lower peak corresponding to off-peak periods with lower heating demand, and the higher peak hours when heating demand is greater.

To verify the predicted HP load for 2025 based on the 2022 training model, a correlation heat map was obtained to examine the influence of different features on

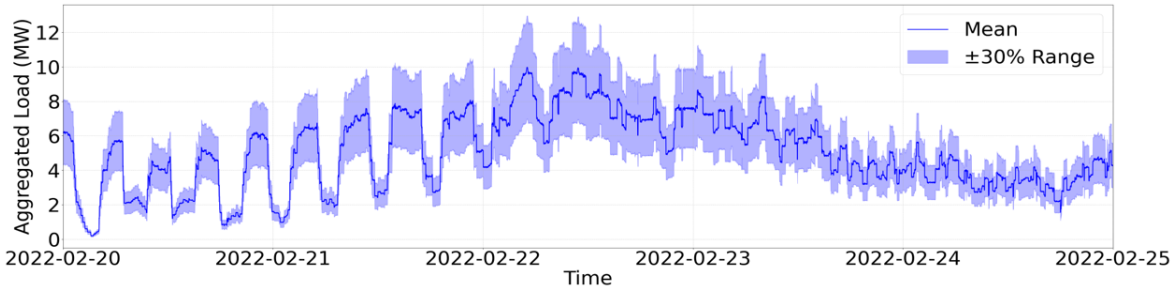

(a)

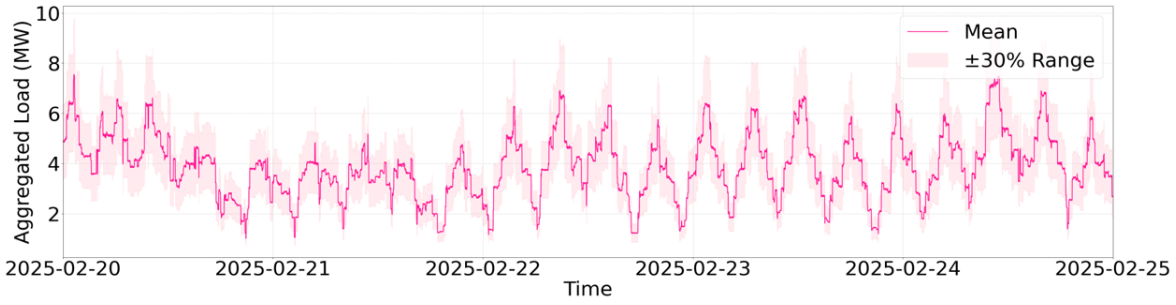

(b)

Figure 5.11: Aggregated HP load profiles in Milton for February (a) 2022 and (b) 2025.

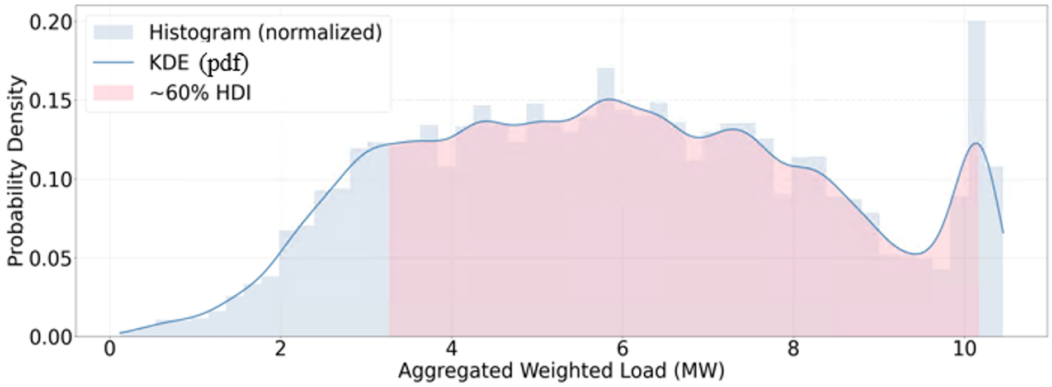

Figure 5.12: Kernel Density Estimation-based pdf of the 2022 dataset spanning January 01 to March 25.

the HP load profile prediction. Different features were considered for the correlation

analysis, including temperature, hour, minute, day, month, day of the week, weekends, solar radiation, and transmission-level power data. This resulted in the HP load being most strongly correlated with temperature, followed by day and month, respectively, which were consistent with the expectation of heating demand.

5.3.6 Heat Pump and Demand Load Power Disaggregation

Based on the aggregated load profiles obtained in Step 9 for 2022 and Step 11 for 2025, and verified in Step 12, the net-load disaggregation for 2022 and 2025 can be obtained in Step 13, depicted in Fig. 5.13a and Fig. 5.13b, respectively. This methodology provides a scalable and robust framework for HP load disaggregation under data-scarce conditions. By combining stochastic modeling, synthetic data generation, and predictive analytics, the approach enables disaggregation of HP load from net load while accounting for input uncertainty. This framework allows utilities to estimate and monitor installed HP capacity using existing measurements, without requiring extensive deployment of advanced metering infrastructure.

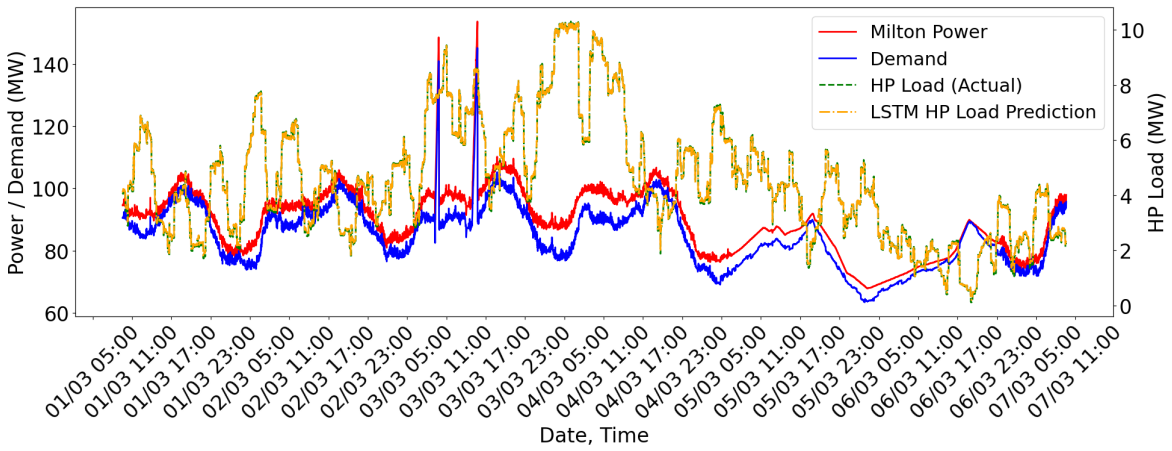

(a)

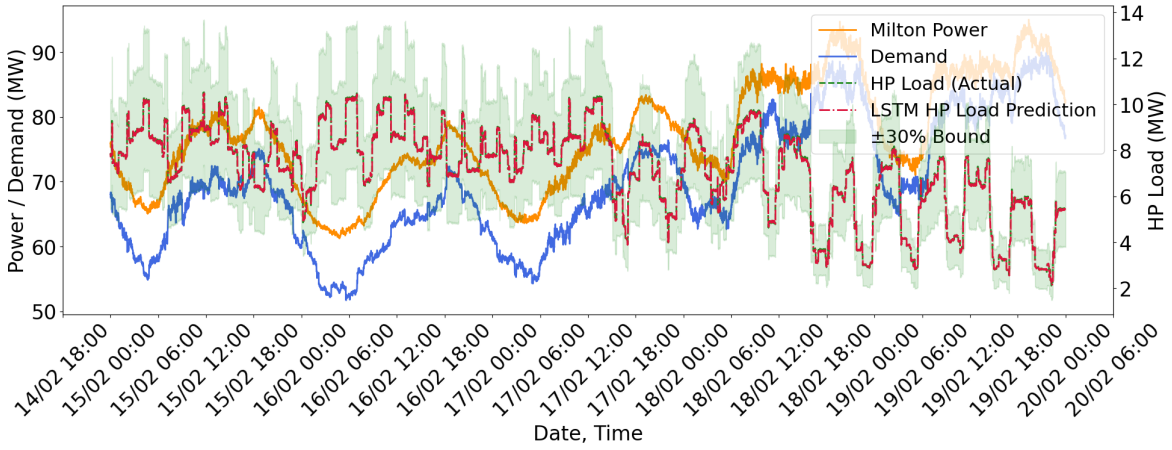

(b)

Figure 5.13: Disaggregation of HP demand using net-load measurements for (a) March 2022 and (b) February 2025.

5.4 Summary

This chapter proposed a methodology for extracting HP load profiles from transmission-level net-load measurements using available datasets. A model was developed to simulate HP consumption, with probabilistic synthetic load profiles being generated using a combination of physics-based simulations and data-driven techniques. GIS data

provided information on typical house characteristics, and AI/ML models were employed for random house selection. Public statistics were used to estimate HP capacities, and weather data informed the generation of multiple synthetic load profiles. An AI/ML framework was further applied for forecasting and disaggregation of aggregated HP demand for future years. The approach was demonstrated using real HV/MV feeder net-load data, with synthetic profiles evaluated via load distribution curves and Pearson correlation coefficients. The results show that the simulated profiles capture temperature-dependent behavior and provide a reasonable approximation of real-world HP loads.

The limitations of the proposed approach include the use of data from only one household in the region of interest and the use of public statistics to estimate regional building characteristics and occupancy. Hence, the reasonable generated synthetic profiles are conditional and intended as substitutes where comprehensive measurement data are unavailable.

Chapter 6

Conclusions, Contributions and Future Work

6.1 Summary and Conclusions

The rapid integration of distributed energy resources and electrified heating technologies has significantly transformed modern power systems, introducing new challenges in monitoring, visibility, and operational planning. In particular, the increasing penetration of DPV systems and HPs has amplified the complexity of net load behavior at both transmission and distribution levels. This thesis addresses these challenges by developing advanced data-driven and physics-informed methodologies, leveraging ML techniques to disaggregate PV generation and model residential HP loads using limited measurements, which are subsequently utilized for HP load disaggregation. By integrating satellite imagery with system-level data, the proposed approaches enhance the observability of behind-the-meter resources. Overall, this work contributes to bridging the gap between HV/MV grid measurements and granular end-use insights, supporting more efficient, reliable, and data-driven operation of future low-carbon power systems.

Chapter 1 presented the motivation for this research by highlighting the need for improved techniques to disaggregate PV generation and HP consumption from net-load measurements at the transmission system level. The chapter reviewed existing methodologies for PV generation disaggregation and HP load estimation, including

residential HP modeling and behavioral analysis, and identified key research gaps. Building on these insights, the research objectives were defined to develop methods for PV power estimation, HP load modeling and validation, and HP load disaggregation. Finally, the chapter provided an overview of the thesis structure and the content of the subsequent chapters.

Chapter 2 provided a comprehensive background for the key systems and underpinning this thesis. The chapter first presented an overview of PV power, including PV load disaggregation, highlighting challenges in estimating large-scale PV generation from aggregate measurements. Then it overviewed HP loads, including HP performance fundamentals and HP demand disaggregation, emphasizing operational behavior and energy consumption patterns. Exciting GIS techniques were introduced for estimating DPV system capacity and for identifying residential building characteristics to support HP load profile estimation. The chapter also reviewed ML/DL techniques for forecasting and disaggregation of energy data. Finally, the use of synthetic data and stochastic analysis was discussed for generating PV power and HP consumption data. These foundational concepts established the basis for the modeling, disaggregation, and analysis studies presented in Chapters 3 through 5.

Chapter 3 described a novel methodology for disaggregating PV generation from HV/MV transmission-level net-load measurements. ML-based algorithms to detect and estimate PV system capacity using satellite imagery were obtained which were validated against actual utility data. The estimated PV generation capacity was integrated into existing software tools to simulate solar power output and generate synthetic PV data, which was then used to reconstruct aggregate DPV loads. This data was further analyzed using multiple ML models to separate aggregated PV generation from transmission feeder net-load measurements for the Waterloo region in Ontario, Canada, demonstrating that the proposed approach provides improved system visibility with minimal additional sensing infrastructure. The primary limitations of the presented work stem from uncertainties in capacity estimation and profile diversity. The reliance on satellite imagery and GIS-based estimation introduces potential errors due to human annotation inaccuracies, inactive or non-functional installations, and off-grid PV systems. Furthermore, the synthetic solar profiles do not account for all real-world variations, such as diverse panel orientations, tilt angles, localized shading effects, and

efficiency degradations, which may affect the overall precision of the aggregated PV disaggregation.

Chapter 4 proposed an ML-framework for modeling the power and energy consumption of a central air-source HP for residential applications using real measurement data. The developed supervised technique, consisting of ANN and LSTM networks, was trained on power measurements, outdoor temperature, temporal variables, and solar radiation. The results of applying the presented techniques to an actual HP in Milton, Ontario household during the winter season showed that the proposed LSTM model achieved superior short-term accuracy for residential HP load estimation compared to an existing physics-based model. The main limitation of the presented work is the reliance on empirical data collected from a single residential household during the winter season. Consequently, the model does not capture variations across different building envelopes, insulation levels, occupant behaviors, and appliance usage patterns. In addition, the framework focuses exclusively on single-mode heating operation, omitting cooling dynamics, which restricts its immediate generalizability to more complex residential setups and to HP cooling applications.

Chapter 5 proposed a methodology for extracting aggregated residential HP load profiles from HV/MV transmission-level net-load measurements. To establish baseline HP capacity, publicly available statistical data were used. A real HP dataset was used for physics-based simulations, with GIS data helping to characterize typical house features. Additionally, ML models and statistical techniques were employed to capture key factors affecting HP consumption, such as temperature and the COP, informed by existing studies and data-driven analyses. Synthetic load profiles were then generated for multiple virtual households using a combination of physics-based simulations and data-driven techniques. Finally, an ML framework was employed for load forecasting and HP disaggregation applications. The resulting framework was demonstrated and tested for forecasting and disaggregation of aggregated HP demand in Milton, Ontario, demonstrating practical relevance for system operators and supporting improved visibility and management of distributed HP loads. The presented approach is constrained by regional specificity and the approximated nature of synthetic profiles. Because the framework is calibrated specifically for the climate zone and network topology of Milton, Ontario, applying it to other regions requires re-tuning the underlying models,

GIS parameters, and load features. Moreover, the generated synthetic HP load profiles rely on probabilistic and physics-informed assumptions, which can be considered surrogates in the absence of comprehensive sub-metering, and may not fully encompass all real-world operational and behavioral stochasticity.

6.2 Contributions

6.2.1 PV Power Disaggregation

- A novel approach is presented based on satellite imagery and image-based DL techniques, for accurate detection of PV panels and estimation of installed PV capacity.
- A scalable and generalizable new framework is proposed for PV disaggregation from net-load measurements, applicable to scenarios with limited, unreliable, or unavailable data sources.
- A novel technique is presented for synthetic data generation of PV power based on simulations and multiple ML/DL models for enhanced net-load disaggregation.
- A practical application of the proposed techniques is demonstrated and validated based on real transmission feeder-head power measurements for disaggregation of PV power generation and downstream demand, considering residential rooftop and ground-mounted PV systems.

6.2.2 Modeling and Validation of Heat Pump Loads

- An accurate data-driven HP model is proposed using ANN and LSTM architectures, leveraging smart meter measurements and weather data.
- A practical validation of the proposed model is presented, highlighting the strengths and limitations of data-driven approaches compared to an existing physics-based model.

6.2.3 Heat Pump Load Disaggregation

- A flexible and scalable framework is proposed for generating aggregated synthetic HP load profiles from limited data, capturing diverse operating conditions and stochastic temporal variability. This framework is based on a physics-based HP model and real-world measurements to approximately represent HP load behavior, integrating satellite imagery, ML-based random sampling of residential building characteristics, and probabilistic modeling of occupancy patterns and comfort levels.

- Development of a methodology to estimate installed HP capacity using publicly available data on regional adoption rates, housing characteristics, and penetration levels, enabling scaling of synthetic HP load profiles to match HV/MV system-level observations.

- An HP load disaggregation approach is presented to extract aggregated HP demand from real HV/MV feeder-head measurements, leveraging synthetic data and advanced DL techniques.

- The proposed disaggregation framework is demonstrated and validated using multi-year real data from Milton, Ontario, without reliance on extensive AMI, highlighting its practical applicability for system operators such as Ontario's IESO.

6.2.4 Applicability

The following needs to be considered when applying and deploying the proposed disaggregation frameworks:

- Generalization:

  PV: The Mask R-CNN and GIS framework transfers across similar urban topologies without model retraining, though direct applicability is limited

by regional variations in panel orientation, tilt angle, shading, and efficiency that require local re-tuning.

HP: The physics-informed and GIS framework generalizes across residential feeders via archetype sampling, yet broader applicability is limited by regional and climate specificity (calibrated for Milton, ON), reliance on single-household data, unmodeled variations in building insulation and occupancy, and the exclusion of dual-use (heating/cooling) or hybrid HP operations.

- Scalability:

  PV: The framework scales effectively to HV/MV transmission feeders without dedicated asset telemetry using satellite capacity estimates and simulation software, though large-scale deployment is limited by capacity estimation uncertainties from human annotation errors, inactive or non-functional units, and off-grid PV systems.

  HP: The bottom-up approach scales non-intrusively to bulk substation levels without customer sub-metering via census statistics and stochastic simulations, though scalability is limited by its reliance on conditional synthetic profiles rather than comprehensive real-world measurement data.

- Robustness:

  PV: The ML disaggregation models remain robust against daily solar irradiance swings when trained on regional meteorological feeds, though operational stability is limited by unmodeled efficiency variations, localized shading, and severe cloud transients.

  HP: Incorporating stochastic resampling and temperature-dependent COP ensures robust macro-level load tracking across weather changes, yet robustness is limited because conditional synthetic assumptions cannot capture all real-world appliance usage patterns, behavioral randomness, or extreme sub-zero nonlinearities.

- Accuracy:

PV: The framework achieves high spatial accuracy (98% capacity accuracy and 65% Intersection over Union (IoU) against utility registries), though aggregated disaggregation precision is limited by limited PV profile variability and capacity estimation uncertainties from inactive or off-grid installations.

HP: The LSTM and bottom-up models achieve strong short-term accuracy and reproduce seasonal load distributions (validated via correlation, KDE, and 60% HDI), though validation and forecasting accuracy are limited by single-household calibration data, unmodeled building characteristics, and the absence of grid-wide sub-metering.

6.3 Future Work

Several potential directions for extending and improving the proposed research can be identified:

- **Regional Adaptation:** Test and adapt the proposed methodology using transmission load profiles from other similar regions and from regions with different climate conditions to determine how the proposed load disaggregation methods can be adjusted or calibrated regionally.
- **Integration of Other DERs:** Extend net-load disaggregation methods to include DERs such as EVs, battery storage, and demand-response loads, enabling a more comprehensive understanding of behind-the-meter contributions based on PV and HP loads.
- **Multi-Household Diversity and Multi-Season HP Simulation:** Expand HP modeling to encompass diverse household archetypes, varying across building types, heating and cooling configurations, and occupancy behaviors, while incorporating empirical measurement data across all seasons to capture operational variability in energy consumption and COP.

References

[1] W. Kanchana and J. G. Singh, "Detection of invisible solar PV installations in power distribution system: A review," in *IEEE International Conference and Utility Exhibition on Energy, Environment and Climate Change (ICUE)*, pp. 1–8, 2022.

[2] International Renewable Energy Agency (IRENA), "Renewable capacity statistics 2020." [Online]. Available: `https://www.irena.org/publications/2020/Mar/Renewable-Capacity-Statistics-2020`, 2020. Accessed: Sep. 20, 2024.

[3] M. D'Incecco, S. Squartini, and M. Zhong, "Transfer learning for non-intrusive load monitoring," *IEEE Transactions on Smart Grid*, vol. 11, no. 2, pp. 1419–1429, 2019.

[4] Ember, "Global solar installations surge 64% in first half of 2025." [Online]. Available: `https://ember-energy.org/latest-updates/global-solar-installations-surge-64-in-first-half-of-2025/`, 2025. Accessed: Feb. 25, 2026.

[5] International Energy Agency (IEA), "Global heat pump sales continue double-digit growth -analysis." [Online]. Available: `https://www.iea.org/commentaries/global-heat-pump-sales-continue-double-digit-growth`, 2023. Accessed: Feb. 25, 2026.

[6] International Energy Agency (IEA), "Installation of about 600 million heat pumps covering 20% of buildings heating needs required by 2030." [Online]. Available: `https://www.iea.org/reports/installation-of-about-`

600-million-heat-pumps-covering-20-of-buildings-heating-needs-required-by-2030, 2024. Accessed: Sep. 27, 2024.

[7] Canada Energy Regulator, "Provincial and territorial energy profiles- Ontario." [Online]. Available: https://www.cer-rec.gc.ca/en/data-analysis/energy-markets/provincial-territorial-energy-profiles/provincial-territorial-energy-profiles-ontario.html, 2026. Accessed: Feb. 25, 2026.

[8] H. McDiarmid, "Air source heat pumps." [Online]. Available: https://www.cleanairalliance.org/wp-content/uploads/2022/01/Heat-Pump-Report-2022-8.5x11-jan-11-v_01.pdf, 2021. Accessed: Sep. 27, 2024.

[9] Natural Resources Canada, "Canada greener homes initiative: Progress update." [Online]. Available: https://natural-resources.canada.ca/energy-efficiency/home-energy-efficiency/canada-greener-homes-initiative/greener-homes-initiative-progress-update-july-2024, 2024. Accessed: Aug. 20, 2025.

[10] Government of Canada, "Heat Pumps Uptake at a Glance." [Online]. Available: https://natural-resources.canada.ca/energy-efficiency/home-energy-efficiency/canada-greener-homes-initiative/heat-pumps-uptake-glance-0, 2025. Published: Jul. 22, 2025. Accessed: Aug. 20, 2025.

[11] Canadian Climate Institute, "Heat pumps pay off: Unlocking lower-cost heating and cooling in Canada." [Online]. Available: https://climateinstitute.ca/wp-content/uploads/2023/09/Heat-Pumps-Pay-Off-Unlocking-lower-cost-heating-and-cooling-in-Canada-Canadian-Climate-Institute.pdf, 2023. Accessed: Sep. 11, 2024.

[12] Canada Energy Regulator, "Provincial and territorial energy profiles – Ontario." [Online]. Available: https://www.cer-rec.gc.ca/en/data-analysis/energy-markets/provincial-territorial-energy-profiles/provincial-territorial-energy-profiles-ontario.html, 2024. Accessed: Nov. 1, 2024.

[13] P. Denholm, M. O'Connell, G. Brinkman, and J. Jorgenson, "Overgeneration from solar energy in California. a field guide to the duck chart," tech. rep., National Renewable Energy Lab. (NREL), Golden, CO (United States), 2015.

[14] B. Bayer, P. Matschoss, H. Thomas, and A. Marian, "The German experience with integrating photovoltaic systems into the low-voltage grids," *Renewable Energy*, vol. 119, pp. 129–141, 2018.

[15] E. Vrettos, E. Kara, E. Stewart, and C. Roberts, "Estimating PV power from aggregate power measurements within the distribution grid," *Journal of Renewable and Sustainable Energy*, vol. 11, no. 2, 2019.

[16] Q. Chen, F. Wang, B.-M. Hodge, J. Zhang, Z. Li, M. Shafie-Khah, and J. P. Catalão, "Dynamic price vector formation model-based automatic demand response strategy for PV-assisted EV charging stations," *IEEE Transactions on Smart Grid*, vol. 8, no. 6, pp. 2903–2915, 2017.

[17] F. Wang, K. Li, C. Liu, Z. Mi, M. Shafie-Khah, and J. P. Catalão, "Synchronous pattern matching principle-based residential demand response baseline estimation: Mechanism analysis and approach description," *IEEE Transactions on Smart Grid*, vol. 9, no. 6, pp. 6972–6985, 2018.

[18] L. Massidda and M. Marrocu, "Decoupling weather influence from user habits for an optimal electric load forecast system," *Energies*, vol. 10, no. 12, p. 2171, 2017.

[19] Y. Yu, X. Wen, J. Zhao, Z. Xu, and J. Li, "Co-planning of demand response and distributed generators in an active distribution network," *Energies*, vol. 11, no. 2, p. 354, 2018.

[20] F. Bu, K. Dehghanpour, Y. Yuan, Z. Wang, and Y. Zhang, "A data-driven game-theoretic approach for behind-the-meter PV generation disaggregation," *IEEE Transactions on Power Systems*, vol. 35, no. 4, pp. 3133–3144, 2020.

[21] D. W. Van der Meer, J. Munkhammar, and J. Widén, "Probabilistic forecasting of solar power, electricity consumption and net load: Investigating the effect of seasons, aggregation and penetration on prediction intervals," *Solar Energy*, vol. 171, pp. 397–413, 2018.

[22] W. Stainsby, D. Zimmerle, and G. P. Duggan, "A method to estimate residential PV generation from net-metered load data and system install date," *Applied Energy*, vol. 267, 2020. Art. no. 114895.

[23] F. Wang, K. Li, X. Wang, L. Jiang, J. Ren, Z. Mi, M. Shafie-khah, and J. P. Catalão, "A distributed PV system capacity estimation approach based on Support Vector Machine with customer net load curve features," *Energies*, vol. 11, no. 7, p. 1750, 2018.

[24] X. Chen and O. Ardakanian, "Data efficient solar disaggregation with behind-the-meter energy resources," *Sustainable Energy, Grids and Networks*, vol. 32, 2022. Art. no. 100813.

[25] E. C. Kara, C. M. Roberts, M. Tabone, L. Alvarez, D. S. Callaway, and E. M. Stewart, "Towards real-time estimation of solar generation from micro-synchrophasor measurements," *arXiv:1607.02919*, 2016.

[26] J. M. Malof, K. Bradbury, L. M. Collins, and R. G. Newell, "Automatic detection of solar photovoltaic arrays in high resolution aerial imagery," *Applied Energy*, vol. 183, pp. 229–240, 2016.

[27] J. de Hoog, S. Maetschke, P. Ilfrich, and R. R. Kolluri, "Using satellite and aerial imagery for identification of solar PV: State of the art and research opportunities," in *ACM International Conference on Future Energy Systems*, pp. 308–313, 2020.

[28] U.S. Energy Information Administration, "Annual energy outlook 2020," tech. rep., Energy Information Administration, Washington, DC, 2020. Accessed: Oct. 31, 2024.

[29] N. Batra, R. Kukunuri, A. Pandey, R. Malakar, R. Kumar, O. Krystalakos, M. Zhong, P. Meira, and O. Parson, "Towards reproducible state-of-the-art energy disaggregation," in *ACM International Conference on Systems for Energy-Efficient Buildings, Cities, and Transportation*, pp. 193–202, 2019.

[30] S. Bahramara, A. Mazza, G. Chicco, M. Shafie-khah, and J. P. S. Catalão, "Comprehensive review on the decision-making frameworks referring to the distribution network operation problem in the presence of distributed energy resources and microgrids," *International Journal of Electrical Power & Energy Systems*, vol. 115, 2020. Art. no. 105466.

[31] T. Brudermueller, M. Kreft, E. Fleisch, and T. Staake, "Large-scale monitoring of residential heat pump cycling using smart meter data," *Applied Energy*, vol. 350, 2023. Art. no. 121734.

[32] M. McDonald, "How will air source heat pumps affect electricity load profiles in buildings in Ireland? a data logger used to model electrical energy profiles," in *International Universities Power Engineering Conference (UPEC)*, pp. 1–6, 2023.

[33] M. Akmal, B. Fox, J. D. Morrow, and T. Littler, "Impact of heat pump load on distribution networks," *IET Generation, Transmission & Distribution*, vol. 8, no. 12, pp. 2065–2073, 2014.

[34] A. Weigert, "Identification and classification of heat pump problems in the field and their implication for a user-centric problem recognition," *Energy Informatics*, vol. 5, no. 1, 2022. Art. no. 70.

[35] T. Brudermueller, F. Wirth, A. Weigert, and T. Staake, "Automatic differentiation of variable and fixed speed heat pumps with smart meter data," in *IEEE International Conference on Communications, Control, and Computing Technologies for Smart Grids*, pp. 412–418, 2022.

[36] F. Wüllhorst, S. Schwarz, N. Fuchs, L. Maier, A. Monti, and D. Müller, "Impact of hybrid heat pump shares and building envelope retrofit rates on load pene-

tration in German low-voltage grids," *Applied Energy*, vol. 388, 2025. Art. no. 125530.

[37] M. Toro-Cárdenas, I. Moreira, H. Morais, P. M. Carvalho, and L. A. Ferreira, "Net load disaggregation at secondary substation level," *Renewable Energy*, vol. 207, pp. 765–771, 2023.

[38] Z. Xiaochen and S. Grijalva, "A data-driven approach for detection and estimation of residential PV installations," *IEEE Transactions on Smart Grid*, vol. 7, no. 5, pp. 2477–2485, 2016.

[39] P. Gotseff, J. Cale, M. Baggu, D. Narang, and K. Carroll, "Accurate power prediction of spatially distributed PV systems using localized irradiance measurements," in *IEEE PES General Meeting*, pp. 1–5, 2014.

[40] J. Alonso-Montesinos, F. Batlles, and J. Bosch, "Beam, diffuse and global solar irradiance estimation with satellite imagery," *Energy Conversion and Management*, vol. 105, pp. 1205–1212, 2015.

[41] X.-Y. Zhang, S. Kuenzel, P. Guo, L. Yin, and C. Watkins, "A hybrid data-driven online solar energy disaggregation system from the grid supply point," *Complex & Intelligent Systems*, vol. 9, no. 4, pp. 3695–3716, 2023.

[42] G.-C. Adalberto, B. Giulia, T. Giovanni, and M. U. Girish, "Computer vision-based reader for analogue energy/water meters in low-cost embedded system: a case study in an office building in Scotland," in *E3S Web of Conferences*, vol. 172, p. 25006, 2020.

[43] X.-Y. Zhang, S. Kuenzel, J.-R. Córdoba-Pachón, and C. Watkins, "Privacy-functionality trade-off: A privacy-preserving multi-channel smart metering system," *Energies*, vol. 13, no. 12, p. 3221, 2020.

[44] H. Shaker, H. Zareipour, and D. Wood, "Estimating power generation of invisible solar sites using publicly available data," *IEEE Transactions on Smart Grid*, vol. 7, no. 5, pp. 2456–2465, 2016.

[45] W. Ling, G. Dalzell, X. Yu, B. McGrath, and P. Sokolowski, "An interpretable classification approach for solar PV load profiles using Decision Trees," in *IEEE International Symposium on Industrial Electronics (ISIE)*, pp. 522–527, 2022.

[46] E. Cook, S. Luo, and Y. Weng, "Solar panel identification via deep semi-supervised learning and deep one-class classification," *IEEE Transactions on Power Systems*, vol. 37, no. 4, pp. 2516–2526, 2021.

[47] A. Altan, S. Karasu, and E. Zio, "A new hybrid model for wind speed forecasting combining long short-term memory neural network, decomposition methods and Grey Wolf optimizer," *Applied Soft Computing*, vol. 100, 2021. Art. no. 106996.

[48] E. G. Vera, C. A. Cañizares, M. Pirnia, T. P. Guedes, and J. D. M. Trujillo, "Two-stage stochastic optimization model for multi-microgrid planning," *IEEE Transactions on Smart Grid*, vol. 14, no. 3, pp. 1723–1735, 2022.

[49] S. Lee, S. Iyengar, M. Feng, P. Shenoy, and S. Maji, "Deeproof: A data-driven approach for solar potential estimation using rooftop imagery," in *ACM SIGKDD International Conference on Knowledge Discovery & Data Mining*, (Anchorage, AK, USA), pp. 2105–2113, 2019.

[50] J. Yu, Z. Wang, A. Majumdar, and R. Rajagopal, "Deepsolar: A machine learning framework to efficiently construct a solar deployment database in the United States," *Joule*, vol. 2, no. 12, pp. 2605–2617, 2018.

[51] L. Breiman, "Random Forests," *Machine learning*, vol. 45, pp. 5–32, 2001.

[52] V. Mnih and G. E. Hinton, "Learning to detect roads in high-resolution aerial images," in *Computer Vision ECCV: European Conference on Computer Vision, Heraklion, Crete, Greece, September 5-11, 2010, Proceedings, Part VI 11*, pp. 210–223, 2010.

[53] X. Chen, S. Xiang, C.-L. Liu, and C.-H. Pan, "Vehicle detection in satellite images by parallel Deep Convolutional Neural Networks," in *IAPR Asian Conference on Pattern Recognition*, pp. 181–185, 2013.

[54] M. Mokhtarzade and M. V. Zoej, "Road detection from high-resolution satellite images using Artificial Neural Networks," *International Journal of Applied Earth Observation and Geoinformation*, vol. 9, no. 1, pp. 32–40, 2007.

[55] S. Madhogaria, P. M. Baggenstoss, M. Schikora, W. Koch, and D. Cremers, "Car detection by fusion of HOG and causal MRF," *IEEE Transactions on Aerospace and Electronic Systems*, vol. 51, no. 1, pp. 575–590, 2015.

[56] P. O. Gislason, J. A. Benediktsson, and J. R. Sveinsson, "Random Forests for land cover classification," *Pattern Recognition Letters*, vol. 27, no. 4, pp. 294–300, 2006.

[57] P. Tokarczyk, J. Montoya, and K. Schindler, "An evaluation of feature learning methods for high resolution image classification," *ISPRS Annals of the Photogrammetry, Remote Sensing and Spatial Information Sciences*, vol. 1, pp. 389–394, 2012.

[58] C. Gonzales and W. Sakla, "Semantic segmentation of clouds in satellite imagery using deep pre-trained U-Nets," in *IEEE Applied Imagery Pattern Recognition Workshop (AIPR)*, pp. 1–7, 2019.

[59] J. M. Malof, L. M. Collins, and K. Bradbury, "A Deep Convolutional Neural Network, with pre-training, for solar photovoltaic array detection in aerial imagery," in *IEEE International Geoscience and Remote Sensing Symposium (IGARSS)*, pp. 874–877, 2017.

[60] Z. Huang, T. Mendis, and S. Xu, "Urban solar utilization potential mapping via deep learning technology: A case study of Wuhan, China," *Applied Energy*, vol. 250, pp. 283–291, 2019.

[61] R. Castello, S. Roquette, M. Esguerra, A. Guerra, and J.-L. Scartezzini, "Deep Learning in the built environment: Automatic detection of rooftop solar panels using Convolutional Neural Networks," *Journal of Physics: Conference Series*, vol. 1343, no. 1, 2019. Art. no. 012034.

[62] P. Li, H. Zhang, Z. Guo, S. Lyu, J. Chen, W. Li, X. Song, R. Shibasaki, and J. Yan, "Understanding rooftop PV panel semantic segmentation of satellite and aerial images for better using machine learning," *Advances in Applied Energy*, vol. 4, 2021. Art. no. 100057.

[63] J. Yuan and Y. Weng, "Enhance unobservable solar generation estimation via constructive Generative Aadversarial Networks," *IEEE Transactions on Power Systems*, vol. 39, no. 1, pp. 2251–2263, 2023.

[64] E. Reiter, K. Ardani, R. Margolis, and R. Edge, "Industry perspectives on advanced inverters for US solar photovoltaic systems. grid benefits, deployment challenges, and emerging solutions," tech. rep., National Renewable Energy Lab. (NREL), Golden, CO (United States), 2015.

[65] L. Waswa, M. J. Chihota, and B. Bekker, "A probabilistic estimation of PV capacity in distribution networks from aggregated net-load data," *IEEE Access*, vol. 9, pp. 140358–140371, 2021.

[66] S. Killinger, F. Braam, B. Müller, B. Wille-Haussmann, and R. McKenna, "Projection of power generation between differently-oriented PV systems," *Solar Energy*, vol. 136, pp. 153–165, 2016.

[67] M. Pierro, M. De Felice, E. Maggioni, D. Moser, A. Perotto, F. Spada, and C. Cornaro, "Data-driven upscaling methods for regional photovoltaic power estimation and forecast using satellite and numerical weather prediction data," *Solar Energy*, vol. 158, pp. 1026–1038, 2017.

[68] F. Sossan, L. Nespoli, V. Medici, and M. Paolone, "Unsupervised disaggregation of photovoltaic production from composite power flow measurements of heterogeneous prosumers," *IEEE Transactions on Industrial Informatics*, vol. 14, no. 9, pp. 3904–3913, 2018.

[69] J. M. Bright, S. Killinger, D. Lingfors, and N. A. Engerer, "Improved satellite-derived PV power nowcasting using real-time power data from reference PV systems," *Solar Energy*, vol. 168, pp. 118–139, 2018.

[70] F. Kabir, N. Yu, W. Yao, R. Yang, and Y. Zhang, "Estimation of behind-the-meter solar generation by integrating physical with statistical models," in *IEEE International Conference on Communications, Control, and Computing Technologies for Smart Grids (SmartGridComm)*, pp. 1–6, 2019.

[71] D. Chen and D. Irwin, "Sundance: Black-box behind-the-meter solar disaggregation," in *International Conference on Future Energy Systems*, pp. 45–55, 2017.

[72] A. Mokaribolhassan, G. Nourbakhsh, G. Ledwich, A. Arefi, and M. Shafiei, "Distribution system state estimation using PV separation strategy in LV feeders with high levels of unmonitored PV generation," *IEEE Systems Journal*, vol. 17, no. 1, pp. 684–695, 2022.

[73] M. Lave, W. Hayes, A. Pohl, and C. W. Hansen, "Evaluation of global horizontal irradiance to plane-of-array irradiance models at locations across the United States," *IEEE Journal of Photovoltaics*, vol. 5, no. 2, pp. 597–606, 2015.

[74] C. A. Gueymard, "Progress in direct irradiance modeling and validation," in *Annual Conf. Phoenix, AZ, USA*, 2010.

[75] H. I. Ruf, *Computation of the load flow at the transformer in distribution grids with a significant number of photovoltaic systems using satellite-derived solar irradiance data*. PhD thesis, University of Agder, 2016.

[76] Y. Wang, N. Zhang, Q. Chen, D. S. Kirschen, P. Li, and Q. Xia, "Data-driven probabilistic net load forecasting with high penetration of behind-the-meter PV," *IEEE Transactions on Power Systems*, vol. 33, no. 3, pp. 3255–3264, 2017.

[77] E. C. Kara, C. M. Roberts, M. Tabone, L. Alvarez, D. S. Callaway, and E. M. Stewart, "Disaggregating solar generation from feeder-level measurements," *Sustainable Energy, Grids and Networks*, vol. 13, pp. 112–121, 2018.

[78] K. Li, F. Wang, Z. Mi, M. Fotuhi-Firuzabad, N. Duić, and T. Wang, "Capacity and output power estimation approach of individual behind-the-meter distributed photovoltaic system for demand response baseline estimation," *Applied Energy*, vol. 253, p. 113595, 2019.

[79] P. Shaffery, R. Yang, and Y. Zhang, "Bayesian structural time series for behind-the-meter photovoltaic disaggregation," in *IEEE Power & Energy Society Innovative Smart Grid Technologies Conference (ISGT)*, pp. 1–5, 2020.

[80] J. Betcke and H. G. Beyer, "Accuracy improvement of irradiation data by combining ground and satellite measurements," in *International Solar Forum: ISES Solar Conference*, vol. 3, p. 933, 2004.

[81] L. M. Aguiar, B. Pereira, P. Lauret, F. Díaz, and M. David, "Combining solar irradiance measurements, satellite-derived data and a numerical weather prediction model to improve intra-day solar forecasting," *Renewable Energy*, vol. 97, pp. 599–610, 2016.

[82] Y.-M. Saint-Drenan, S. Bofinger, B. Ernst, T. Landgraf, and K. Rohrig, "Regional nowcasting of the solar power production with PV-plant measurements and satellite images," in *Solar World Congress*, 2011.

[83] L. Langer and T. Volling, "An optimal home energy management system for modulating heat pumps and photovoltaic systems," *Applied Energy*, vol. 278, 2020. Art. no. 115661.

[84] H. Wolisz, T. Schütz, T. Blanke, M. Hagenkamp, M. Kohrn, M. Wesseling, and D. Müller, "Cost optimal sizing of smart buildings' energy system components considering changing end-consumer electricity markets," *Energy*, vol. 137, pp. 715–728, 2017.

[85] M. Dongellini, C. Naldi, and G. L. Morini, "Seasonal performance evaluation of electric air-to-water heat pump systems," *Applied Thermal Engineering*, vol. 90, pp. 1072–1081, 2015.

[86] M. Dongellini, C. Naldi, and G. L. Morini, "Influence of sizing strategy and control rules on the energy saving potential of heat pump hybrid systems in a residential building," *Energy Conversion and Management*, vol. 235, 2021. Art. no. 114022.

[87] P. Yin, M. Pate, and F. Battaglia, "In-field performance evaluation and economic analysis of residential ground source heat pumps in heating operation," *Journal of Building Engineering*, vol. 26, 2019. Art. no. 100932.

[88] F. Oldewurtel, A. Parisio, C. N. Jones, D. Gyalistras, M. Gwerder, V. Stauch, B. Lehmann, and M. Morari, "Use of model predictive control and weather forecasts for energy efficient building climate control," *Energy and buildings*, vol. 45, pp. 15–27, 2012.

[89] J. Laustsen, "Energy efficiency requirements in building codes, energy efficiency policies for new buildings." IEA Information Paper, International Energy Agency (IEA), Paris, France. [Online]. Available: `https://www.iea.org/reports/energy-efficiency-requirements-in-building-codes`, 2008. Accessed: Aug. 20, 2025.

[90] J. Vivian, E. Prataviera, F. Cunsolo, and M. Pau, "Demand side management of a pool of air source heat pumps for space heating and domestic hot water production in a residential district," *Energy Conversion and Management*, vol. 225, 2020. Art. no. 113457.

[91] Z. Xu, H. Li, S. Shao, W. Xu, Z. Wang, Y. Wang, X. Sun, Q. Yang, C. Xu, and W. Zhao, "A semi-theoretical model for energy efficiency assessment of air source heat pump systems," *Energy Conversion and Management*, vol. 228, 2021. Art. no. 113667.

[92] L. Danza, L. Belussi, I. Meroni, M. Mililli, and F. Salamone, "Hourly calculation method of air source heat pump behavior," *Buildings*, vol. 6, no. 2, p. 16, 2016.

[93] A. Zendehboudi, J. Zhao, and X. Li, "Data-driven modeling of residential air source heat pump system for space heating," *Journal of Thermal Analysis and Calorimetry*, vol. 145, pp. 1863–1876, 2021.

[94] F. Maranghi, L. Gosselin, J. Raymond, and M. Bourbonnais, "Modeling of solar-assisted ground-coupled heat pumps with or without batteries in remote high north communities," *Renewable Energy*, vol. 207, pp. 484–498, 2023.

[95] Y. Chen, E. Liang, U. Berardi, J. Yang, X. Jiang, and G. Cui, "A model-based predictive control method of the ground-source heat pump system for maintaining thermal comfort in low-energy buildings," in *2022 7th International Conference on Power and Renewable Energy (ICPRE)*, pp. 1080–1085, IEEE, 2022.

[96] A. Gabaldón, S. Valero-Verdu, A. García-Garre, C. Senabre, C. Álvarez-Bel, M. López, E. Peñalvo, and E. P. Sánchez, "A physically-based model of heat pump water heaters for demand response policies: Evaluation and testing," in *2018 International Conference on Smart Energy Systems and Technologies (SEST)*, pp. 1–6, IEEE, 2018.

[97] Y. Xie, P. Hu, N. Zhu, F. Lei, L. Xing, L. Xu, and Q. Sun, "A hybrid short-term load forecasting model and its application in ground source heat pump with cooling storage system," *Renewable Energy*, vol. 161, pp. 1244–1259, 2020.

[98] H. Dagdougui, F. Bagheri, H. Le, and L. Dessaint, "Neural Network model for short-term and very-short-term load forecasting in district buildings," *Energy and Buildings*, vol. 203, 2019. Art. no. 109408.

[99] T. Ahmad, H. Chen, Y. Guo, and J. Wang, "A comprehensive overview on the data driven and large scale based approaches for forecasting of building energy demand: A review," *Energy and Buildings*, vol. 165, pp. 301–320, 2018.

[100] S. Hochreiter and J. Schmidhuber, "Long short-term memory," *Neural Computation*, vol. 9, no. 8, pp. 1735–1780, 1997.

[101] M. Cai, M. Pipattanasomporn, and S. Rahman, "Day-ahead building-level load forecasts using deep learning vs. traditional time-series techniques," *Applied Energy*, vol. 236, pp. 1078–1088, 2019.

[102] Z. E. Lee and K. M. Zhang, "Scalable identification and control of residential heat pumps: A minimal hardware approach," *Applied Energy*, vol. 286, 2021. Art. no. 116544.

[103] K. Fürst, P. Chen, and I. Y.-H. Gu, "Hierarchical LSTM-based classification of household heating types using measurement data," *IEEE Transactions on Smart Grid*, vol. 15, no. 2, pp. 2261–2270, 2023.

[104] A. Weigert, K. Hopf, N. Weinig, and T. Staake, "Detection of heat pumps from smart meter and open data," *Energy Informatics*, vol. 3, 2020. Art. no. 21.

[105] G. Le Ray, M. H. Christensen, and P. Pinson, "Detection and characterization of domestic heat pumps," in *IEEE Milan PowerTech*, (Milan, Italy), pp. 1–6, 2019.

[106] C. M. R. Do Carmo and T. H. Christensen, "Cluster analysis of residential heat load profiles and the role of technical and household characteristics," *Energy and Buildings*, vol. 125, pp. 171–180, 2016.

[107] L. Semmelmann, P. Jaquart, and C. Weinhardt, "Generating synthetic load profiles of residential heat pumps: A K-means Clustering approach," *Energy Informatics*, vol. 6, no. Suppl 1, 2023. Art. no. 37.

[108] G. G. Pillai, G. A. Putrus, and N. M. Pearsall, "Generation of synthetic benchmark electrical load profiles using publicly available load and weather data," *International Journal of Electrical Power & Energy Systems*, vol. 61, pp. 1–10, 2014.

[109] D. Fischer, A. Härtl, and B. Wille-Haussmann, "Model for electric load profiles with high time resolution for German households," *Energy and Buildings*, vol. 92, pp. 170–179, 2015.

[110] D. Fischer, T. Wolf, J. Scherer, and B. Wille-Haussmann, "A stochastic bottom-up model for space heating and domestic hot water load profiles for German households," *Energy and Buildings*, vol. 124, pp. 120–128, 2016.

[111] J. V. Paatero and P. D. Lund, "A model for generating household electricity load profiles," *International Journal of Energy Research*, vol. 30, no. 5, pp. 273–290, 2006.

[112] C. Bucher and G. Andersson, "Generation of domestic load profiles-an adaptive top-down approach," in *Proceedings of PMAPS*, vol. 2012, pp. 10–14, 2012.

[113] T. Zufferey, D. Toffanin, D. Toprak, A. Ulbig, and G. Hug, "Generating stochastic residential load profiles from smart meter data for an optimal power matching at an aggregate level," in *2018 Power Systems Computation Conference (PSCC)*, pp. 1–7, IEEE, 2018.

[114] Y. Chen, Y. Wang, D. Kirschen, and B. Zhang, "Model-free renewable scenario generation using generative adversarial networks," *IEEE Transactions on Power Systems*, vol. 33, no. 3, pp. 3265–3275, 2018.

[115] J. Love, A. Z. P. Smith, S. Watson, E. Oikonomou, A. Summerfield, C. Gleeson, P. Biddulph, L. F. Chiu, J. Wingfield, C. Martin, A. Stone, and R. Lowe, "The addition of heat pump electricity load profiles to GB electricity demand: Evidence from a heat pump field trial," *Applied Energy*, vol. 204, pp. 332–342, 2017.

[116] S. D. Watson, J. Crawley, K. J. Lomas, and R. A. Buswell, "Predicting future GB heat pump electricity demand," *Energy and Buildings*, vol. 286, 2023. Art. no. 112917.

[117] C. Protopapadaki and D. Saelens, "Heat pump and PV impact on residential low-voltage distribution grids as a function of building and district properties," *Applied Energy*, vol. 192, pp. 268–281, 2017.

[118] F. L. Müller and B. Jansen, "Large-scale demonstration of precise demand response provided by residential heat pumps," *Applied Energy*, vol. 239, pp. 836–845, 2019.

[119] S. Makonin, B. Ellert, I. V. Bajić, and F. Popowich, "Electricity, water, and natural gas consumption of a residential house in Canada from 2012 to 2014," *Scientific Data*, vol. 3, no. 1, pp. 1–12, 2016.

[120] O. Ruhnau, L. Hirth, and A. Praktiknjo, "Time series of heat demand and heat pump efficiency for energy system modeling," *Scientific data*, vol. 6, no. 1, p. 189, 2019.

[121] B. Yang, W. Li, Y. Zhao, and X. He, "Design and analysis of a grid-connected photovoltaic power system," *IEEE Transactions on Power Electronics*, vol. 25, no. 4, pp. 992–1000, 2009.

[122] R. Khezri and A. Mahmoudi, "Review on the state-of-the-art multi-objective optimisation of hybrid standalone/grid-connected energy systems," *IET Generation, Transmission Distribution*, vol. 14, no. 20, pp. 4285–4300, 2020.

[123] O. M. Toledo, D. Oliveira Filho, and A. S. A. C. Diniz, "Distributed photovoltaic generation and energy storage systems: A review," *Renewable and Sustainable Energy Reviews*, vol. 14, no. 1, pp. 506–511, 2010.

[124] M. Mendelsohn, T. Lowder, and B. Canavan, "Utility-scale concentrating solar power and photovoltaic projects: A technology and market overview," tech. rep., National Renewable Energy Lab. (NREL), Golden, CO (United States), 2012.

[125] T. E. Kuhn, C. Erban, M. Heinrich, J. Eisenlohr, F. Ensslen, and D. H. Neuhaus, "Review of technological design options for building integrated photovoltaics (BIPV)," *Energy and Buildings*, vol. 231, 2021. Art. no. 110381.

[126] I. J. Perez-Arriaga and C. Batlle, "Impacts of intermittent renewables on electricity generation system operation," *Economics of Energy & Environmental Policy*, vol. 1, no. 2, pp. 3–18, 2012.

[127] M. Obi and R. Bass, "Trends and challenges of grid-connected photovoltaic systems: A review," *Renewable and Sustainable Energy Reviews*, vol. 58, pp. 1082–1094, 2016.

[128] T. Chen, H. Sun, K. F. Tai, and C. K. Heng, "Analysis of the barriers to implementing building integrated photovoltaics in Singapore using an interpretive structural modelling approach," *Journal of Cleaner Production*, vol. 365, 2022. Art. no. 132652.

[129] M. Shafiullah, S. D. Ahmed, and F. A. Al-Sulaiman, "Grid integration challenges and solution strategies for solar PV systems: A review," *IEEE Access*, vol. 10, pp. 52233–52257, 2022.

[130] J. Hu, J. Zhu, and D. G. Dorrell, "Model predictive control of grid-connected inverters for PV systems with flexible power regulation and switching frequency reduction," *IEEE Transactions on Industry Applications*, vol. 51, no. 1, pp. 587–594, 2014.

[131] Q. Li, L. Zhu, Y. Sun, L. Lu, and Y. Yang, "Performance prediction of building integrated photovoltaics under no-shading, shading and masking conditions using a multi-physics model," *Energy*, vol. 213, 2020. Art. no. 118795.

[132] X. Wang, L. Xia, C. Bales, X. Zhang, B. Copertaro, S. Pan, and J. Wu, "A systematic review of recent air source heat pump (ASHP) systems assisted by solar thermal, photovoltaic and photovoltaic/thermal sources," *Renewable Energy*, vol. 146, pp. 2472–2487, 2020.

[133] A. Hepbasli and Y. Kalinci, "A review of heat pump water heating systems," *Renewable and Sustainable Energy Reviews*, vol. 13, no. 6-7, pp. 1211–1229, 2009.

[134] P. Christodoulides, L. Aresti, and G. Florides, "Air-conditioning of a typical house in moderate climates with ground source heat pumps and cost comparison with air source heat pumps," *Applied Thermal Engineering*, vol. 158, 2019. Art. no. 113772.

[135] R. Wu *et al.*, "Energy efficiency technologies: air source heat pump vs. ground source heat pump," *Journal of Sustainable Development*, vol. 2, no. 2, pp. 14–23, 2009.

[136] A. S. Gaur, D. Z. Fitiwi, and J. Curtis, "Heat pumps and our low-carbon future: A comprehensive review," *Energy Research & Social Science*, vol. 71, 2021. Art. no. 101764.

[137] F. Ren, Z. Wei, and X. Zhai, "A review on the integration and optimization of distributed energy systems," *Renewable and Sustainable Energy Reviews*, vol. 162, 2022. Art. no. 112440.

[138] T. Péan, *Heat pump controls to exploit the energy flexibility of building thermal loads*. Springer Nature, 2021.

[139] E. M. Wanjiru, S. M. Sichilalu, and X. Xia, "Model predictive control of heat pump water heater-instantaneous shower powered with integrated renewable-grid energy systems," *Applied Energy*, vol. 204, pp. 1333–1346, 2017.

[140] L. Schibuola, M. Scarpa, and C. Tambani, "Demand response management by means of heat pumps controlled via real time pricing," *Energy and Buildings*, vol. 90, pp. 15–28, 2015.

[141] I. Sarbu and C. Sebarchievici, "General review of ground-source heat pump systems for heating and cooling of buildings," *Energy and Buildings*, vol. 70, pp. 441–454, 2014.

[142] T. El Samad, A. Żabnieńska-Góra, H. Jouhara, and A. I. Sayma, "A review of compressors for high temperature heat pumps," *Thermal Science and Engineering Progress*, vol. 53, 2024. Art. no. 102603.

[143] P. Rockett and E. A. Hathway, "Model-predictive control for non-domestic buildings: a critical review and prospects," *Building Research & Information*, vol. 45, no. 5, pp. 556–571, 2017.

[144] F. Mancini, G. Lo Basso, and L. de Santoli, "Energy use in residential buildings: Impact of building automation control systems on energy performance and flexibility," *Energies*, vol. 12, no. 15, p. 2896, 2019.

[145] S. Gonzato, J. Chimento, E. O'Dwyer, G. Bustos-Turu, S. Acha, and N. Shah, "Hierarchical price coordination of heat pumps in a building network controlled using model predictive control," *Energy and Buildings*, vol. 202, 2019. Art. no. 109421.

[146] T. Brudermueller, F. Breer, and T. Staake, "Disaggregation of heat pump load profiles from low-resolution smart meter data," in *International Conference on Systems for Energy-Efficient Buildings, Cities, and Transportation*, pp. 228–231, 2023.

[147] Z. Lee, K. Gupta, K. J. Kircher, and K. M. Zhang, "Mixed-integer model predictive control of variable-speed heat pumps," *Energy and Buildings*, vol. 198, pp. 75–83, 2019.

[148] C. Verhelst, F. Logist, J. Van Impe, and L. Helsen, "Study of the optimal control problem formulation for modulating air-to-water heat pumps connected to a residential floor heating system," *Energy and Buildings*, vol. 45, pp. 43–53, 2012.

[149] M. Abuelhamd and C. A. Cañizares, "Dynamic model of integrated electricity and district heating for remote communities," *Applied Energy*, vol. 376, 2024. Art. no. 124337.

[150] G. O. Reddy, "Geographic information system: principles and applications," *Geospatial Technologies in Land Resources Mapping, Monitoring and Management*, pp. 45–62, 2018.

[151] M. F. Goodchild, "Geographic information science and systems for environmental management," *Annual Review of Environment and Resources*, vol. 28, no. 1, pp. 493–519, 2003.

[152] X. Zhu, *GIS for environmental applications: a practical approach*. Routledge, 2016.

[153] S. Xhafa and A. Kosovrasti, "Geographic Information Systems (GIS) in urban planning," *European Journal of Interdisciplinary Studies*, vol. 1, no. 1, pp. 74–81, 2015.

[154] S. Zambrano-Asanza, J. Quiros-Tortos, and J. F. Franco, "Optimal site selection for photovoltaic power plants using a GIS-based multi-criteria decision making and spatial overlay with electric load," *Renewable and Sustainable Energy Reviews*, vol. 143, 2021. Art. no. 110853.

[155] S. N. Shorabeh, H. K. Firozjaei, M. K. Firozjaei, M. Jelokhani-Niaraki, M. Homaee, and O. Nematollahi, "The site selection of wind energy power plant using GIS-multi-criteria evaluation from economic perspectives," *Renewable and Sustainable Energy Reviews*, vol. 168, 2022. Art. no. 112778.

[156] S. Ali, J. Taweekun, K. Techato, J. Waewsak, and S. Gyawali, "GIS based site suitability assessment for wind and solar farms in Songkhla, Thailand," *Renewable Energy*, vol. 132, pp. 1360–1372, 2019.

[157] Z. Deng, Y. Chen, X. Pan, Z. Peng, and J. Yang, "Integrating GIS-based point of interest and community boundary datasets for urban building energy modeling," *Energies*, vol. 14, no. 4, p. 1049, 2021.

[158] M. M. Moein, A. Saradar, K. Rahmati, S. H. G. Mousavinejad, J. Bristow, V. Aramali, and M. Karakouzian, "Predictive models for concrete properties using machine learning and deep learning approaches: A review," *Journal of Building Engineering*, vol. 63, 2023. Art. no. 105444.

[159] J. D. Kelleher, *Deep Learning*. MIT Press, 2019.

[160] I. Goodfellow, *Deep Learning*. MIT Press, 2016.

[161] D.-M. Petroșanu and A. Pîrjan, "Electricity consumption forecasting based on a Bidirectional long-short-term memory artificial neural network," *Sustainability*, vol. 13, no. 1, p. 104, 2020.

[162] T. Ahmad and H. Chen, "A review on machine learning forecasting growth trends and their real-time applications in different energy systems," *Sustainable Cities and Society*, vol. 54, 2020. Art. no. 102010.

[163] M. Zou, S. Zhu, J. Gu, L. M. Korunovic, and S. Z. Djokic, "Heating and lighting load disaggregation using frequency components and Convolutional Bidirectional Long Short-Term Memory method," *Energies*, vol. 14, no. 16, p. 4831, 2021.

[164] B. Zhao, M. Ye, L. Stankovic, and V. Stankovic, "Non-intrusive load disaggregation solutions for very low-rate smart meter data," *Applied Energy*, vol. 268, 2020. Art. no. 114949.

[165] OpenCV, "Open computer vision library." [Online]. Available: `https://opencv.org/`, 2026. Accessed: Feb. 2, 2026.

[166] H. Safari, C. A. Cañizares, D. Sohm, E. Ahmed, I. El-Samahy, and M. Dusseault, "Disaggregating distributed PV power from aggregate measurements in transmission systems," *IEEE Transactions on Smart Grid*, pp. 1–1, 2025.

[167] J. Chen, J. S. Kim, and C. Rabiti, "Probabilistic analysis of hybrid energy systems using synthetic renewable and load data," in *2017 American Control Conference (ACC)*, pp. 4723–4728, IEEE, 2017.

[168] J. Heine, E. E. Fowler, A. Berglund, M. J. Schell, and S. Eschrich, "Techniques to produce and evaluate realistic multivariate synthetic data," *Scientific Reports*, vol. 13, no. 1, p. 12266, 2023.

[169] C. G. Corlu, A. Akcay, and W. Xie, "Stochastic simulation under input uncertainty: A review," *Operations Research Perspectives*, vol. 7, 2020. Art. no. 100162.

[170] H. Li, J. H. Yeo, A. L. Bornsheuer, and T. J. Overbye, "The creation and validation of load time series for synthetic electric power systems," *IEEE Transactions on Power Systems*, vol. 36, no. 2, pp. 961–969, 2020.

[171] K. M. Gegner, A. B. Birchfield, T. Xu, K. S. Shetye, and T. J. Overbye, "A methodology for the creation of geographically realistic synthetic power flow models," in *2016 IEEE Power and Energy Conference at Illinois (PECI)*, pp. 1–6, IEEE, 2016.

[172] A. B. Birchfield, T. Xu, K. M. Gegner, K. S. Shetye, and T. J. Overbye, "Grid structural characteristics as validation criteria for synthetic networks," *IEEE Transactions on Power Systems*, vol. 32, no. 4, pp. 3258–3265, 2016.

[173] V. Champaney, F. Chinesta, and E. Cueto, "Engineering empowered by physics-based and data-driven hybrid models: A methodological overview," *International Journal of Material Forming*, vol. 15, no. 3, p. 31, 2022.

[174] M. Rayati, P. D. Falco, D. Proto, M. Bozorg, and M. Carpita, "Generation data of synthetic high frequency solar irradiance for data-driven decision-making in electrical distribution grids," *Energies*, vol. 14, no. 16, p. 4734, 2021.

[175] N. Damianakis, G. R. C. Mouli, and P. Bauer, "Grid impact of photovoltaics, electric vehicles and heat pumps on distribution grids: An overview," *Applied Energy*, vol. 380, 2025. Art. no. 125000.

[176] O. Bamisile, C. Acen, D. Cai, Q. Huang, and I. Staffell, "The environmental factors affecting solar photovoltaic output," *Renewable and Sustainable Energy Reviews*, vol. 208, 2025. Art. no. 115073.

[177] I. L. Carreno, R. Ramakrishna, A. Scaglione, D. Arnold, C. Roberts, S.-T. Ngo, S. Peisert, and D. Pinney, "Soda: An irradiance-based synthetic solar data generation tool," in *2020 IEEE International Conference on Communications, Control, and Computing Technologies for Smart Grids (SmartGridComm)*, pp. 1–6, IEEE, 2020.

[178] M. Miozzo, D. Zordan, P. Dini, and M. Rossi, "SolarStat: Modeling photovoltaic sources through stochastic Markov processes," in *2014 IEEE International Energy Conference (ENERGYCON)*, pp. 688–695, IEEE, 2014.

[179] D. A. R. de Jesús, P. Mandal, T. Senjyu, and S. Kamalasadan, "Unsupervised hybrid deep generative models for photovoltaic synthetic data generation," in *2021 IEEE Power & Energy Society General Meeting (PESGM)*, pp. 1–5, IEEE, 2021.

[180] P. R. Mishra, S. Rathore, and V. Jain, "PVSyst enabled real time evaluation of grid connected solar photovoltaic system," *International Journal of Information Technology*, vol. 16, no. 2, pp. 745–752, 2024.

[181] M. Muller, K. Anderson, and M. Deceglie, "Generating synthetic time series photovoltaic data with real-world physical challenges and noise for use in algorithm test and validation," tech. rep., National Renewable Energy Laboratory (NREL), Golden, CO (United States), 2023.

[182] N. Salazar-Pena, A. Tabares, and A. Gonzalez-Mancera, "Sequential stochastic and bootstrap methods to generate synthetic solar irradiance time series of high

temporal resolution based on historical observations," *Solar Energy*, vol. 264, 2023. Art. no. 112030.

[183] H. Palahalli, P. Maffezzoni, and G. Gruosso, "Gaussian copula methodology to model photovoltaic generation uncertainty correlation in power distribution networks," *Energies*, vol. 14, no. 9, p. 2349, 2021.

[184] D. Pylorof and H. E. Garcia, "Uncertainty-aware photovoltaic generation estimation through fusion of physics with harmonics information using bayesian neural networks," in *2023 IEEE Power & Energy Society Innovative Smart Grid Technologies Conference (ISGT)*, pp. 1–5, IEEE, 2023.

[185] N. Lindsay, Q. Libois, J. Badosa, A. Migan-Dubois, and V. Bourdin, "Errors in pv power modelling due to the lack of spectral and angular details of solar irradiance inputs," *Solar Energy*, vol. 197, pp. 266–278, 2020.

[186] M. Ehrendorfer, "Predicting the uncertainty of numerical weather forecasts: A review," *Meteorologische Zeitschrift-Berlin-*, vol. 6, pp. 147–183, 1997.

[187] H.-L. Xue, X.-S. Shen, and J.-F. Chou, "A forecast error correction method in numerical weather prediction by using recent multiple-time evolution data," *Advances in Atmospheric Sciences*, vol. 30, no. 5, pp. 1249–1259, 2013.

[188] N. D. Brenowitz, Y. Cohen, J. Pathak, A. Mahesh, B. Bonev, T. Kurth, D. R. Durran, P. Harrington, and M. S. Pritchard, "A practical probabilistic benchmark for AI weather models," *Geophysical Research Letters*, vol. 52, no. 7, p. e2024GL113656, 2025.

[189] D. Orrell, L. Smith, J. Barkmeijer, and T. N. Palmer, "Model error in weather forecasting," *Nonlinear processes in geophysics*, vol. 8, no. 6, pp. 357–371, 2001.

[190] H. A. Kazem and M. T. Chaichan, "Effect of humidity on photovoltaic performance based on experimental study," *International Journal of Applied Engineering Research (IJAER)*, vol. 10, no. 23, pp. 43572–43577, 2015.

[191] N. Gökmen, W. Hu, P. Hou, Z. Chen, D. Sera, and S. Spataru, "Investigation of wind speed cooling effect on pv panels in windy locations," *Renewable Energy*, vol. 90, pp. 283–290, 2016.

[192] K. Barhmi, C. Heynen, S. Golroodbari, and W. van Sark, "A review of solar forecasting techniques and the role of artificial intelligence," in *Solar*, vol. 4, pp. 99–135, MDPI, 2024.

[193] R. P. Kenny, G. Friesen, D. Chianese, A. Bernasconi, and E. D. Dunlop, "Energy rating of PV modules: comparison of methods and approach," in *3rd World Conference on Photovoltaic Energy Conversion, 2003. Proceedings of*, vol. 2, pp. 2015–2018, IEEE, 2003.

[194] T. Huld, M. Šúri, and E. D. Dunlop, "Geographical variation of the conversion efficiency of crystalline silicon photovoltaic modules in Europe," *Progress in photovoltaics: Research and applications*, vol. 16, no. 7, pp. 595–607, 2008.

[195] L. Le Cam, *Asymptotic methods in statistical decision theory*. Springer Science & Business Media, 2012.

[196] E. Cramer, L. R. Gorjao, A. Mitsos, B. Schäfer, D. Witthaut, and M. Dahmen, "Validation methods for energy time series scenarios from deep generative models," *IEEE access*, vol. 10, pp. 8194–8207, 2022.

[197] I. Staffell, D. Brett, N. Brandon, and A. Hawkes, "A review of domestic heat pumps," *Energy Environmental Science*, vol. 5, no. 11, pp. 9291–9306, 2012.

[198] T. Marsik, V. Stevens, R. Garber-Slaght, C. Dennehy, R. T. Strunk, and A. Mitchell, "Empirical study of the effect of thermal loading on the heating efficiency of variable-speed air source heat pumps," *Sustainability*, vol. 15, no. 3, 2023. Art. no. 1880.

[199] Z. Wei, T. Zhang, B. Yue, Y. Ding, R. Xiao, R. Wang, and X. Zhai, "Prediction of residential district heating load based on Machine Learning: A case study," *Energy*, vol. 231, 2021. Art. no. 120950.

[200] M. Akmal, B. Fox, D. Morrow, and T. Littler, "Impact of high penetration of heat pumps on low voltage distribution networks," in *2011 IEEE Trondheim PowerTech*, (Trondheim, Norway), pp. 1–7, IEEE, 2011.

[201] Z. Liu, X. Yang, and S. A. Kalogirou, "Empowering building flexibility service through thermal energy storage with ground source heat pump from demand side," *Energy*, vol. 314, 2026. Art. no. 140854.

[202] Z. Yang, H. Xiao, W. Shi, M. Zhang, and B. Wang, "Analysis and determination of a seasonal performance evaluation for air source heat pumps," *Journal of Building Engineering*, vol. 43, 2021. Art. no. 102574.

[203] Independent Electricity System Operator (IESO), "Supply overview: Transmission-connected generation." [Online]. Available: `https://www.ieso.ca/en/Power-Data/Supply-Overview/Transmission-Connected-Generation`, 2024. Accessed: Aug. 28, 2024.

[204] A. Voulodimos, N. Doulamis, A. Doulamis, and E. Protopapadakis, "Deep learning for computer vision: A brief review," *Computational Intelligence and Neuroscience*, vol. 2018, no. 1, p. 7068349, 2018.

[205] H. Li, B. Herfort, and A. Zipf, "Estimating openstreetmap missing built-up areas using pre-trained deep neural networks," in *GILE Conference on Geographic Information Science*, pp. 17–20, 2019.

[206] National Renewable Energy Laboratory (NREL), "NREL system advisor model (SAM) weather data." [Online]. Available: `https://sam.nrel.gov/weather-data/weather-data-publications.html`, 2024. Accessed: Sep. 11, 2024.

[207] P. Anandhi and E. Nathiya, "Application of linear regression with their advantages, disadvantages, assumption and limitations," *International Journal of Statistics and Applied Mathematics*, vol. 8, pp. 133–137, 2023.

[208] Y. Dong, X. Ma, and T. Fu, "Electrical load forecasting: A Deep Learning approach based on K-nearest neighbors," *Applied Soft Computing*, vol. 99, 2021. Art. no. 106900.

[209] V. Prasath, H. A. A. Alfeilat, A. Hassanat, O. Lasassmeh, A. S. Tarawneh, M. B. Alhasanat, and H. S. E. Salman, "Distance and similarity measures effect on the performance of K-nearest neighbor classifier: A review," *arXiv preprint arXiv:1708.04321*, p. 39, 2017.

[210] S. Preda, S.-V. Oprea, A. Bâra, and A. Belciu, "PV forecasting using support vector machine learning in a big data analytics context," *Symmetry*, vol. 10, no. 12, p. 748, 2018.

[211] K.-L. Du, B. Jiang, J. Lu, J. Hua, and M. N. S. Swamy, "Exploring Kernel Machines and Support Vector Machines: Principles, techniques, and future directions," *Mathematics*, vol. 12, no. 24, 2024. Art. no. 3888.

[212] S.-C. Lim, J.-H. Huh, S.-H. Hong, C.-Y. Park, and J.-C. Kim, "Solar power forecasting using CNN-LSTM hybrid model," *Energies*, vol. 15, no. 21, p. 8233, 2022.

[213] U. Javed, K. Ijaz, M. Jawad, I. Khosa, E. A. Ansari, K. S. Zaidi, M. N. Rafiq, and N. Shabbir, "A novel short receptive field based dilated causal Convolutional Network integrated with Bidirectional LSTM for short-term load forecasting," *Expert Systems with Applications*, vol. 205, 2022. Art. no. 117689.

[214] C. Ma, G. Dai, and J. Zhou, "Short-term traffic flow prediction for urban road sections based on time series analysis and LSTM–BiLSTM method," *IEEE Transactions on Intelligent Transportation Systems*, vol. 23, no. 6, pp. 5615–5624, 2021.

[215] Esri, "ArcGIS pretrained models: Introduction to the model." [Online]. Available: `https://doc.arcgis.com/en/pretrained-models/latest/imagery/introduction-to-solar-panel-detection-usa.htm`, 2024. Accessed: Aug. 28, 2024.

[216] National Renewable Energy Laboratory (NREL), "NREL system advisor model (SAM)." [Online]. Available: `https://sam.nrel.gov/download`, 2024. Accessed: Sep. 11, 2024.

[217] C. Seger, "An investigation of categorical variable encoding techniques in machine learning: Binary versus one-hot and feature hashing." [Online]. Available: https://www.diva-portal.org/smash/record.jsf?pid=diva2%3A1259073&dswid=-6062, 2018. Accessed: Sep. 11, 2024.

[218] A. Géron, *Hands-on machine learning with Scikit-Learn, Keras, and TensorFlow*. O'Reilly Media, 2022.

[219] A. F. M. Jaramillo, D. M. Laverty, D. J. Morrow, J. M. del Rincon, and A. M. Foley, "Load modelling and non-intrusive load monitoring to integrate distributed energy resources in low and medium voltage networks," *Renewable Energy*, vol. 179, pp. 445–466, 2021.

[220] M. Everingham, L. Van Gool, C. K. Williams, J. Winn, and A. Zisserman, "The Pascal Visual Object Classes (VOC) challenge," *International Journal of Computer Vision*, vol. 88, pp. 303–338, 2010.

[221] M. Zech, H.-P. Tetens, and J. Ranalli, "Toward global rooftop PV detection with deep active learning," *Advances in Applied Energy*, vol. 16, 2024. Art. no. 100191.

[222] L. Wang, Y. Shoulin, H. Alyami, A. A. Laghari, M. Rashid, J. Almotiri, H. J. Alyamani, and F. Alturise, "A novel deep learning-based single shot multibox detector model for object detection in optical remote sensing images," *Geoscience Data Journal*, vol. 11, pp. 237–251, 2024.

[223] Z. Hameed and B. Garcia-Zapirain, "Sentiment classification using a single-layered BiLSTM model," *IEEE Access*, vol. 8, pp. 73992–74001, 2020.

[224] D. P. Kingma, "Adam: A method for stochastic optimization," *arXiv preprint arXiv:1412.6980*, 2014.

[225] A. T. Prihatno, H. Nurcahyanto, M. F. Ahmed, M. H. Rahman, M. M. Alam, and Y. M. Jang, "Forecasting PM2.5 concentration using a single-dense layer BiLSTM method," *Electronics*, vol. 10, no. 15, p. 1808, 2021.

[226] C. Guo, G. Liu, and C.-H. Chen, "Air pollution concentration forecast method based on the deep ensemble neural network," *Wireless Communications and Mobile Computing*, vol. 2020, no. 1, p. 8854649, 2020.

[227] C. M. Bishop and N. M. Nasrabadi, *Pattern recognition and machine learning*, vol. 4. Springer, 2006.

[228] O. Tarkhaneh and H. Shen, "Training of feedforward Neural Networks for data classification using hybrid particle Swarm optimization, Mantegna Lévy flight and neighborhood search," *Heliyon*, vol. 5, no. 4, 2019.

[229] H. Safari, C. A. Cañizares, D. Sohm, E. Ahmed, I. El-Samahy, and M. Dusseault, "Modeling of air-source heat pumps in smart residential applications," *IEEE Innovative Smart Grid Technologies (ISGT)*, 2026.

[230] H. Safari, M. Abuelhamd, C. Cañizares, M. B. Dusseault, D. Sohm, E. Ahmed, and I. El-Samahy, "Modeling of air-source heat pumps in smart residential applications," 2026. Preprint, TechRxiv. [Online]. Available: http://dx.doi.org/10.36227/techrxiv.177220023.38309352/v1. Accessed: 2026.

[231] A. Ouammi, D. Zejli, H. Dagdougui, and R. Benchrifa, "Artificial neural network analysis of Moroccan solar potential," *Renewable and Sustainable Energy Reviews*, vol. 16, no. 7, pp. 4876–4889, 2012.

[232] H. Safari, C. A. Cañizares, M. B. Dusseault, D. Sohm, E. Ahmed, and I. El-Samahy, "Transmission-level disaggregation of distributed PV power using data-driven methods," in *IEEE Electrical Power and Energy Conference (EPEC)*, p. 447, 2025.

[233] Mitsubishi Electric Sales Canada Inc., "Zuba cold climate heat pumps." [Online]. Available: `https://www.mitsubishielectric.ca/en/hvac/professionals/zuba`, 2025. Accessed: Aug. 20, 2025.

[234] Solcast, "Solcast global solar irradiance data and forecasting." [Online]. Available: `https://solcast.com/`, 2026. Accessed: Feb. 25, 2026.

[235] I. Calero, C. A. Canizares, K. Bhattacharya, and R. Baldick, "Duck-curve mitigation in power grids with high penetration of PV generation," *IEEE Transactions on Smart Grid*, vol. 13, no. 1, pp. 314–329, 2021.

[236] M. Dahl, A. Brun, O. S. Kirsebom, and G. B. Andresen, "Improving short-term heat load forecasts with calendar and holiday data," *Energies*, vol. 11, no. 7, p. 1678, 2018.

[237] M. Sirati, W. O'Brien, and C. A. Cruickshank, "Analyzing smart thermostat data to uncover trends in remote work behaviors," *Energy and Buildings*, vol. 330, 2025. Art. no. 115320.

[238] Yukon Energy Mines and Resources, "Air source heat pump pilot project: Technical report, winter 2020-21." [Online]. Available: `https://yukon.ca/en/air-source-heat-pump-pilot-project-technical-report-winter-2021`, 2021. Accessed: Jan. 30, 2026.

[239] G. F. Tzortzis and A. C. Likas, "Multiple view clustering using a weighted combination of exemplar-based mixture models," *IEEE Transactions on Neural Networks*, vol. 21, no. 12, pp. 1925–1938, 2010.

[240] Hydro One Networks Inc., "Needs assessment report: Greater Toronto area (GTA) west region." [Online]. Available: `https://www.hydroone.com/abouthydroone/CorporateInformation/regionalplans/gtawest/Documents/Needs%20Assessment%20Report%20GTA%20West%202019.pdf`, 2019. Accessed: Jan. 29, 2026.

[241] Mitsubishi Electric, "ZUBA cold climate hyper-heat (H2i™): MESCA." [Online]. Available: `https://www.mitsubishielectric.ca/en/hvac/homeowners/zuba`, 2026. Accessed: Jan. 29, 2026.

[242] ClimateData.ca, "Download data – ClimateData.ca." [Online]. Available: `https://climatedata.ca/download/`, 2026. Accessed: Jan. 29, 2026.

[243] Canada Energy Regulator, "Heat pumps could significantly reduce GHG emissions from Canada's buildings." [Online]. Available: https://www.cer-rec.gc.ca/en/data-analysis/energy-markets/market-snapshots/2023/market-snapshot-heat-pumps-could-significantly-reduce-ghg-emissions-from-canadas-buildings.html, 2024. Accessed: Jan. 29, 2026.

[244] Natural Resources Canada, "Heat pumps uptake at a glance." [Online]. Available: https://natural-resources.canada.ca/energy-efficiency/home-energy-efficiency/canada-greener-homes-initiative/heat-pumps-uptake-glance-0, 2026. Accessed: Jan. 29, 2026.

[245] Statistics Canada, "Focus on geography series, 2021 census: Ontario." [Online]. Available: https://www12.statcan.gc.ca/census-recensement/2021/as-sa/fogs-spg/page.cfm?lang=E&topic=3&dguid=2021A000235, 2023. Accessed: Jan. 29, 2026.

[246] Dynamic Heating & Cooling, "Best heat pump brands in Canada: Recommendations 2025." [Online]. Available: https://dynamicheatandcool.ca/best-heat-pump-brands-canada-recommends-2025/, 2026. Accessed: Jan. 29, 2026.

[247] Carrier, "Central AC units: Air conditioners, residential." [Online]. Available: https://www.carrier.com/residential/en/ca/products/air-conditioners/, 2026. Accessed: Jan. 29, 2026.